

UNIVERSITY OF KWAZULU-NATAL



Investigation of Different Graphite Precursors for Graphene Oxide Supercapacitors

by

Solan Perumal

Supervised by:
Dr. A.L.L. Jarvis

A dissertation submitted in fulfilment for
the degree of Master of Science in
Engineering

in the
Discipline of Electrical, Electronic and Computer Engineering,
College of Agriculture, Engineering and Science,
University of KwaZulu-Natal, Durban, South Africa

Date: March 2021

Declaration of Authorship

I, SOLAN PERUMAL, declare that this dissertation titled, 'INVESTIGATION OF DIFFERENT GRAPHITE PRECURSORS FOR GRAPHENE OXIDE SUPERCAPACITORS' and the work presented in it are my own. I confirm that:

- The research reported in this dissertation, except where otherwise indicated, is my original work.
- This dissertation has not been submitted for any degree or examination at any other university.
- This dissertation does not contain other persons data, pictures, graphs or other information unless specifically acknowledged as being sourced from other persons.
- This dissertation does not contain other persons writing unless specifically acknowledged as being sourced from other researchers. Where other written sources have been quoted, then: i) their words have been re-written, but the general information attributed to them has been referenced and ii) where their exact words have been used, their writing has been placed inside quotation marks and referenced.
- Where I have reproduced a publication of which I am an author, co-author or editor, I have indicated in detail which part of the publication was written by myself alone and have fully referenced such publications.
- This dissertation does not contain text, graphics or tables copied and pasted from the Internet, unless specifically acknowledged, and the source being detailed in the dissertation and the References sections.

Signed:

Date:

As the candidate's supervisor, I, ALAN LAWRENCE LEIGH JARVIS, agree to the submission of this dissertation.

Signed:

Date

Abstract

Master of Science in Engineering

by Solan Perumal

The impact of non-renewable energy sources has had adverse effects on the environment resulting in climate change. Many countries have undertaken a call for renewable energy sources as a cleaner and more sustainable alternative. With the change towards renewable energy sources, storing this energy has become a challenge due to its intermittent nature.

An energy storage device that could help solve the above problem is a supercapacitor due to its high power density, long cycle life, and high rate capability, which are desirable characteristics for energy storage devices. Supercapacitors downfall is their low energy density. Improvement in the electrode material of the supercapacitor may help address the low energy density issue. A promising candidate is graphene oxide (GO). GO has shown notable potential as electrode material in past research due to the pseudocapacitance effect. The primary precursor for the synthesis of GO is graphite. Varying graphite precursors may yield GO with different properties.

In this research, graphite precursors with different characteristics were investigated to determine the effect they have on GO supercapacitor energy storage capabilities. Eight graphite precursors were used to synthesise GO. The samples were characterised using High-Resolution Transmission Electron Microscopy (HRTEM), Scanning Electron Microscopy (SEM), Elemental Analysis, Fourier Transform Infrared (FTIR) Spectroscopy and Raman Spectroscopy. GO supercapacitors were fabricated using GO as an active electrode material, stainless steel plates as current collectors, and phosphoric acid (H_3PO_4) hydrogel polymer as electrolyte and separator. The electrochemical testing conducted on GO electrode material were Cyclic Voltammetry (CV) at different scan rates to determine specific capacitance and energy density.

It was found that increasing flake size of natural graphite precursors produced GO with higher specific capacitance with an implicit limiting point. With the lack of peaks between the voltage limits of the CV curves for GO produced from natural graphite precursors, this indicated that the pseudocapacitance effect from oxygen functional groups is insignificant to the overall specific capacitance for these samples. These results led to further research into other possible factors that can be playing a role in GO's high specific capacitance.

It was observed that GO produced from the smallest flake size (0.045 mm) synthetic graphite precursor had the highest specific capacitance compared to GO produced from natural graphite precursor of all flake sizes investigated in this research. Firstly, the synthetic GO sample

produced from smallest flake size had higher crystallinity compared to natural GO samples which were estimated using Raman spectroscopy. Secondly, high oxygen content shown in elemental analysis and peaks observed between voltage limits of CV curves provided a high pseudocapacitance effect that is significant to the overall capacitance. Thirdly, low amount of defects determined from low I_D/I_G (Intensity of D band/Intensity of G band) ratio in Raman spectrum may enable the ions from the electrolyte to move through the GO structure efficiently. It is the combination of these characteristics that attribute to GO produced from smallest flake size (0.045 mm) synthetic graphite precursor that improved energy storage capabilities and be an excellent electrode material to use in supercapacitors.

Acknowledgements

I would like to express my heartfelt gratitude and appreciation foremost to my supervisor Dr A.L.L. Jarvis for all your invaluable guidance, mentorship, and continued encouragement throughout my research. Your expert advice and recognised extensive knowledge in the field of material science and engineering have been a permanent source of great assistance.

I would like to express my love and gratitude to my mum and dad for their faith, encouragement, support and allowing me this opportunity to further my studies. To my girlfriend, Jilane Naidoo, thank you for listening to my theories and ideas, sometimes giving me company during late-night experiments and making me focus when I strayed off matters at hand.

I would like to thank Mohammed Gaffoor (Mo) for his assistance and advice with experimentation and support throughout my research. Thanks to the technicians at the Machinery Workshop for their assistance and lending of tools when needed. I would like to give thanks to the following technicians: Thiloshini Naidoo (Anita) for smooth processing of samples for characterisation, Vishal Bharuth for teaching me how to use the Scanning Electron Microscope (SEM) and Energy Dispersive X-ray (EDX), Sizwe Zamisa for slotting me into your busy schedule to use the Raman machine. I am forever grateful to everyone mentioned above.

Saving the best for last, to God, I thank you for giving me the strength to continue through the tough times and when things were not working; also, for the joyful rewards of hard work and the incredible experience.

“I have no special talent. I am only passionately curious.”

~ Albert Einstein

List of Symbols and Units

A	Area of the electrode (cm^2)
C	Capacitance (F)
C_{SA}	Areal Specific Capacitance ($\text{F}\cdot\text{cm}^{-2}$)
C_{SG}	Gravimetric Specific Capacitance ($\text{F}\cdot\text{g}^{-1}$)
C_{SV}	Volumetric Specific Capacitance ($\text{F}\cdot\text{cm}^{-3}$)
ΔV_{ESR}	Voltage drop at the beginning of the galvanostatic discharging curve (V)
E	Energy Density ($\text{kJ}\cdot\text{kg}^{-1}$)
E_1	Low Limit Potential on CV Curve (V)
E_2	High Limit Potential on CV Curve (V)
ESR	Equivalent Series Resistance (Ω)
I	Current (A)
I_{2D}	Intensity of 2D band (a.u.)
I_D	Intensity of D band (a.u.)
I_G	Intensity of G band (a.u.)
L_a	Estimated Crystallite Size (nm)
λ_L	Laser Line Wavelength (nm)
m	Mass of sample (g)
ν	Scan Rate ($\text{V}\cdot\text{s}^{-1}$)
P_{MAX}	Maximum Power Density ($\text{kW}\cdot\text{kg}^{-1}$)
Q	Charge (C)
t	Time (s)
V	Operating Voltage/Voltage Window (V)

Acronyms

2D	Two-Dimensional
3D	Three-Dimensional
BMD	Bockris-Müller-Devanathan
CE	Counter Electrode
CNT	Carbon Nanotubes
CV	Cyclic Voltammetry
EDLC	Electric Double Layer Capacitor
FTIR	Fourier Transform Infrared
FWHM	Full Width at Half Maximum
G	Graphene
GO	Graphene Oxide
HRTEM	High-Resolution Transmission Electron Microscopy
PAN	Polyacrylonitrile
PANI	Polyaniline
PVA	Poly(Vinyl Alcohol)
RE	Reference Electrode
rGO	Reduced Graphene Oxide
SEM	Scanning Electron Microscope
WE	Working Electrode

Contents

Declaration of Authorship	i
Abstract	ii
Acknowledgements	iv
List of Symbols and Units	v
Acronyms	vi
List of Figures	ix
List of Tables	xii
1 Introduction	1
1.1 Electrochemical Energy Storage Technologies	1
1.2 Overview of Supercapacitor Technology	3
1.3 Research Objectives	5
1.4 Contributions	6
References	8
2 Literature Review	9
2.1 Specific Capacitance (C_s).....	9
2.2 Energy Density (E).....	13
2.3 Operating Voltage Window (V).....	17
2.4 Equivalent Series Resistance (ESR).....	19
2.5 Power Density (P)	21
2.6 Graphite	23
2.7 Graphene Oxide.....	25
References	27
3 Journal Article 1	30
3.1 Abstract.....	32
3.2 Introduction	33
3.3 Background.....	35
3.4 Experimental.....	39
3.4.1 Synthesis of GO	39
3.4.2 Fabrication of current collectors	39
3.4.3 Preparation of GO electrode	40
3.4.4 Synthesis of electrolyte	41
3.4.5 Assembly of GO supercapacitor	41
3.4.6 GO characterisation.....	42

3.4.7 GO supercapacitor electrochemical measurement	43
3.5 Results and Discussion	44
3.6 Conclusion	53
3.7 Acknowledgments	54
References	55
4 Journal Article 2.....	57
4.1 Abstract.....	59
4.2 Introduction	60
4.3 Background.....	62
4.4 Experimental.....	64
4.4.1 Synthesis of GO	64
4.4.2 Elemental Analysis	64
4.4.3 Fourier Transform Infrared (FTIR) Spectroscopy	64
4.4.4 Raman Spectroscopy.....	65
4.4.5 Cyclic Voltammetry	65
4.5 Results and Discussion	67
4.6 Conclusion	75
4.7 Acknowledgments	76
References	77
5 Conclusions and Recommendations	78
5.1 Conclusion.....	78
5.2 Recommendation for Further Studies.....	79
6 Appendix A	80
7 Appendix B.....	82
B.1 Abstract.....	83
B.2 Introduction.....	84
B.3 Background	85
B.4 Experimental.....	87
B.4.1 Synthesis of GO.....	87
B.4.2 Fabrication of current collectors.....	87
B.4.3 Preparation of GO electrode	88
B.4.4 Synthesis of electrolyte	89
B.4.5 Assembly of GO supercapacitor.....	89
B.4.6 GO characterisation	89
B.4.7 GO supercapacitor electrochemical measurement	90
B.5 Results and Discussion	91
B.6 Conclusion	95
B.7 Acknowledgments.....	96
References.....	97

List of Figures

Figure 2.1 : Typical CV curve used for Capacitance Calculation	10
Figure 2.2 : Working principle of energy storage in supercapacitor	13
Figure 2.3 : Circuit diagram to determine the energy density of a supercapacitor	13
Figure 2.4 : Categorisation of electrolytes for supercapacitors	17
Figure 2.5 : Internal components of supercapacitor.....	19
Figure 2.6 : Typical galvanostatic charge/discharge curve for a supercapacitor	19
Figure 2.7 : Die press used for sandwiching electrodes.....	20
Figure 2.8 : Circuit diagram used to determine the power density of a supercapacitor.....	21
Figure 2.9 : Crystal structure of graphite.....	23
Figure 2.10 : Categorisation of graphite precursors.....	23
Figure 2.11 : Graphite and GO powders.....	25
Figure 2.12 : Structure of GO	26
Figure 3.1 : Categorisation of supercapacitors	35
Figure 3.2 : Schematic diagram of supercapacitor showing EDLC.....	36
Figure 3.3 : Process of energy storage in supercapacitor	37
Figure 3.4 : Structure of GO showing carbonyl, carboxyl and hydroxyl on the sheet edge and epoxide on the basal plane	38
Figure 3.5 : GO Samples (a) AN1-GO, (b) AN2-GO, (c) AN3-GO, (d) AN4-GO.....	39
Figure 3.6 : Stainless steel current collector with dimensions	40
Figure 3.7 : Drop-casting of GO on stainless steel current collectors	40
Figure 3.8 : Soft steel die sandwiching electrodes.....	41
Figure 3.9 : HRTEM of (a) AN1-GO, (b) AN2-GO, (c) AN3-GO, (d) AN4-GO.....	44
Figure 3.10 : FTIR spectra of AN1-Graphite and AN4-Graphite.....	46
Figure 3.11 : FTIR spectra of AN1-GO and AN4-GO	46
Figure 3.12 : Raman spectra of graphite precursors	47
Figure 3.13 : Raman spectra of GO samples	47

Figure 3.14 : CV curves for GO samples at 10 mV.s ⁻¹ scan rate	48
Figure 3.15 : CV curves for GO samples at 20 mV.s ⁻¹	49
Figure 3.16 : CV curves for GO samples at 100 mV.s ⁻¹	49
Figure 3.17 : Gravimetric Capacitance vs. Scan Rate.....	50
Figure 3.18 : Energy Density vs. Scan Rate	50
Figure 3.19 : Specific capacitance as a function of average particle size at scan rate 10 mV.s ⁻¹	51
Figure 3.20 : Specific capacitance as a function of the scan rate.....	52
Figure 4.1 : Structure of graphite	62
Figure 4.2 : Categorisation of graphite	62
Figure 4.3 : GO as-prepared powder samples	64
Figure 4.4 : Typical CV curve showing critical values.....	66
Figure 4.5 : FTIR spectra of: AN1-Graphite and AS1-Graphite (left); and AN4-Graphite and AS4-Graphite (right)	68
Figure 4.6 : FTIR spectra of: AN1-GO and AS1-GO (left); and AN4-GO and AS4-GO (right)...	69
Figure 4.7 : Raman spectra of natural graphite precursor samples	70
Figure 4.8 : Raman spectra of synthetic graphite precursor samples.....	71
Figure 4.9 : Raman spectra of natural GO samples	71
Figure 4.10 : Raman spectra of synthetic GO samples	72
Figure 4.11 : CV curves for natural GO samples at: 10 mV.s ⁻¹ (left); and 20 mV.s ⁻¹ (right)	72
Figure 4.12 : CV curves for synthetic GO samples at: 10 mV.s ⁻¹ (left); and 20 mV.s ⁻¹ (right)	73
Figure 4.13 : Specific gravimetric capacitance of GO samples vs average particle size of graphite precursors.....	74
Figure A.1 : Discoloured gel electrolyte.....	80
Figure A.2 : Clear gel electrolyte: top view (left); and side view (right).....	80
Figure A.3 : Hydraulic press sandwiching supercapacitor electrodes together	81
Figure A.4 : Fully assembled GO supercapacitor.....	81
Figure B.1 : Categorisation of supercapacitors.....	85
Figure B.2 : Schematic of supercapacitor	86

Figure B.3 : GO samples.....	87
Figure B.4 : Stainless current collector with dimensions	88
Figure B.5 : Drop-casting of GO on stainless steel current collectors.....	88
Figure B.6 : Soft steel die sandwiching electrodes	89
Figure B.7 : Typical CV curve.....	90
Figure B.8 : HRTEM of (a) AN1-GO, (b) AN2-GO, (c) AN3-GO, (d) AN4-GO	91
Figure B.9 : CV curves for GO samples at 10 mV.s ⁻¹	92
Figure B.10 : CV curves for GO samples at 20 mV.s ⁻¹	92
Figure B.11 : CV curves for GO samples at 100 mV.s ⁻¹	93
Figure B.12 : Specific Capacitance as a function of average particle size at scan rate 10 mV.s ⁻¹	94
Figure B.13 : Specific capacitance as a function of scan rate.....	94

List of Tables

Table 3.1 : Elemental Analysis Results	45
Table 3.2 : Raman Results for Graphite Precursors	47
Table 3.3 : Raman Results for GO samples.....	48
Table 4.1 : Yield results of GO samples from GO synthesis process	67
Table 4.2 : Elemental analysis results of graphite precursors and GO samples.....	68
Table 4.3 : Results obtained from Raman spectra for all samples	69
Table 4.4 : Results obtained from CV curves for natural and synthetic GO samples.....	73
Table B.1 : Elemental Analysis Results	92
Table B.2 : Results calculated from CV curves	93

Chapter 1

Introduction

1.1 Electrochemical Energy Storage Technologies

Energy storage technology is required to store energy until needed that are harvested from energy sources specifically renewable energy sources like solar and wind. Energy storage technologies are categorised into four general types which are mechanical, chemical, electrochemical, and electrical [1]. Electrochemical energy storage falls under the scope of this dissertation.

The working principle of electrochemical energy storage is based on three processes which include separating charge, transporting charged species, and recombining of charge. The technologies that have these basic principles include electrolytic capacitors, fuel cells, batteries, and supercapacitors. However, their operating principles use different mechanisms that come with their advantages, disadvantages, challenges, and shortfalls to achieve energy storage. Depending on the application, certain electrochemical energy storage technologies are better suited.

Electrolytic capacitors are a second-generation capacitor which yield capacitance in the range of 0.1 μF to 1 F with a voltage range of 50 to 400 V [1] [2]. The different types of electrolytic capacitor include aluminum, tantalum and ceramic where they use solid/liquid electrolytes with a separator between symmetrical anode and cathode. The applications for electrolytic capacitors include power supplies and LED driver modules. Electrolytic capacitors work well in these applications because they have a high power density within the range of 1 kW.kg^{-1} to 10 000 kW.kg^{-1} [3]. Their energy density can be from 0.036 kJ.kg^{-1} to 0.18 kJ.kg^{-1} [3]. This makes electrolytic capacitors not suitable for high energy applications.

Fuel cells on the other hand have a very high energy density. Fuel cells store this energy by using a continuous supply of fuel such as hydrogen, natural gas, or methanol and an oxidant such as oxygen, air, or hydrogen peroxide. The energy density of fuel cells is in the range of 1080 kJ.kg^{-1} and 4320 kJ.kg^{-1} [4]. Fuels cells have a power density between 0.005 kW.kg^{-1} and 0.5 kW.kg^{-1} . Fuel cell's high energy density and low power density show that it is suitable for long term storage [4]. The disadvantages of fuel cells is the high storage cost in the range of R 7500.00 per kilowatt and R 150 000.00 per kilowatt and low efficiency of 20 % to 50 % [4].

Batteries are much more widely used with global energy storage power capacity shares of 1120 MW for lithium-ion (Li-ion) batteries, 220 MW for sodium-sulphur (NaS) and zebra batteries (Na-NiCl₂) batteries, 80 MW lead acid (Pb-acid) batteries, 47 MW flow batteries

30 MW for nickel-cadmium (NiCd) batteries compared to 80 MW for capacitors and 50 MW for other electrochemical energy storage technologies in 2017 [4]. The lithium-ion battery being the most popular of all batteries indicated by its large global energy storage power capacity share has an energy density in the range of 288 kJ.kg⁻¹ to 720 kJ.kg⁻¹. Lithium-ion batteries high energy density makes them suitable as a long-term energy storage device. The disadvantage of using lithium-ion batteries is their low power density in the range of 0.05 kW.kg⁻¹ to 2 kW.kg⁻¹.

Supercapacitors bridges the gap between the electrolytic capacitors and batteries in terms of energy density and power density. The power density of supercapacitors is much higher in the range of 0.01 kW.kg⁻¹ to 1000 kW.kg⁻¹ resulting in fast charging speed (< 5 ms) compared to lithium-ion batteries [3]. This high power density is due to their energy storage mechanism described as surface adsorption reactions of charged species on an electrode material compared to batteries that store their energy in the bulk of the material [5]. Supercapacitors have high energy efficiency (85 to 98 %) and long life cycle (> 100000 cycles).

The other characteristic that has shown recent interest related to battery and supercapacitor technologies is environmentally friendliness. Batteries use hazardous chemicals which can ignite during charging/discharging or be released into the environment upon disposal [6]. Supercapacitors are environmentally friendlier than batteries as no thermal heat or hazardous substances are released during their discharge.

Since supercapacitors store energy on the surface of the electrode material, their energy density is low in the range of 0.18 kJ.kg⁻¹ to 72 kJ.kg⁻¹ compared to batteries [3]. The low energy density of supercapacitors is a technical problem that is still under research in the field of supercapacitors today [7] [8] [9] which provided the focus for this dissertation.

The dissertation is structured in the following way; Chapter 1 is an introduction discussing the electrochemical energy storage technologies, overview of supercapacitor technology, setting out research objectives and highlighting how these research objectives were achieved and key findings in the contributions presented as chapters in this dissertation; Chapter 2 is a Literature Review examining the improvement of energy storage capabilities of supercapacitors by using carbon-based electrode materials, providing background information on precursor material graphite and electrode material graphene oxide (GO); Chapter 3 is a journal article showing effect of flake size of precursor material graphite on improving the energy storage capabilities of supercapacitor electrode material GO, Chapter 4 is a journal article presenting influence of graphite precursor type on GO supercapacitor energy storage; Chapter 5 is the conclusion offering recommendations for further studies.

1.2 Overview of Supercapacitor Technology

Capacitor technology used for electrical energy storage began in 1745 with the invention of the Leiden jar discovered independently by German cleric Ewald Georg von Kleist and by Dutch scientist Pieter van Musschenbroek of Leiden [10].

Supercapacitor technology dates back to the discovery of the concept of electric double layer by Helm Hermann Ludwig Ferdinand von Helmholtz in 1853 [11]. This discovery was the first explanation of the theory of electric double layer that occurs at the electrode and electrolyte interface. Helmholtz described the interface of an electrode, and the electrolyte is like a capacitor. A positively charged electrode will attract the anions from the electrolyte and form a uniform negatively charged sheet of ions to create a charge balance [12]. A negatively charged electrode will attract the cations from the electrolyte and form a uniform positively charged sheet of ions to create a charge balance. This initial model for the double layer charge was known as Helmholtz Model. Over the years, by 1947, this model was refined to the Grahame-Stern Combined Model [13]. One of the newer models used to explain the electric double layer is Bockris-Müller-Devanathan (BMD) model formulated in 1963 by, John O'Mara Bockris, a South African electrochemist together with Klaus Müller a German chemist and Michael Angelo Vincent Devanathan, a Sri Lankan chemist [14].

In 1957, the electric double layer concept was first implemented practically by Howard Becker at the General Electric Corporation where he invented the Low Voltage Electrolytic Capacitor and has a patent on carbon-based electrolytic capacitors [15]. The electrode material used was fire tar lampblack, a type of carbon. This design showed that a high surface area porous carbon material immersed in the electrolyte could be used to obtain high capacitances of 0.61 F.cm^{-3} (0.237 F.cm^{-2}) at 1.5 V d.c.

In 1970, Donald L. Boos invented the first electric double-layer capacitor (EDLC) for the commercial purpose at Sohio Corporation in Cleveland [16]. He used activated carbon as the electrode material with a surface area of $500\text{-}1500 \text{ m}^2.\text{g}^{-1}$ in a non-aqueous solvent comprising of tetra alkyl ammonium salt-based electrolyte and combined the two to form a paste. The capacitance obtained was 22.88 F.cm^{-3} at 1 V.

In 1978, the term “supercapacitor” was first used by a Japanese multinational Information Technology provider called NEC, who marketed the double layer capacitor technology for the memory back up in computers [17]. The primary issue with this supercapacitor was the low specific energy value. Thus, began the search to improve the energy storage capabilities of supercapacitors.

One of the main factors that affect the energy storage capabilities of supercapacitors is the electrode material. Porous carbons have proven to be a suitable electrode material for supercapacitors because of their large surface area, easy processability, low electrical

resistance and low cost. These porous carbons are either produced from physical activation or chemical activation of carbon precursors. In the new millennia, nanomaterials have also shown great promise for being a suitable electrode material in supercapacitors which include carbon nanotubes (CNT), graphene (G) and graphene oxide (GO).

1.3 Research Objectives

In this research, the intention was to understand aspects of energy storage of GO supercapacitors. The electrode material, GO, was selected as the supercapacitor component to study in order to see its effects on energy storage:

1. Execute a method for synthesising GO that can be characterised and be used as an electrode material for supercapacitors.
2. Synthesise electrode material GO using various graphite precursors, i.e. different flake size and type (natural versus synthetic).
3. Characterise the physical properties (morphology and structure) and chemical characteristics (chemical bonds and elemental composition) of graphite precursors and GO electrode materials using the following techniques High-Resolution Transmission Electron Microscopy (HRTEM), Fourier Transform Infrared (FTIR) Spectroscopy and Raman Spectroscopy.
4. Synthesise a suitable electrolyte that is compatible with the electrode material GO.
5. Fabricate suitable current collectors for the GO supercapacitors.
6. Evaluate the electrochemical properties of the GO electrode material synthesised from the various graphite precursors such as specific capacitance and energy density.
7. Identify essential characteristics in the graphite precursors and GO electrode materials synthesised from them and the impacts they have on the energy storage capabilities of the GO supercapacitors.

1.4 Contributions

The research presented in this dissertation consists of two research articles, one journal paper that is submitted and one journal paper in manuscript form. The conference paper titled “Effect of flake size of graphite precursors of graphene oxide supercapacitors for energy storage” included in Appendix B was selected to be further extended to the journal paper titled “Effect of graphite precursor flake size on energy storage capabilities of graphene oxide supercapacitors”. This journal paper is developed further in a journal paper titled “Influence of type of graphite precursor on energy storage characteristics of graphene oxide supercapacitor”.

Conference Paper (Included in Appendix B)

Title: Effect of flake size of graphite precursor on graphene oxide supercapacitors for energy storage.

Authors: Solan Perumal, Alan Lawrence Leigh Jarvis and Mohammed Zaahid Gaffoor

Publication Type: Conference Article – peer-reviewed

Status: Published in Proceedings of the International Southern African Universities Power Engineering Conference (SAUPEC), March 2020

In this paper, the GO electrode materials that were tested were made from only natural graphite precursors with varying flakes sizes. The samples were named AN1-GO, AN2-GO, AN3-GO, and AN4-GO synthesised from graphite precursors with flake sizes 0.045 mm, 0.105 mm, 0.1250 mm and 0.4500 mm respectively. The current collectors were fabricated from stainless steel. The electrolyte was a hydrogel polymer electrolyte made with PVA, water and H₃PO₄. CV was used to determine the specific capacitance and energy density of the as-prepared electrode material in H₃PO₄ electrolyte. The expected result was for the higher oxygen content sample, which was AN1-GO to have the highest specific capacitance due to the pseudocapacitance effect. The GO electrode material made with the largest flake size natural graphite precursor, which is AN4-GO had the highest specific capacitance and energy density. This sample had the lowest oxygen content as seen by Elemental Analysis. This result showed that the pseudocapacitance effect was not predominant in contributing to the overall capacitance. Therefore, another factor must be playing a role in the increase of capacitance. Thus, it led to further investigation and resulting in paper 2.

Paper 1 (Chapter 3)

Title: Effect of Graphite Precursor Flake Size on Energy Storage Capabilities of Graphene Oxide Supercapacitors

Authors: Solan Perumal, Alan Lawrence Leigh Jarvis, and Mohammed Zaahid Gaffoor

Publication Type: Journal Article - peer-reviewed

Status: Submitted camera-ready paper to SAIEE Africa Research Journal

The conference paper was flagged by the SAIEE Africa Research Journal committee to further develop into a journal paper, which resulted in Paper 1. Further background on graphene oxide was included, and additional characterisation such as FTIR and Raman spectroscopy on natural graphite precursors and GO samples were added. Elemental analysis was expanded to include the natural graphite precursors with varying flake size. The results obtained from additional characterisation was evaluated on their effects on specific capacitance and energy density.

Paper 2 (Chapter 4)

Title: Influence of type of graphite precursor on energy storage characteristics of graphene oxide supercapacitor

Authors: Solan Perumal, Alan Lawrence Leigh Jarvis and Ajay Bissessur

Publication Type: Journal Article - peer-reviewed

Status: To be submitted (in manuscript form)

In this paper, natural and synthetic graphite precursors with analogous flake sizes were used to synthesise GO electrode material for supercapacitors. The samples AS1-GO, AS2-GO, AS3-GO, AS4-GO, AN1-GO, AN2-GO, AN3-GO and AN4-GO were characterised and tested. The characterisation of the graphite precursors and GO samples were done by Elemental Analysis to determine the elemental composition, Fourier Transform Infrared (FTIR) spectroscopy to determine bonds formed and Raman spectroscopy to determine the structural characteristics, i.e. estimated crystallite size and amount of defects, these are other factors that could be playing a role in the increase in capacitance and energy density. GO synthesised from synthetic graphite precursor with smallest flake size (0.045 mm) had the highest specific gravimetric capacitance, therefore, having the highest energy density. This outcome was due to a combination of high oxygen content, high crystallinity and low amount of defects.

References

- [1] T. M. Gür, "Review of electrical energy storage technologies, materials and systems: challenges and prospects for large-scale grid storage," *Energy & Environmental Science*, vol. 11, no. 10, pp. 2696-2767, 2018.
- [2] M. Jayalakshmi and K. Balasubramanian, "Simple Capacitors to Supercapacitors - An Overview," *International Journal Of Electrochemical Science*, vol. 3, pp. 1196-1217, 2008.
- [3] S. Koochi-Fayegh and M. A. Rosen, "A review of energy storage types, applications and recent developments," *Journal of Energy Storage*, vol. 27, pp. 1-23, 2020.
- [4] M. C. Argyrou, P. Christodoulides and S. A. Kalogirou, "Energy storage for electricity generation and related processes: Technologies appraisal and grid scale applications," *Renewable and Sustainable Energy Reviews*, vol. 94, pp. 804-821, 2018.
- [5] S. Huang, X. Zhu, S. Sarkar² and Y. Zhao, "Challenges and opportunities for supercapacitors," *APL Materials*, vol. 7, no. 10, pp. 1-9, 2019.
- [6] K. M. Winslow, S. J. Laux and T. G. Townsend, "A review on the growing concern and potential management strategies of waste lithium-ion batteries," *Resources, Conservation and Recycling*, vol. 129, pp. 263-277, 2018.
- [7] D. Tie, S. Huang, J. Wang, J. Ma, J. Zhang and Y. Zhao, "Hybrid energy storage devices: Advanced electrode materials and matching principles," *Energy Storage Materials*, vol. 21, pp. 22-40, 2019.
- [8] Y. Zhao, W. Ran, J. He, Y. Song, C. Zhang, D.-B. Xiong, F. Gao, J. Wu and Y. Xia, "Oxygen-Rich Hierarchical Porous Carbon Derived from Artemia Cyst Shells with Superior Electrochemical Performance," *ACS Applied Materials & Interfaces*, vol. 7, no. 2, p. 1132–1139, 2015.
- [9] Yufeng Zhao, Z. Zhang, Y. Ren, W. Ran, X. Chen, J. Wu and F. Gao, "Vapor deposition polymerization of aniline on 3D hierarchical porous carbon with enhanced cycling stability as supercapacitor electrode," *Journal of Power Sources*, vol. 286, pp. 1-9, 2015.
- [10] F. Scholz, "From the Leiden jar to the discovery of the glass electrode by Max Cremer," *Journal of Solid State Electrochemistry*, no. 15, pp. 5-14, 2011.
- [11] H. v. Helmholtz, "Some laws concerning the distribution of electric currents in volume conductors with applications to experiments on animal electricity," *Proceedings of the IEEE*, vol. 92, no. 5, pp. 868-870, 2004.
- [12] A. E. Woodruff, "The Contributions of Hermann von Helmholtz to Electrodynamics," *Isis*, vol. 59, no. 3, pp. 300-311, 1968.
- [13] D. C. Grahame, "The Electrical Double Layer and the Theory of Electrocapillarity," *Chemical Reviews*, vol. 41, no. 3, pp. 441-501, 1947.
- [14] J. O. Bockris and M. A. V. D. Klaus Müller, "On the structure of charged interfaces," in *Proceedings of the First Australian Conference*, Sydney, 1963.
- [15] H. Becker, "Low Voltage Electrolytic Capacitor". United States of America Patent 2,800,616, 23 July 1957.
- [16] D. L. Boos, "Electrolytic capacitor having carbon paste electrodes". United States of America Patent 3,536,963, 27 October 1970.
- [17] M. Endo, T. Takeda, Y. J. Kim, K. Koshiba and K. Ishii, "High power electric double layer capacitor (EDLC's); from operating principle to pore size control in advanced activated carbons," *Carbon Letters*, vol. 1, no. 3, pp. 117-128, 2001.

Chapter 2

Literature Review

This section looks at how using different electrode materials improves the energy storage capabilities of supercapacitors and provides background information on precursor material graphite and electrode material graphene oxide.

2.1 Specific Capacitance (C_S)

Capacitance is the ability of the supercapacitor to store electrical charge. Capacitance is also known as the ratio of charge (Q) and voltage (V). The capacitance of supercapacitors is in orders of magnitude larger than conventional capacitors [1] [2] [3]. For comparison of capacitance values within research, capacitance is represented as a specific capacitance which is the capacitance normalised by electrode mass (in grams) called Gravimetric Specific Capacitance (C_{SG}), volume (in cm^3) called Volumetric Specific Capacitance (C_{SV}), or area (in cm^2) called Areal Specific Capacitance (C_{SA}).

Specific capacitance can be determined using cyclic voltammetry (CV). A typical CV curve for a supercapacitor is shown in **Figure 2.1**. The derivation for the equation for specific capacitance from CV is shown below.

From the definition of capacitance which is the ratio of Q and V :

$$C = \frac{dQ}{dV} \quad (2.1)$$

$$C = \frac{dQ}{dt} \times \frac{dt}{dV} \quad (2.2)$$

Since $I = dQ/dt$, then:

$$C = I \times \frac{dt}{dV} \quad (2.3)$$

Rearranging the above equation, it becomes:

$$C = \frac{I}{dV/dt} \quad (2.4)$$

CV is performed at a specific scan rate (ν) with units $\text{V}\cdot\text{s}^{-1}$, that means $\nu = dV/dt$. Hence,

$$C = \frac{I}{\nu} \quad (2.5)$$

I is not constant, and hence an average need to be determined. Using the mean value theorem:

$$C = \frac{\int_{E_1}^{E_2} I(V)dV}{(E_2 - E_1)v} \quad (2.6)$$

There are two sweeps of voltage, one is positive, and one is negative. Only one sweep needs to be used to determine capacitance. Since the CV curve is not ideally symmetric, the entire integral area of the CV is calculated and divided by 2. Hence,

$$C = \frac{\int_{E_1}^{E_2} I(V)dV}{2(E_2 - E_1)v} \quad (2.7)$$

where the integral part which is the area under the curve as shown in Figure 2.1 represents the total voltammetric charge, E_2 and E_1 and the limits of the high and low potential (V) respectively, v is the scan rate ($V.s^{-1}$).

$$C_{SG} = \frac{C}{m} \quad (2.8)$$

where C_{SG} is the gravimetric capacitance; m is the mass of the active electrode material.

$$C_{SA} = \frac{C}{A} \quad (2.9)$$

where C_{AG} is the areal capacitance; A is the area of the electrode.

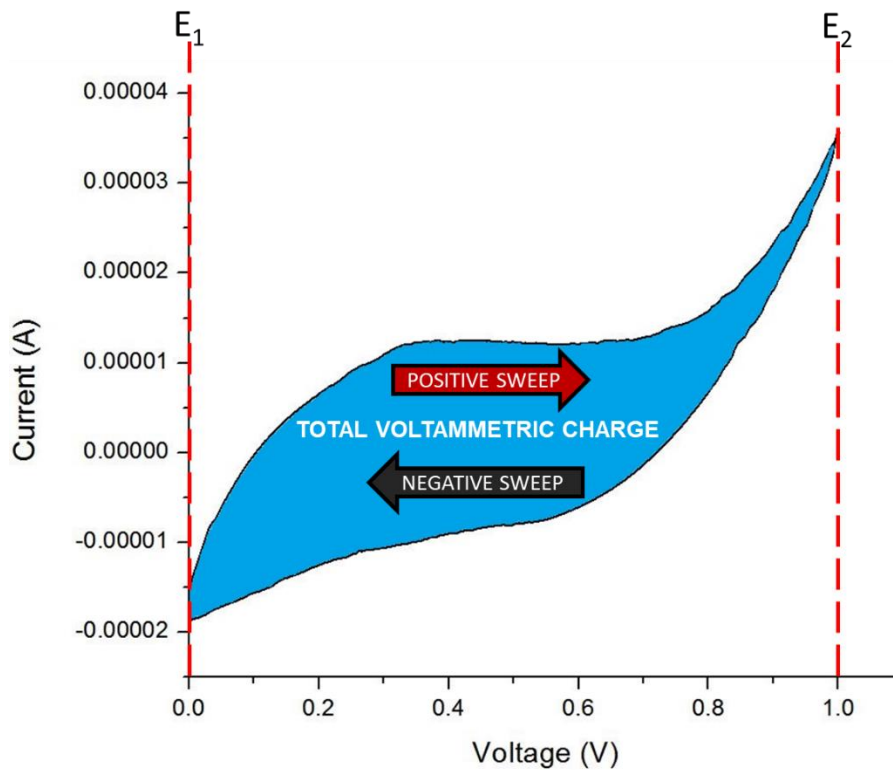


Figure 2.1 : Typical CV curve used for Capacitance Calculation

Reduced graphene oxide (rGO), which is G that has been chemically reduced from GO has been reported by many as a suitable electrode material for supercapacitors. Meryl D. Stoller *et al.* was able to attain specific gravimetric capacitances of 100 F.g⁻¹ and 99 F.g⁻¹ at 20 mV.s⁻¹ scan rate in aqueous (1 V) and organic (2.7 V) electrolyte respectively using rGO as an electrode material with appropriate chemical stability, large surface area and high electrical conductivity [4]. However, the agglomeration and limited surface area of the rGO made it difficult for the electrolyte ions to penetrate the pores of the electrode material. A nanocomposite of polyaniline (PANI) doped with GO had a synergistic effect regarding their current density (A.g⁻¹) responses at 10 mV.s⁻¹ which could be seen from the CV curves [5]. However, their specific capacitance values from CV curves were not specified. The synergy of PANI and GO was attributed to the interaction of the nitrogen atoms in the –NH– group in PANI and oxygen functional groups in GO [5].

To address the limited surface area and make the pores of the rGO more accessible Yanwu Zhu *et al.* chemically activated microwave exfoliated GO using potassium hydroxide (KOH) to increase the surface area, which is a common method to synthesise porous carbons [6]. Yanwu Zhu *et al.* were the first to employ this method for GO to use as an electrode material for supercapacitors. The specific capacitance obtained was 200 F.g⁻¹ at 200 mV.s⁻¹ scan rate and operating voltage window of 0 V to 3.5 V.

Guoxiong Zhang *et al.* improved the specific capacitance of the supercapacitor going the eco-friendly route by using an electrode material biomass carbon from bamboo activated using KOH [7]. The specific capacitance obtained was 253 F.g⁻¹ at a current density of 0.5 A.g⁻¹ using an activation temperature of 1000 °C. This high activation temperature used makes the activated biomass carbon very costly. To reduce the cost of electrode material, Boris Dyatkin *et al.* investigated carbon electrode material derived from titanium carbide (TiC) precursor with varying grain size. Higher grain size TiC precursor is cheaper than lower grain size TiC precursor due to less milling required. It was previously thought that larger particle size electrodes impede ion transport and small particle size electrodes are required for supercapacitors. However, Boris Dyatkin and co-authors showed that a higher grain size (250 µm) had a high capacitance of 110 F.g⁻¹ at scan rate 10 mV.s⁻¹ compared to a lower grain size (70 µm).

Chen-To Hsieh *et al.* showed that polyacrylonitrile (PAN) based carbon fibre by oxygen treatment had an increase in pseudocapacitance with an increase in oxidation with a minor change in the double-layer capacitance. This result showed that more oxygen content in the electrode material contributes to a higher capacitance. Bin Xu *et al.* compared GO and graphene as an electrode material for supercapacitors and found that GO had a specific capacitance of 189 F.g⁻¹, higher than that of graphene. Their reason for this was an additional

pseudocapacitance effect of attached oxygen-functional groups on the basal plane in the GO electrode material.

In this research, GO electrode material was synthesised from natural graphite precursors with different flake sizes to determine flake size affects specific capacitance. GO synthesised from a larger flake size (0.450 mm) graphite precursor with lower oxygen content was found to have a higher specific capacitance compared to the GO synthesised from a smaller flake size (0.045 mm) graphite precursor. Oxygen content and specific capacitance were determined using Elemental Analysis and CV, respectively. The results obtained showed that the pseudocapacitance effect in GO is insignificant on the overall capacitance than previously thought; also, that another factor must be playing a role in the increase of specific capacitance in GO supercapacitors.

2.2 Energy Density (E)

Energy density is the amount of energy the supercapacitor can store and is presented as a specific energy density measured in J.kg^{-1} [8]. This characteristic is lacking in supercapacitors as compared to batteries more specifically lithium-ion batteries which are known to have a large energy density [9] [1]. The process in which supercapacitor stores its energy is shown in Figure 2.2.

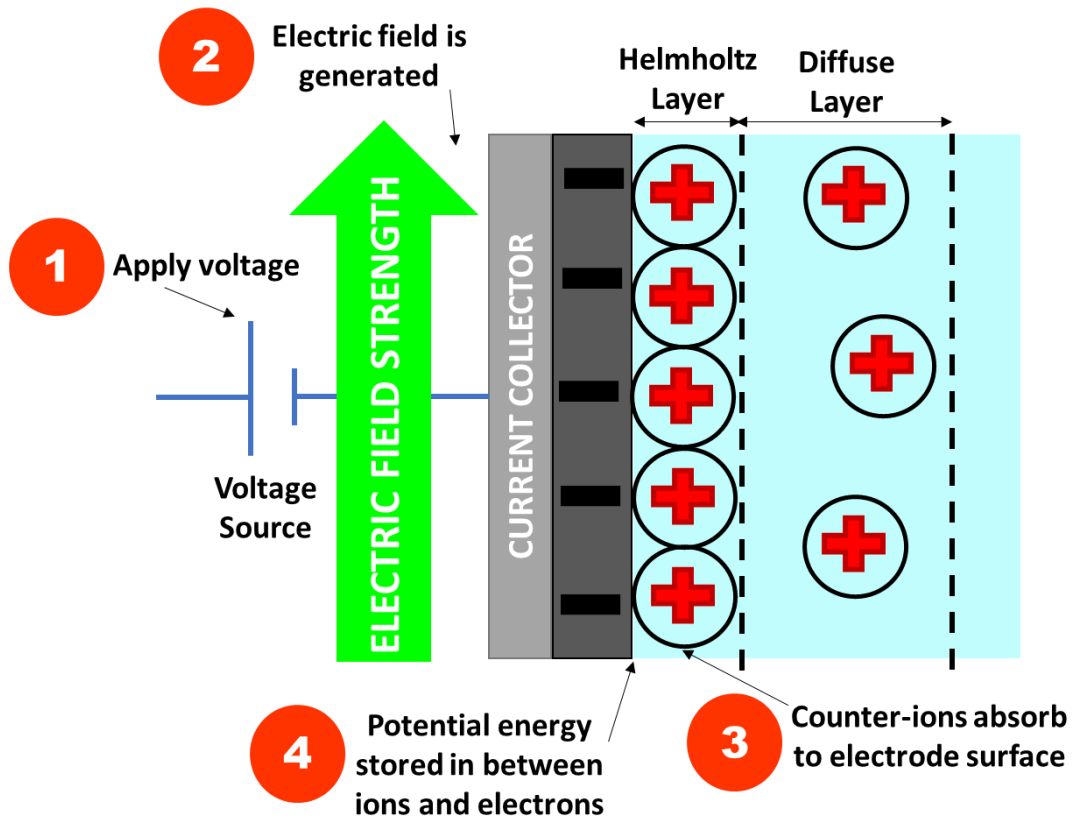


Figure 2.2 : Working principle of energy storage in supercapacitor

To determine the equation for the energy density of a supercapacitor, refer to Figure 2.3 and the derivation that follows.

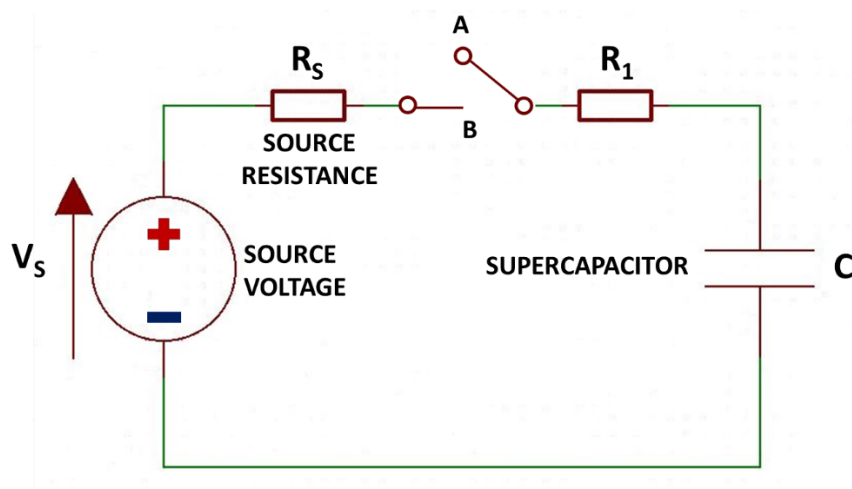


Figure 2.3 : Circuit diagram to determine the energy density of a supercapacitor

Assuming the supercapacitor is completely discharged when the switch is at position A. When the switch moves from position A to position B, the supercapacitor begins to charge. Using Kirchhoff's Voltage Law:

$$V_S = iR_S + iR_1 + \frac{1}{C} \int_0^t i(t) dt \quad (2.10)$$

$$V_S = i(R_S + R_1) + \frac{1}{C} \int_0^t i(t) dt \quad (2.11)$$

Simplifying R_S and R_1 in series to R_T :

$$V_S = i(R_T) + \frac{1}{C} \int_0^t i(t) dt \quad (2.12)$$

At $t = 0$:

$$V_S = i(R_T) + \frac{1}{C} \int_0^0 i(t) dt \quad (2.13)$$

$$V_S = iR_T \quad (2.14)$$

Rearranging the above equation:

$$i = \frac{V_S}{R_T} \quad (2.15)$$

To determine i of the supercapacitor after some time, differentiate the following equation:

$$V_S = i(R_T) + \frac{1}{C} \int_0^t i(t) dt \quad (2.16)$$

$$\frac{dV_S}{dt} = R_T \frac{di}{dt} + \frac{1}{C} i \quad (2.17)$$

Since, V_S is a d.c. voltage source meaning constant voltage with time, therefore:

$$0 = R_T \frac{di}{dt} + \frac{1}{C} i \quad (2.18)$$

Rearranging the above equation:

$$\frac{di}{i} = -\frac{1}{R_T C} dt \quad (2.19)$$

Integrating both sides:

$$\ln(i) = -\frac{1}{R_T C} t + K \quad (2.20)$$

The constant K is equal to i at $t = 0$, called I_0 :

$$\ln(i) = -\frac{1}{R_T C} t + I_0 \quad (2.21)$$

Taking the exponential on both sides of the equation:

$$i(t) = I_0 e^{-\left(\frac{t}{RC}\right)} \quad (2.22)$$

$$i(t) = \frac{V_S}{R_T} e^{-\left(\frac{t}{RC}\right)} \quad (2.23)$$

To find the energy stored in the supercapacitor:

$$E = \int_0^{\infty} P(t) dt \quad (2.24)$$

$$E = \int_0^{\infty} R_T i^2 dt \quad (2.25)$$

$$E = \int_0^{\infty} R_T \left(\frac{V_S}{R_T} e^{-\left(\frac{t}{RC}\right)} \right)^2 dt \quad (2.26)$$

$$E = \int_0^{\infty} \frac{V_S^2}{R_T} e^{-2\left(\frac{t}{RC}\right)} dt \quad (2.27)$$

$$E = \frac{V_S^2 R_T C}{R_T \cdot 2} \quad (2.28)$$

$$E = \frac{1}{2} C V_S^2 \quad (2.29)$$

In this research, the parameters capacitance (C) which was determined from CV and voltage window (V) also used in CV was used to calculate the energy density of the supercapacitor.

Different electrode materials that have been suitably designed has shown an increase in the supercapacitor's energy storage capabilities. Tae Young Kim *et al.* fabricated an activated GO-based electrode that was crumpled from aerosol spray drying GO and microwaved creating hierarchical porous architecture that had mesopores within the macro-structure of the graphene attained after activation [10]. This type of architecture solved the issue of the agglomeration of graphene sheets and was able for the electrolyte to efficiently penetrate the pores of the electrode material, therefore storing more energy with an energy density of 266.4 kJ.kg^{-1} . Long

Zhang *et al.* also found a way to synthesise graphene electrode material with lower agglomeration by hydrothermal carbonisation of biomass/polymer mixed with GO and KOH activation producing high surface area porous three-dimensional (3D) graphene structures [11]. The energy density of the 3D graphene obtained was 352.8 kJ.kg^{-1} . An eco-friendly electrode material was investigated by Sung Hoon Jung *et al.* made from glucose that was polymerised, carbonised, graphitised and then activated to produce graphene [12]. The energy density obtained was 266.4 kJ.kg^{-1} . These processes are relatively expensive and require specialised equipment to synthesise the above electrode materials making scalability challenging to reach.

A significant drawback of using graphene as an electrode material is the agglomeration and restacking of the graphene sheets, which reduces the electrode material accessible surface area resulting in poor energy storage. An electrode material that does not tend to agglomerate is GO making it a better option. Also GO is cheaper to manufacture because it is the precursor to graphene and has deionised water as an inexpensive solvent. In 2018, Michael Down *et al.* fabricated supercapacitors using GO screen-printed with conductive ink as an electrode material and obtaining an energy density of 41.76 kJ.kg^{-1} . In this research, it was shown that the energy density of the supercapacitor made from GO electrode material could be improved by using a suitable graphite precursor. GO synthesised from large flake (0.4500 mm) natural graphite precursor had an energy density of $102.11 \text{ kJ.kg}^{-1}$ compared to GO synthesised from smallest flake (0.0450 mm) natural graphite precursor. A different outcome was obtained from GO synthesised from synthetic graphite precursor. GO synthesised from synthetic graphite precursor with smallest flake size (0.045 mm) showed the highest energy density of $521.49 \text{ kJ.kg}^{-1}$.

2.3 Operating Voltage Window (V)

The operating voltage window for a supercapacitor is the voltage range between which a supercapacitor can be utilised. This parameter is highly dependent on the electrolyte used [13]. It is the electrolyte's electrochemical stability that determines the operating voltage of the supercapacitor. In other words, the voltage that decomposes the electrolyte into its constituent elements is the limiting factor for the voltage of the supercapacitor. There are many electrolytes with varying voltage windows. The categorisation of electrolytes with their respective operating voltage windows are shown in Figure 2.4.

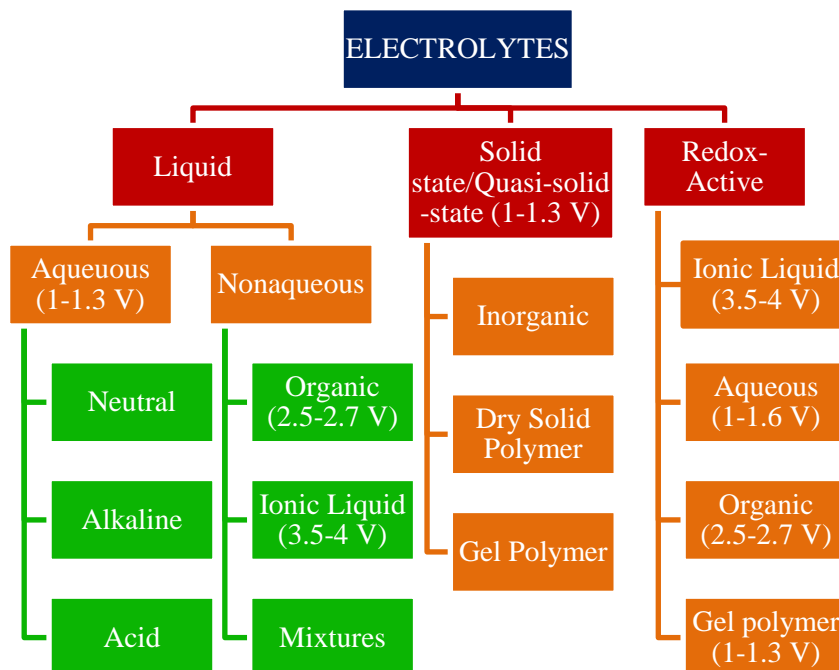


Figure 2.4 : Categorisation of electrolytes for supercapacitors

There are other factors to take into consideration when choosing an electrolyte for a supercapacitor other than electrochemical stability such as electrolyte conductivity, salt effect, solvent effect and thermal stability [14]. There are observed trade-offs for these factors. For example, aqueous electrolytes have a low operating voltage window (1 – 1.3 V) but a high conductivity that attains higher capacitances [15]. On the other hand, nonaqueous organic electrolytes have a high operating voltage window (2.5 – 2.7 V) and low conductivity, giving lower capacitances [15].

For this research, the focus was on the electrode material and minimal emphasis on the electrolyte material. The electrolyte chosen in this research was a quasi-solid-state electrolyte made of gel polymer with poly(vinyl alcohol) (PVA) as a host matrix, deionised water as a plasticiser and phosphoric acid (H_3PO_4) as the electrolyte solution. The reasons for choosing this type of electrolyte was the easy processability, low cost, and eliminating the need for a separator since the gel polymer electrolyte provides ions as well as acts as a separator. Since this electrolyte is inorganic and comprises of water (H_2O) which splits into hydrogen (H_2) and

oxygen (O₂) gases at a voltage of 1.23 V, the supercapacitor was operated between 0 V and 1 V to avoid decomposition of the electrolyte. During the synthesis process, instantaneous heating of 80 °C caused the gel electrolyte to discolour, as shown in Figure A.1. After many attempts, the correct procedure was realised which is gradual heating from room temperature to 80 °C which is not specified by other researchers to obtain a transparent hydro polymer gel electrolyte as shown in Figure A.2.

2.4 Equivalent Series Resistance (ESR)

ESR is the accumulated resistance of the internal components of a supercapacitor such as current collectors, electrode material, electrolyte and separator [16]. The internal components of the supercapacitor are shown in Figure 2.5.

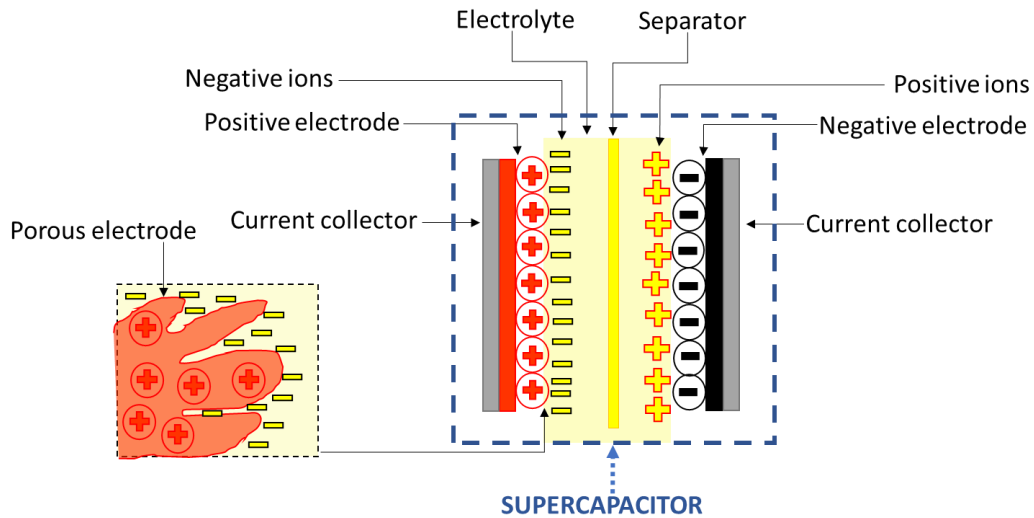


Figure 2.5 : Internal components of supercapacitor

ESR can be obtained from determining the voltage drop at the start of galvanostatic (constant current) discharging curve, as shown in Figure 2.6. Then using (2.30), ESR can be calculated [17].

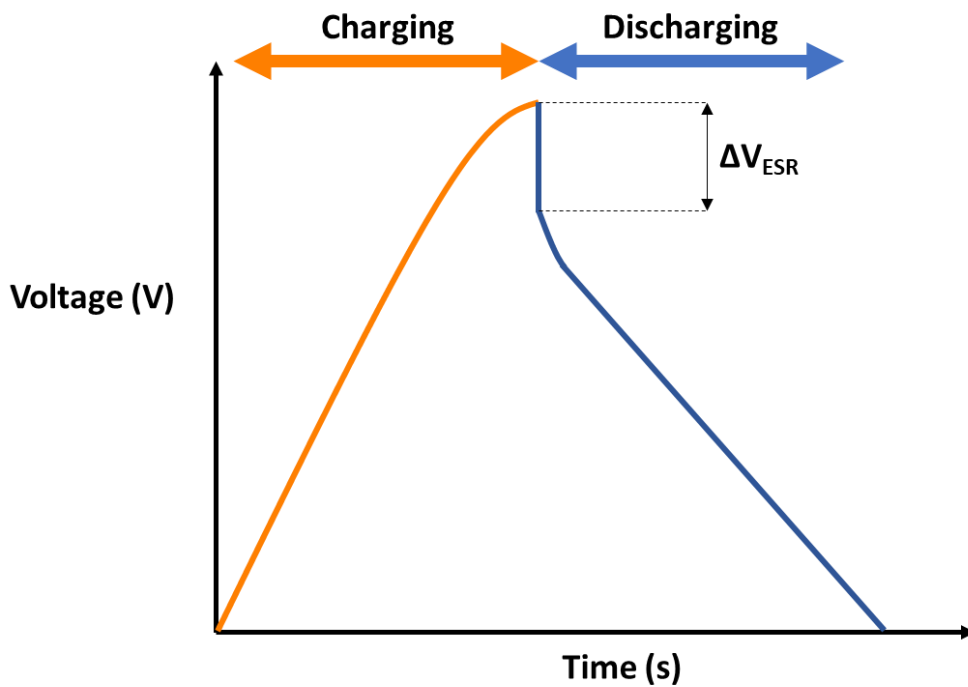


Figure 2.6 : Typical galvanostatic charge/discharge curve for a supercapacitor

$$ESR = \frac{\Delta V_{ESR}}{|I_{charge}| + |I_{discharge}|} = \frac{\Delta V_{ESR}}{2I} \quad (2.30)$$

where,

ESR = Equivalent series resistance (Ω)

ΔV_{ESR} = Voltage drop at the beginning of the galvanostatic discharge curve (V)

I = Constant charging/discharging current (A)

B. N. M Dolah *et al.* found using biomass carbon made from oil palm empty fruit bunch fibres mixed with a small amount of carbon nanotubes as an electrode material lowers the ESR than using biomass carbon alone [18]. Electrode material made from reduced GO–silica–polyaniline composite was seen to have a lower ESR than its main constituent PANI showing that reduced GO can decrease the ESR [19].

Laser reduced GO electrode material in two configurations, i.e. in-plane and sandwich were investigated by Wei Gao *et al.* and showed that sandwiched electrodes have a lower ESR than in-plane electrodes [20]. Hence, in this research, sandwiched electrode configuration was implemented as shown in **Figure 2.7**; this was executed using a die press fabricated from soft steel. The pressure was applied using a hydraulic press, as shown in Figure A.3.

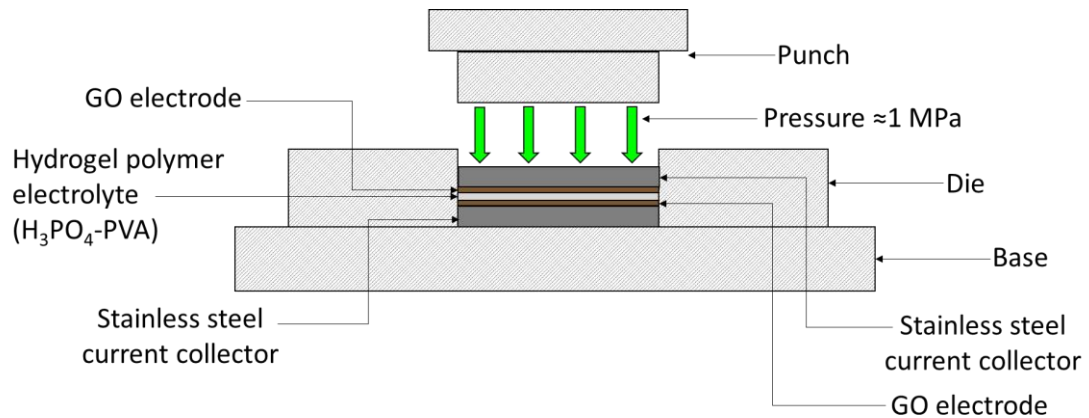


Figure 2.7 : Die press used for sandwiching electrodes

2.5 Power Density (P)

Power density is how quickly a supercapacitor takes to charge and discharge the energy stored. Supercapacitors have a higher power density compared to batteries [21]. The energy of the supercapacitor is stored on the surface of the electrode material through ion adsorption; hence the energy delivery is quick as compared to batteries where the energy is stored in the chemical reactions that occur between the electrode material and electrolyte [22]. Therefore, supercapacitors can be seen in high power applications which include regenerative braking in electric vehicles [23], as a transitional power source in renewable energy [24] and smart street lighting [25].

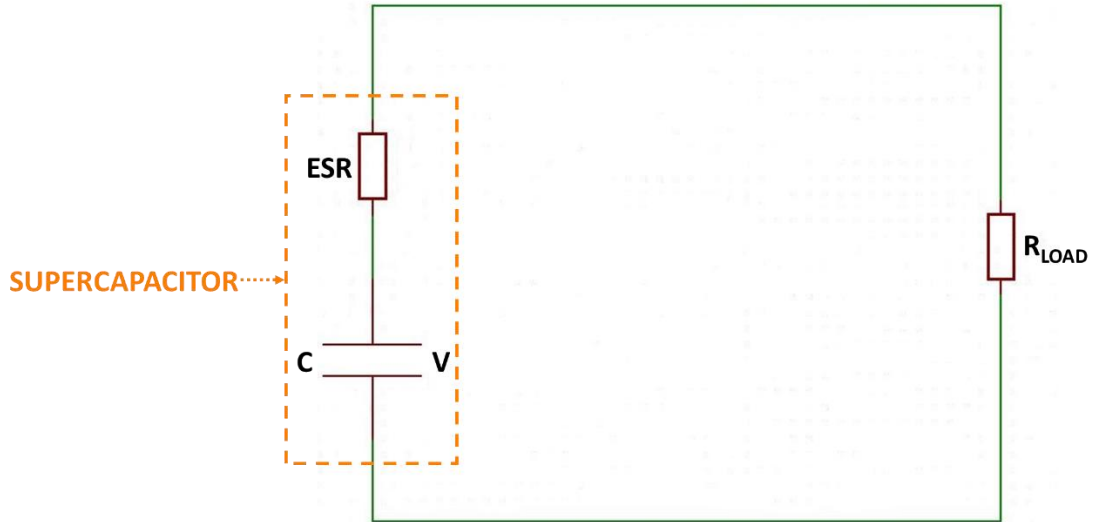


Figure 2.8 : Circuit diagram used to determine the power density of a supercapacitor

The maximum power density of a supercapacitor (P_{MAX}) with voltage rating V and internal resistance ESR delivered to a load R_{LOAD} can be derived as follows using **Figure 2.8**:

$$P = i^2 ESR \quad (2.31)$$

$$P = \left(\frac{V}{R_{LOAD} + ESR} \right)^2 ESR \quad (2.32)$$

Differentiating both sides of the equation:

$$\frac{dP}{dt} = \frac{d}{dESR} \left\{ \left(\frac{V}{R_{LOAD} + ESR} \right)^2 \right\} \quad (2.33)$$

$$\frac{dP}{dt} = V^2 \left\{ \left(\frac{1}{R_{LOAD} + ESR} \right)^2 + ESR \frac{d}{dESR} \left(\frac{1}{R_{LOAD} + ESR} \right)^2 \right\} \quad (2.34)$$

$$\frac{dP}{dt} = V^2 \left\{ \left(\frac{1}{R_{LOAD} + ESR} \right)^2 - 2ESR \left(\frac{1}{R_{LOAD} + ESR} \right)^3 \right\} \quad (2.35)$$

For maximum power density, let $\frac{dP}{dt} = 0$:

$$0 = V^2 \left\{ \left(\frac{1}{R_{LOAD} + ESR} \right)^2 - 2ESR \left(\frac{1}{R_{LOAD} + ESR} \right)^3 \right\} \quad (2.36)$$

$$2ESR = R_{LOAD} + ESR \quad (2.37)$$

$$R_{LOAD} = ESR \quad (2.38)$$

$$\therefore P_{MAX} = \frac{V^2}{4ESR} \quad (2.39)$$

As shown in (2.39), power performance is dependent immensely on the ESR of the supercapacitor and operating voltage. Improving the electrode material can increase the power density of the supercapacitor. Jun Yan *et al.* showed that highly corrugated graphene sheets made from a thermal reduction of GO and rapid cooling using liquid nitrogen could give a higher power density of 34 kW.kg⁻¹ with 68.04 kJ.kg⁻¹ energy density compared to just thermally reduced GO [26]. Majid Beidaghi *et al.* fabricated graphene nanoplatelets using electrostatic spray deposition and obtained a 75.46 kW.kg⁻¹ power density at scan rate 5 V.s⁻¹ [27]. It can be seen that the power density of supercapacitors is not a significant challenge that requires improvement and is already far superior to batteries, but the foremost drawback of supercapacitors is the low energy density. Therefore, the research focus has been in improving the energy storage of supercapacitors.

2.6 Graphite

Graphite is an allotrope of carbon [28]. The structure is a layered type with carbon atoms in a hexagonal pattern. One layer of graphite is known as graphene [29]. The in-plane lattice parameter of graphite is 1.42 Å, and the out-of-plane lattice parameter is 3.35 Å [30]. The crystal structure of graphite is shown in Figure 2.9.

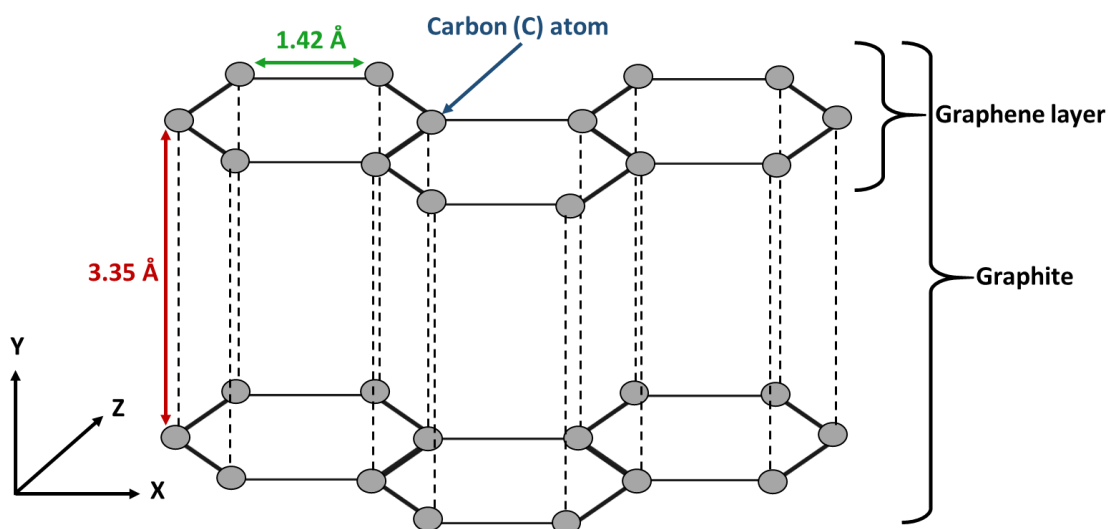


Figure 2.9 : Crystal structure of graphite

Graphite is the primary precursor to GO synthesis. A precursor is a material that following a reaction becomes an intrinsic part of a product. For the graphene oxide synthesis, graphite is regarded as a precursor because it is a material that, following the graphene oxide synthesis process becomes an intrinsic part of the product which is graphene oxide. Types of graphite differ in source, production method and structure. The categorisation of graphite is shown in Figure 2.10. From the different types of graphite, natural flake and synthetic are most commonly used for GO synthesis [31].

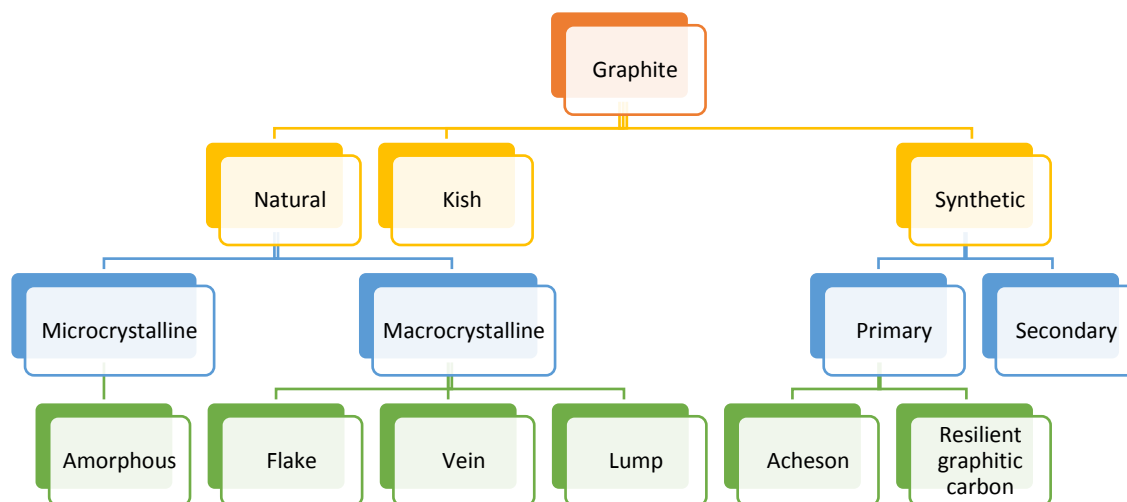


Figure 2.10 : Categorisation of graphite precursors

When purchasing graphite for GO synthesis, one must consider the type of graphite and flake size. These factors affect GO synthesised. Natural graphite precursor has seen to have a higher GO yield compared to synthetic precursor graphite [32]. GO produced from synthetic graphite with smaller flake size (45 μm) exhibits higher oxidation than GO produced from synthetic graphite with larger flake size (150 μm) [33]. There is much research regarding how characteristics of graphite precursors affect GO as a material but little research on the impact on applications. This research aims to show the relationship and direct link between the precursor graphite used for GO supercapacitors and its energy storage capabilities.

2.7 Graphene Oxide

Graphene oxide is a two-dimensional (2D) material that is synthesised from oxidising graphite with a strong oxidising agent such as potassium chlorate (KClO_3) and potassium permanganate (KMnO_4) [34]. When oxidised well, the blackish-grey graphite powder turns to yellowish-brown GO powder, as shown in **Figure 2.11**.

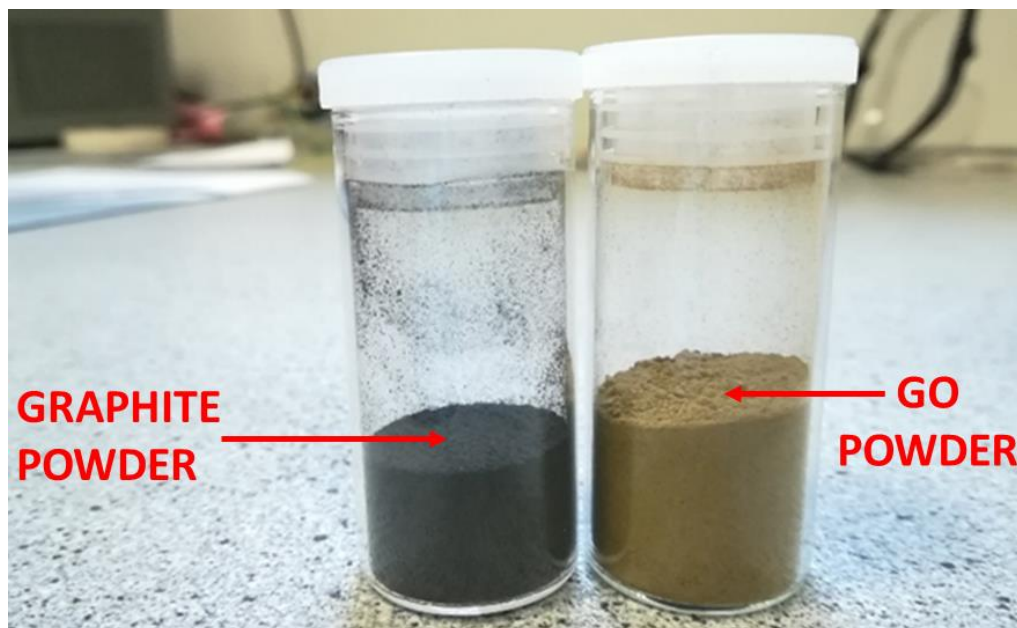


Figure 2.11 : Graphite and GO powders

GO has some desirable properties, which include hydrophilic, which means it has good wettability [35]. This property is essential for electrode materials in supercapacitors as it can soak up electrolyte easily. The structure of GO is a single sheet of graphite which is graphene with oxygen functional groups which include carbonyl, carboxyl and hydroxyl on the sheet edge and epoxide on the basal plane as shown in **Figure 2.12** [36].

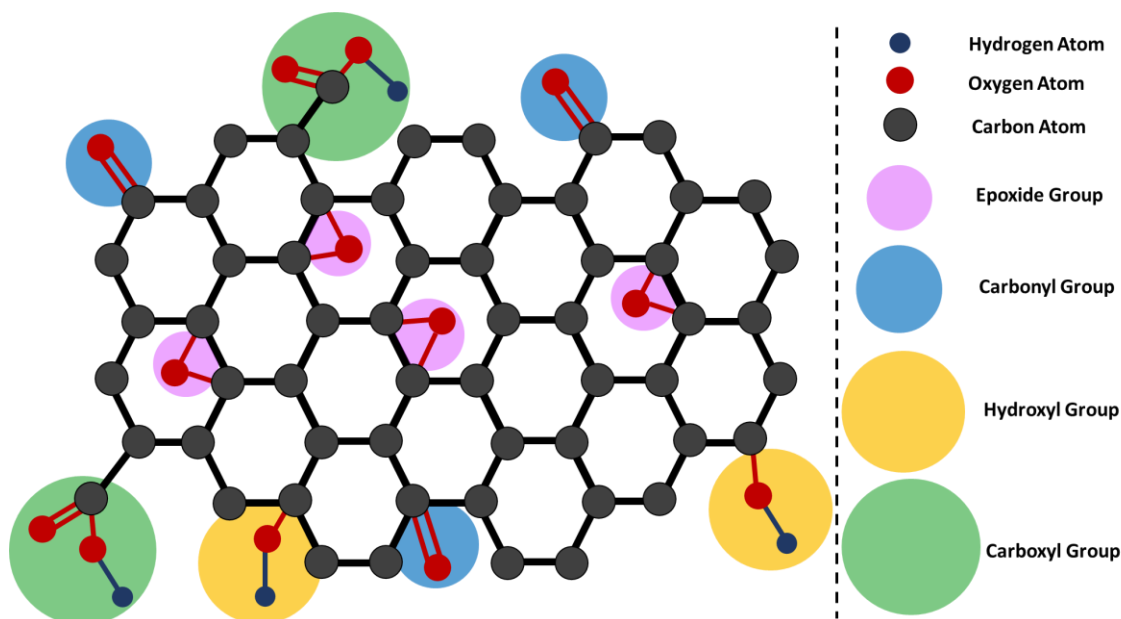


Figure 2.12 : Structure of GO

In 1859, Sir Benjamin Collins Brodie, 2nd Baronet, a British chemist, first prepared graphitic oxide also known as graphitic acid by repeated treatment of Ceylon graphite with an oxidation mixture consisting of KClO_3 and fuming nitric acid (HNO_3) at 60°C for four days and obtained what he called ‘carbonic acid’ [37]. It was Sun Hwa Lee *et al.* who confirmed that Brodie observed a suspension of tiny crystals of graphene oxide, that is, a graphene sheet densely covered with hydroxyl and epoxide groups [38]. In 1898, L Staudenmaier improved Brodie’s method by making it more straightforward and practicable by using concentrated sulfuric acid (H_2SO_4), about two-thirds less fuming HNO_3 , and adding the KClO_3 in multiple aliquots all in a single reaction vessel [39]. The most common method used today is Hummer’s Method since it is the most practical and safest method compared to the others [40] [41]. Variations of all three methods have been developed over the years [42]. In this research, GO was synthesised using Hummer’s method with additional KMnO_4 [43]; and used as the active electrode material for the supercapacitor.

References

- [1] A. Burke, "Ultracapacitors: why, how, and where is the technology," *Journal of Power Sources*, vol. 91, no. 1, pp. 37-50, 2000.
- [2] R.Kötz and M.Carlen, "Principles and applications of electrochemical capacitors," *Electrochimica Acta*, vol. 45, no. 15-16, pp. 2483-2498, 2000.
- [3] A. S. Aricò, P. Bruce, B. Scrosati, J.-M. Tarascon and W. V. Schalkwijk, "Nanostructured materials for advanced energy conversion and storage devices," *Nature Materials*, vol. 4, pp. 366-377, 2005.
- [4] M. D. Stoller, S. Park, Y. Zhu, J. An and R. S. Ruoff, "Graphene-Based Ultracapacitors," *Nano Letters*, vol. 8, no. 10, pp. 3498-3502, 2008.
- [5] H. Wang, Q. Hao, X. Yang, L. Lu and X. Wang, "Graphene oxide doped polyaniline for supercapacitors," *Electrochemistry Communications*, vol. 11, no. 6, p. 2009, 1158-1161.
- [6] Y. Zhu, S. Murali, M. D. Stoller, K. J. Ganesh, W. Cai, P. J. Ferreira, A. Pirkle, R. M. Wallace, K. A. Cychoz, M. Thommes, D. Su, E. A. Stach and R. S. Ruoff, "Carbon-Based Supercapacitors Produced by Activation of Graphene," *Science*, vol. 332, no. 6037, pp. 1537-1541, 2011.
- [7] G. Zhang, Y. Chen, Y. Chen and H. Guo, "Activated biomass carbon made from bamboo as electrode material for supercapacitors," *Materials Research Bulletin*, vol. 102, pp. 391-398, 2018.
- [8] W. K. Chee, H. N. Lim, Z. Zainal, N. M. Huang, I. Harrison and Y. Andou, "Flexible Graphene-Based Supercapacitors: A Review," *The Journal of Physical Chemistry C*, vol. 120, no. 8, pp. 4153-4172, 2016.
- [9] X. Yu, B. Lu and Z. Xu, "Super Long-Life Supercapacitors Based on the Construction of Nanohoneycomb-Like Strongly Coupled CoMoO₄-3D Graphene Hybrid Electrodes," *Advanced Materials*, vol. 26, no. 7, pp. 1044-1051, 2014.
- [10] T. Y. Kim, G. Jung, S. Yoo, K. S. Suh and R. S. Ruoff, "Activated Graphene-Based Carbons as Supercapacitor Electrodes with Macro- and Mesopores," *ACS Nano*, vol. 7, no. 8, pp. 6899-6905, 2013.
- [11] L. Zhang, F. Zhang, X. Yang, G. Long, Y. Wu, T. Zhang, K. Leng, Y. Huang, Y. Ma, A. Yu and Y. Chen, "Porous 3D graphene-based bulk materials with exceptional high surface area and excellent conductivity for supercapacitors," *Scientific Reports*, vol. 3, pp. 1-9, 2013.
- [12] S. H. Jung, Y. Myung, B. N. Kim, I. G. Kim, I.-K. You and T. Y. Kim, "Activated Biomass-derived Graphene-based Carbons for Supercapacitors with High Energy and Power Density," *Scientific Reports*, vol. 8, no. 1915, pp. 1-8, 2018.
- [13] C. Zhong, Y. Deng, W. Hu, J. Qiao, L. Zhang and J. Zhang, "A review of electrolyte materials and compositions for electrochemical supercapacitors," *Chemical Society Reviews*, vol. 44, no. 21, pp. 7484-7539, 2015.
- [14] B. Pal, S. Yang, S. Ramesh, V. Thangadurai and R. Jose, "Electrolyte selection for supercapacitive devices: a critical review," *Nanoscale Advances*, vol. 1, no. 1, pp. 3807-3835, 2019.
- [15] M. Kaempgen, C. K. Chan, J. Ma, Y. Cui and G. Gruner, "Printable Thin Film Supercapacitors Using Single-Walled Carbon Nanotubes," *Nano Letters*, vol. 9, no. 5, pp. 1872-1876, 2009.
- [16] A. Noori, M. F. El-Kady, M. S. Rahmanifar, R. B. Kaner and M. F. Mousavi, "Towards establishing standard performance metrics for batteries, supercapacitors and beyond," *Chemical Society Reviews*, vol. 48, no. 5, pp. 1272-1341, 2019.
- [17] M. Notarianni, J. Liu, K. Vernon and N. Motta, "Synthesis and applications of carbon nanomaterials for," *Journal of Nanotechnology*, vol. 7, pp. 149-196, 2016.
- [18] B. N. M. Dolah, M. Deraman, M. .. R. Othmana, R. Farmaab, E. Taer, Awitdrus, N. H. Basri, I. A. Talib, R. Omara and N. S. M. Nor, "A method to produce binderless supercapacitor electrode monoliths from biomass carbon and carbon nanotubes," *Materials Research Bulletin*, vol. 60, pp. 10-19, 2014.

- [19] U. Male, S. Uppugalla and P. Srinivasan, "Effect of reduced graphene oxide–silica composite in polyaniline: electrode material for high-performance supercapacitor," *Journal of Solid State Electrochemistry*, vol. 19, no. 11, pp. 3381-3388, 2015.
- [20] W. Gao, N. Singh, L. Song, Z. Liu, A. L. M. Reddy, L. Ci, R. Vajtai, Q. Zhang, B. Wei and P. M. Ajayan, "Direct laser writing of micro-supercapacitors on hydrated graphite oxide films," *Nature Nanotechnology*, vol. 6, pp. 496-500, 2011.
- [21] M. F. El-Kady, Y. Shao and R. B. Kaner, "Graphene for batteries, supercapacitors and beyond," *Nature Reviews Materials*, vol. 1, no. 1, pp. 1-14, 2016.
- [22] N. Choi, Z. Chen, S. A. Freunberger, X. Ji, Y. Sun, K. Amine, G. Yushin, L. F. Nazar, J. Cho and P. G. Bruce, "Challenges Facing Lithium Batteries and Electrical Double-Layer Capacitors," *Angewandte Chemie International Edition*, vol. 51, no. 40, pp. 9994-10024, 2012.
- [23] F. Naseri, E. Farjah and T. Ghanbari, "An Efficient Regenerative Braking System Based on Battery/Supercapacitor for Electric, Hybrid, and Plug-In Hybrid Electric Vehicles With BLDC Motor," *IEEE Transactions on Vehicular Technology*, vol. 66, no. 5, pp. 3724 - 3738, 2016.
- [24] S. Wang, T. Wei and Z. Qi, "Supercapacitor Energy Storage Technology and its Application in Renewable Energy Power Generation System," in *Proceedings of ISES World Congress: Solar Energy and Human Settlement*, Berlin, 2007.
- [25] K. Haque, M. R. Khan, N. Nowrin and H. U. Zaman, "Smart Street Lights using Piezoelectric Materials," in *International Conference on Microelectronics, Computing and Communications (MicroCom)*, Durgapur, 2016.
- [26] J. Yan, J. Liu, Z. Fan, T. Wei and L. Zhang, "High-performance supercapacitor electrodes based on highly corrugated graphene sheets," *Carbon*, vol. 50, no. 6, pp. 2179-2188, 2012.
- [27] M. Beidaghi, Z. Wang, L. Gu and C. Wang, "Electrostatic spray deposition of graphene nanoplatelets for high-power thin-film supercapacitor electrodes," *Journal of Solid State Electrochemistry*, vol. 16, pp. 3341-3348, 2012.
- [28] W. Gao, M. K. Siddiqui, M. Naeem and N. A. Rehman, "Topological Characterization of Carbon Graphite and Crystal Cubic Carbon Structures," *Molecules*, vol. 22, no. 9, pp. 1496-1508, 2017.
- [29] M. Matsumoto, Y. Saito, C. Park, T. Fukushima and T. Aida, "Ultrahigh-throughput exfoliation of graphite into pristine 'single-layer' graphene using microwaves and molecularly engineered ionic liquids," *Nature Chemistry*, vol. 7, pp. 730-736, 2015.
- [30] D. D. L. Chung, "Review Graphite," *Journal of Materials Science*, vol. 37, pp. 1475-1489, 2002.
- [31] A. Ambrosi, C. K. Chua, B. Khezri, Z. Sofer, R. D. Webster and M. Pumera, "Chemically reduced graphene contains inherent metallic impurities present in parent natural and synthetic graphite," *Proceedings of the National Academy of Sciences of the United States of America*, vol. 109, no. 32, p. 12899–12904, 2012.
- [32] C. Botas, A. M. Pérez-Mas, P. Álvarez, R. Santamaría, M. Granda, C. Blanco and R. Menéndez, "Optimization of the size and yield of graphene oxide sheets in the exfoliation step," *Carbon*, vol. 63, pp. 576-578, 2013.
- [33] D. R. Chowdhury, C. Singh and A. Paul, "Role of graphite precursor and sodium nitrate in graphite oxide synthesis," *RSC Advances*, vol. 4, no. 29, pp. 15138-15145, 2014.
- [34] J. G. S. Moo, B. Khezri, R. D. Webster and M. Pumera, "Graphene Oxides Prepared by Hummers', Hofmann's, and Staudenmaier's Methods: Dramatic Influences on Heavy-Metal-Ion Adsorption," *ChemPhysChem*, vol. 15, no. 14, pp. 2922-2929, 2014.
- [35] D. A. Dikin, S. Stankovich, E. J. Zimney, R. D. Piner, G. H. B. Dommett, G. Evmenenko, S. T. Nguyen and R. S. Ruoff, "Preparation and characterization of graphene oxide paper," *Nature*, vol. 448, p. 457–460, 2007.
- [36] C. Botas, P. Álvarez, C. Blanco, R. Santamaría, M. Granda, P. Ares, F. Rodríguez-Reinoso and R. Menéndez, "The effect of the parent graphite on the structure of graphene oxide," *Carbon*, vol. 50, no. 1, pp. 275-282, 2012.
- [37] B. C. Brodie, "On the atomic weight of graphite," *Philosophical Transactions*, vol. 149, pp. 249-

259, 1859.

- [38] S. H. Lee, D. R. Dreyer, J. An, A. Velamakanni, R. D. Piner, S. Park, Y. Zhu, S. O. Kim, C. W. Bielawski and R. S. Ruoff, "Polymer Brushes via Controlled, Surface-Initiated Atom Transfer Radical Polymerization (ATRP) from Graphene Oxide," *Macromolecular Rapid Communications*, vol. 31, no. 3, pp. 281-288, 2010.
- [39] L. Staudenmaier, "Process for the Preparation of Graphitic Acid," *Reports of the German Chemical Society*, vol. 31, no. 2, pp. 1481-1487, 1898.
- [40] W. S. Hummers and R. E. Offeman, "Preparation of Graphitic Oxide," *Journal of the American Chemical Society*, vol. 80, no. 6, p. 1339, 1958.
- [41] J. W. S. Hummers, "Preparation of Graphitic Acid". United States of America Patent 2,798,878, 9 July 1957.
- [42] Y. Zhu, S. Murali, W. Cai, X. Li, J. W. Suk, J. R. Potts and R. S. Ruoff, "Graphene and Graphene Oxide: Synthesis, Properties, and Applications," *Advanced Materials*, vol. 22, no. 35, pp. 3906-3924, 2010.
- [43] D. C. Marcano, D. V. Kosynkin, J. M. Berlin, A. Sinitskii, Z. Sun, A. Slesarev, L. B. Alemany, W. Lu and J. M. Tour, "Improved Synthesis of Graphene Oxide," *ACS Nano*, vol. 4, no. 8, pp. 4806-4814, 2010.

Chapter 3

Journal Article 1

Effect of Graphite Precursor Flake Size on Energy Storage Capabilities of Graphene Oxide Supercapacitors

Solan Perumal, Alan Lawrence Leigh Jarvis, and
Mohammed Zaahid Gaffoor

Accepted : SAIEE Africa Research Journal

In this chapter, the following research objectives were achieved. Executing a method for synthesising GO was performed by Hummer's method with additional potassium permanganate. GO was synthesised from natural graphite precursors with varying flake size. A suitable powder form of GO in order to characterise it was achieved. The morphology of GO was characterized by High-Resolution Transmission Electron Microscopy (HRTEM). The structure of GO was characterized by Raman. Fourier Transform Infrared (FTIR) spectroscopy was used to determine chemical bonds in GO. Elemental composition of GO was tested by Elemental Analysis. A liquid solution of the GO powder and deionized water was made to be used as an electrode material for supercapacitors. A hydrogel polymer electrolyte was made using poly(vinyl alcohol) (PVA) as a host matrix, water as a plasticiser and phosphoric acid (H_3PO_4) that is compatible with the electrode material GO. Stainless steel current collectors were fabricated for GO supercapacitors. Specific capacitance and energy density of GO electrode material from natural graphite precursors with varying flake size were evaluated. The key finding was that GO synthesised from a natural graphite precursor with large flake size (0.450 mm) has a higher energy density compared to GO synthesised from a natural graphite precursor with small flake size (0.0405 mm), even though GO synthesised from a natural graphite precursor with large flake size has a greater oxygen compared GO synthesised from a natural graphite precursor with small flake size.

3.1 Abstract

In this research supercapacitors were fabricated using graphene oxide (GO) as the electrode material. GO was synthesised using natural graphite precursor with varying flake sizes. GO was characterised by High-Resolution Transmission Electron Microscopy (HRTEM), Elemental Analysis, Fourier Transform Infrared (FTIR) spectroscopy and Raman spectroscopy. Cyclic voltammetry was carried out at different scan rates to determine the specific capacitance and energy density of the electrode material. An increase in specific capacitance was seen with an increase in graphite precursor flake size. A specific capacitance and energy density of 204.22 F.g^{-1} and $102.11 \text{ kJ.kg}^{-1}$ respectively at scan rate 10 mV.s^{-1} was obtained for the GO sample synthesised from graphite precursor with an average particle size of $0.45 \text{ }\mu\text{m}$. This sample also had the highest specific capacitance for all scan rates.

3.2 Introduction

Eskom, South Africa's primary electricity provider, cannot meet energy demand with their current non-renewable energy-based power plants [1]. In 2018, the Department of Energy pledged to get more renewable energy across the country and especially to rural areas [2]. The intermittent nature of renewable energy sources, however, creates many challenges in energy storage. Therefore, there has been considerable interest in finding efficient energy storage devices for renewable energy [3]. A promising candidate is a supercapacitor due to its high power density and excellent rate capability, which is desirable in energy storage devices [4]. There are other possible candidates that include batteries, fuel cells and flywheels.

This promising candidacy of supercapacitors has resulted in the supercapacitor technology having undergone considerable research and development in recent years. Supercapacitors have a high power density and a low energy density as compared to lithium batteries [5]. For supercapacitors to realise their potential, their energy density must be improved [6]. A meaningful way to address this is to develop advanced electrode materials. One of the unusual materials to use as the electrodes of the supercapacitor is graphene oxide (GO). GO acts as a cathode and separator in batteries due to its insulating nature thus avoiding short circuit in the battery [7]. GO has also been shown to improve battery performance [8] [9] [10] [11] [12].

GO is a two-dimensional (2-D) material made from oxidising graphite. Graphene oxide research is important considering the abundance of carbon sources in South Africa. GO is hydrophilic meaning it is readily dispersible in water. Therefore, it is easy to work with, no expensive solvent or binders are required. GO was first reported as an electrode material for supercapacitors in 2011 by Bin Xu *et al.* [13]. GO had a specific capacitance of 189 F.g⁻¹, higher than that of graphene. This result was attributed by an additional pseudocapacitance effect of attached oxygen-functional groups on the basal plane [14]. In 2018, GO proved to be an excellent electrode material when combined with conductive electrode bulk ink with a specific capacitance of 423 F.g⁻¹ [15]. The properties of GO can be tailored by varying the graphite precursor used for synthesis. By using graphite precursors with different flake sizes, the size and structure of GO are affected [16]. Oxidation of GO is greater when graphite precursor with shorter crystallite sizes was used [17]. So if GO were synthesised with a graphite precursor of smaller flake size, it would be better oxidised and therefore have more oxygen functional groups. This more significant amount of oxygen functional groups would give more pseudocapacitance effect and therefore have a higher capacitance than GO synthesised from graphite precursor with larger flake size. When purchasing commercially available natural graphite, the only difference in choice of natural graphite is varying flake sizes.

In this paper, an investigation into the link between the flake size of the graphite precursor used to synthesise GO and the energy storage characteristics of the GO supercapacitor is presented.

3.3 Background

A supercapacitor is an energy storage device with high surface area porous electrodes and a thin dielectric (electrolyte) [18]. The interface between the electrolyte and the electrode is the electric double layer. The capacitances gained from this type of architecture is orders of magnitude higher than conventional capacitors. Supercapacitors are categorised as per **Figure 3.1**, initially by the charge storage mechanism (type), thereafter, by the electrode material used, i.e. Electrochemical Double Layer Capacitor (EDLC) and GO respectively.

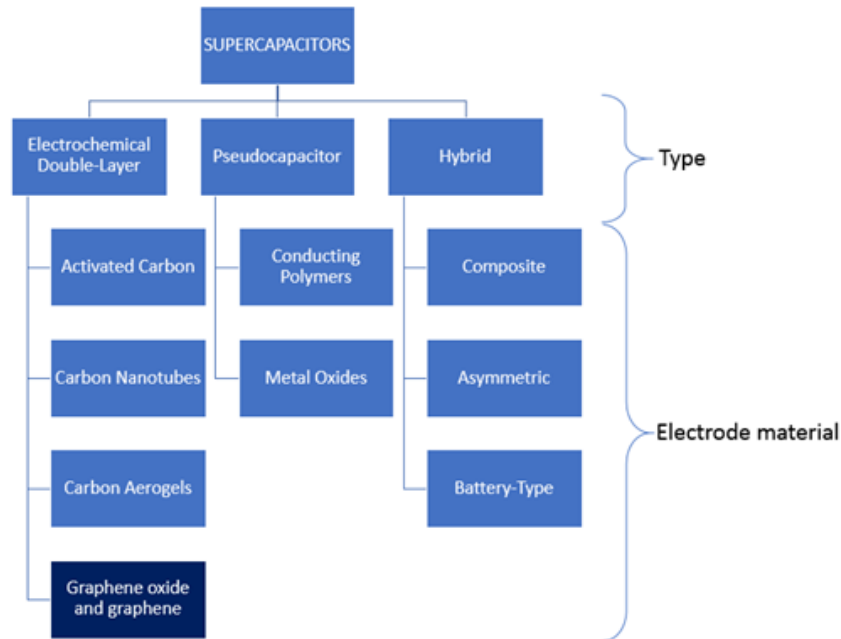


Figure 3.1 : Categorisation of supercapacitors

EDLC's mechanism for storing charge is non-Faradaic, which means charges are distributed on surfaces by physical processes that do not involve the making or breaking of chemical bonds [19]. The double-layer in name 'electrochemical double-layer capacitor' refers to the double layer of charge. One layer of charge accumulates on the electrode surface due to the voltage applied. The other layer of charge is the ions from the electrolyte that diffuse across the separator into the pores of the electrode of the opposite charge, as seen in **Figure 3.2**. The capacitance gained from this mechanism is known as double-layer capacitance.

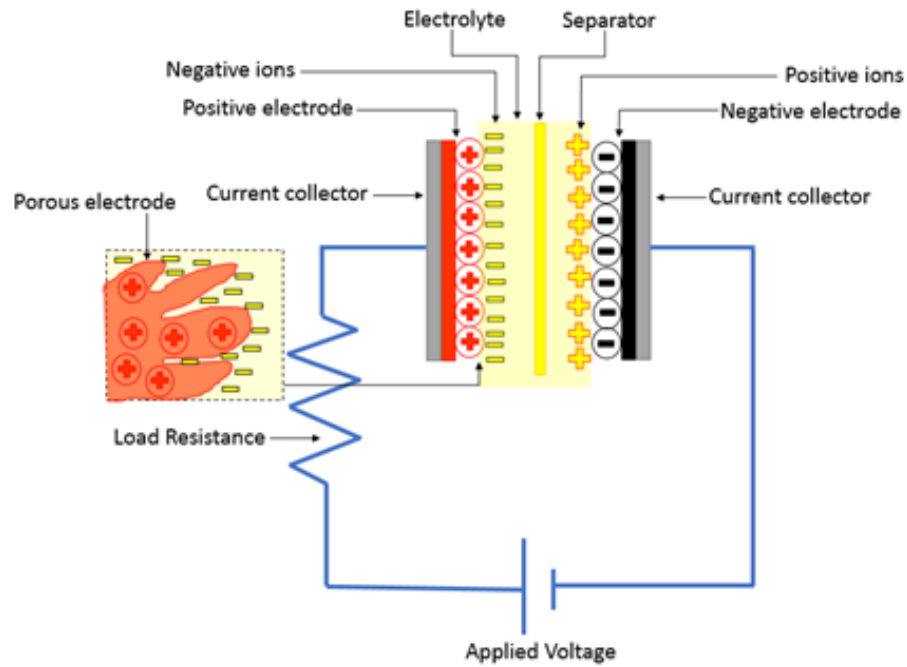


Figure 3.2 : Schematic diagram of supercapacitor showing EDLC

The capacitance of porous carbon materials like GO is mainly contributed by double-layer capacitance from electrostatic charge accumulation, and about 1-5 % is contributed by pseudocapacitance [20]. This pseudocapacitance comes from the high content of oxygen functional groups [21] which is inherent in GO. Pseudocapacitance charge storing mechanism is Faradaic, unlike double-layer capacitance and occurs as quick surface reduction and oxidation (redox) reactions.

The critical parameters for supercapacitors are specific capacitance, equivalent series resistance (ESR), energy density and power density. Specific capacitance is the capacitance normalised by electrode mass (in grams), volume (in cm^3), or area (in cm^2). ESR is the internal resistance of the supercapacitor. Energy density is the amount of energy the supercapacitor can store and is presented as a specific energy density measured in J.kg^{-1} [22]. The process in which supercapacitor stores its energy is shown in **Figure 3.3** demonstrated with a simple Gouy-Chapman Electric Double Layer Model [23] [24] (the second earliest supercapacitor model) of the supercapacitor. There are more recent complex supercapacitor models which include Bockris-Müller-Devanathan (BMD) model [25] formulated in 1963 by John O'Mara Bockris, a South African electrochemist together with Klaus Müller a German chemist and Michael Angelo Vincent Devanathan, a Sri Lankan chemist.

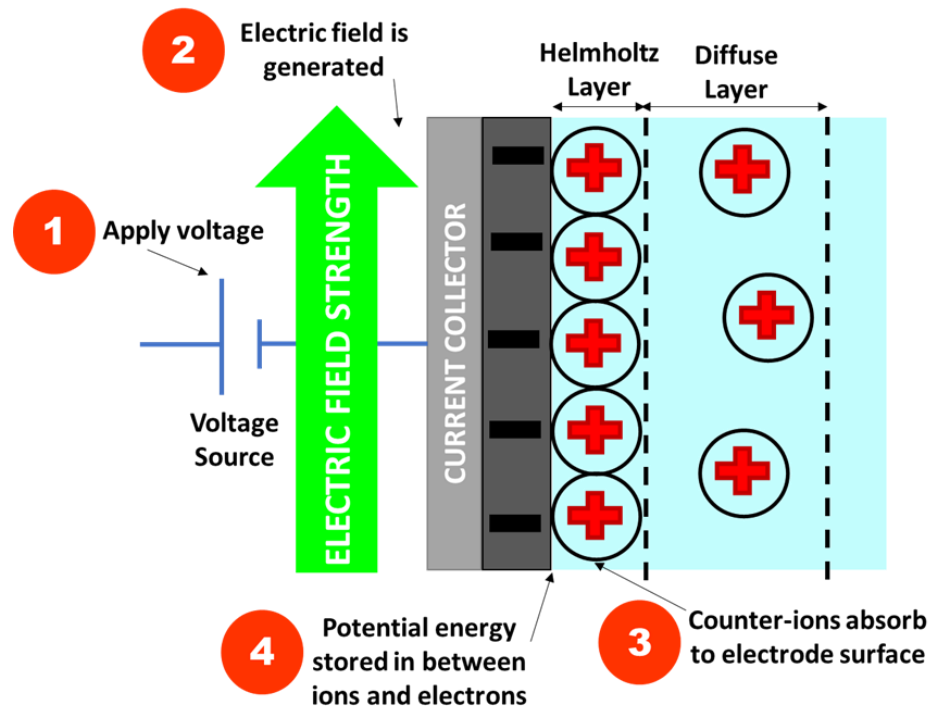


Figure 3.3 : Process of energy storage in supercapacitor

Obtaining the supercapacitor characteristics are most commonly done by cyclic voltammetry (CV). CV can be performed to evaluate capacitance of the as-prepared active electrode material GO and the operating voltage window of the electrolyte. CV is an analytical technique in which current produced via a redox reaction is monitored as a function of the scanned potential applied to an electrode [26]. The instrumentation used in CV analysis consists of a signal generator, potentiostat, working electrode (WE), reference electrode (RE) and counter electrode (CE). CV can either be done using a two-electrode system or three-electrode system [27]. Three-electrode system is accurate in controlling the voltage at the WE while measuring the current flowing from the WE to CE since it uses a RE that is ideally non-polarisable proving to be consistent and reliable [20]. It is found that the three-electrode system is also advantageous due to the quick electrode preparation.

Graphene oxide is synthesised from oxidising graphite with a strong oxidising agent such as potassium chlorate (KClO_3) and potassium permanganate (KMnO_4) [28]. GO has good wettability since it is hydrophilic which is a desirable property for supercapacitor electrode material [29] [30]. Having good wettability is essential for electrode materials in supercapacitors as it can soak up electrolyte easily and thus improving ion transport within the supercapacitor. The structure of GO is a single sheet of graphite which is graphene with oxygen functional groups which include carbonyl, carboxyl and hydroxyl on the sheet edge and epoxide on the basal plane as shown in **Figure 3.4** [31].

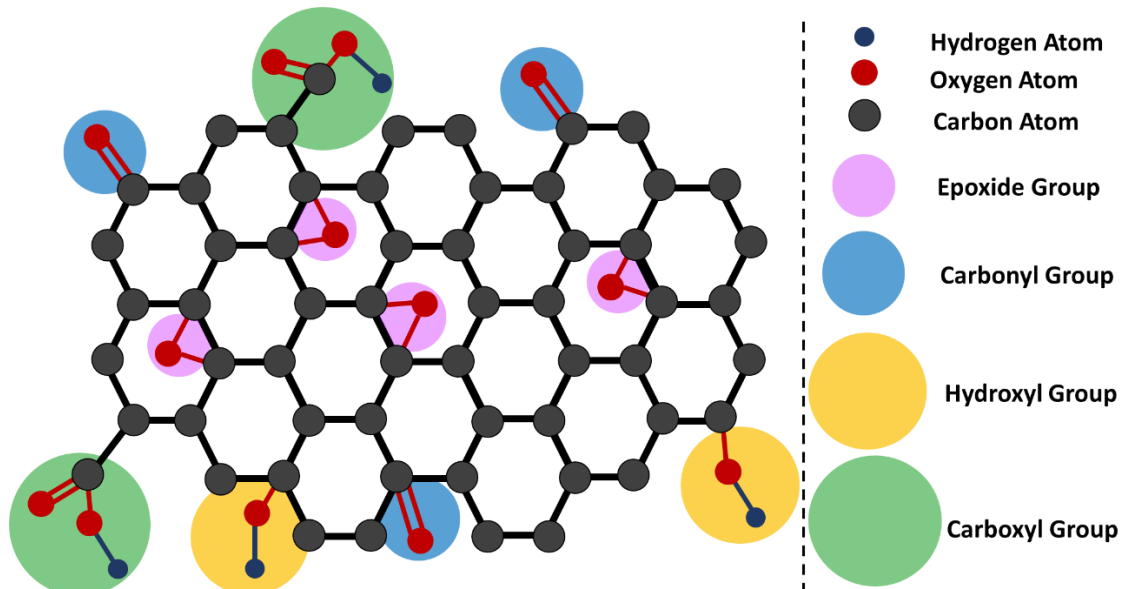


Figure 3.4 : Structure of GO showing carbonyl, carboxyl and hydroxyl on the sheet edge and epoxide on the basal plane

3.4 Experimental

The GO supercapacitor is comprised of three parts viz. electrode material, current collectors, electrolyte. The current collector and electrolyte were kept constant for all samples, and the electrode material was varied.

3.4.1 Synthesis of GO

Four different graphite precursors from Asbury Carbons were used viz. Grade 230U, 3243, 3160 and 3061 and were called AN1-GO, AN2-GO, AN3-GO and AN4-GO respectively for easy identification. The average particle sizes for AN1-GO, AN2-GO, AN3-GO and AN4-GO are 0.045 mm, 0.105 mm, 0.1250 mm and 0.4500 mm respectively. These graphite precursor average particle sizes were obtained from the graphite precursor datasheets received from Asbury Carbons. Graphite precursors were used as received. GO was synthesised by oxidising the graphite precursor using the Hummers method with additional potassium permanganate [32]. The GO powders obtained at the end of the synthesis process is shown in **Figure 3.5**.



Figure 3.5 : GO Samples (a) AN1-GO, (b) AN2-GO, (c) AN3-GO, (d) AN4-GO

3.4.2 Fabrication of current collectors

The design of the current collector was drawn using SolidWorks software, as shown in **Figure 3.6**. The active electrode area on the stainless steel current collector, 24 mm x 24 mm, which was arbitrarily selected does match previously reported supercapacitor electrode sizes [33]. The current collectors were fabricated using stainless steel with 0.5 mm thickness. Symmetric current collectors were made by laser cutting. Stainless steel was chosen due to its low corrosion rate. This property is a requirement due to the use of an acidic electrolyte. Stainless steel has been used as a current collector in many commercially available supercapacitors.

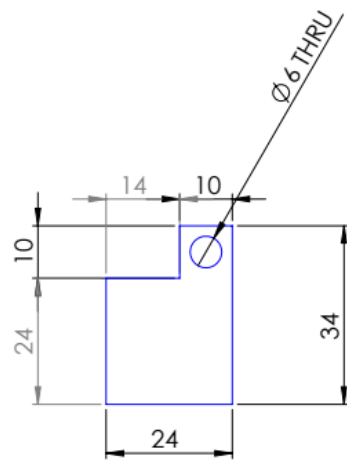


Figure 3.6 : Stainless steel current collector with dimensions

3.4.3 Preparation of GO electrode

GO solution with 0.1 %wt concentration was made by adding 0.03 g of GO powder to 30 ml of deionised water. This concentration is considered to be low, and along with an initial 1-hour sonication and 10 minutes sonication before each coat, mitigated agglomeration of GO [34]. The solution was drop-casted onto stainless steel substrate (Refer to **Figure 3.7**) and left to dry in air overnight at room temperature. In order to attain a homogenous GO deposit on the substrate, five separate individual coats were applied [34].

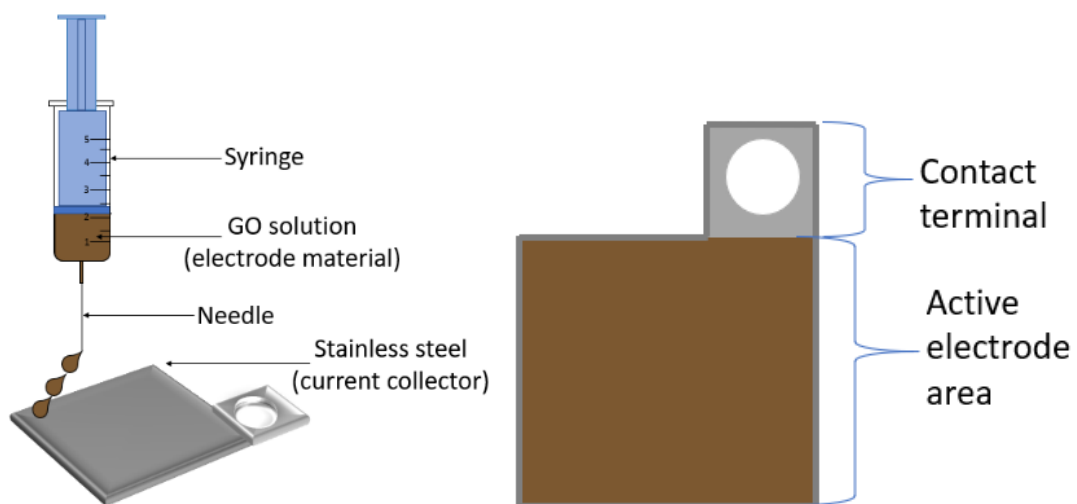


Figure 3.7 : Drop-casting of GO on stainless steel current collectors

3.4.4 Synthesis of electrolyte

The hydrogel polymer electrolyte was made using poly(vinyl alcohol) (PVA) as a host matrix, water as a plasticiser and phosphoric acid (H_3PO_4) as the electrolyte solution. The preparation of the hydrogel polymer electrolyte began with mixing with a magnetic stirrer 1 g of PVA powder and 10 ml of deionised water into a 50 ml beaker [35] [36]. The mixture was then heated up to $\sim 80^\circ\text{C}$ until it turned from white to transparent. This solution was cooled down to 50°C and then 0.03 mol (2.94 g) of H_3PO_4 electrolyte was added to the solution. The viscous solution was mixed thoroughly for one hour. After that, the clear, viscous solution was drop-cast into a glass Petri dish left overnight in the air to allow the excess water to evaporate.

Previous research has shown the capacitance properties increase as H_3PO_4 electrolyte concentration increases in the range 0.01 mol to 0.09 mol and became steady from 0.09 mol to 0.15 mol [36]. During synthesis of electrolyte in this research, it was found that at low concentration (0.01 mol to 0.02 mol) the electrolyte consistency was too stiff to practically work with; and at high concentrations (0.04 mol to 0.09 mol), the electrolyte consistency was too “runny”. At 0.03 mol concentration, the electrolyte gel had a suitable gel consistency and fell in the applicable electrolyte concentration range [36].

3.4.5 Assembly of GO supercapacitor

PVA gel electrolyte is applied to the GO coated electrodes. The electrodes are then sandwiched together using a die-press that was manufactured from soft steel, as seen in **Figure 3.8**. A pressure of ~ 1 MPa was applied to encapsulate the supercapacitor structure. A load of 90 kg was used to achieve this pressure.

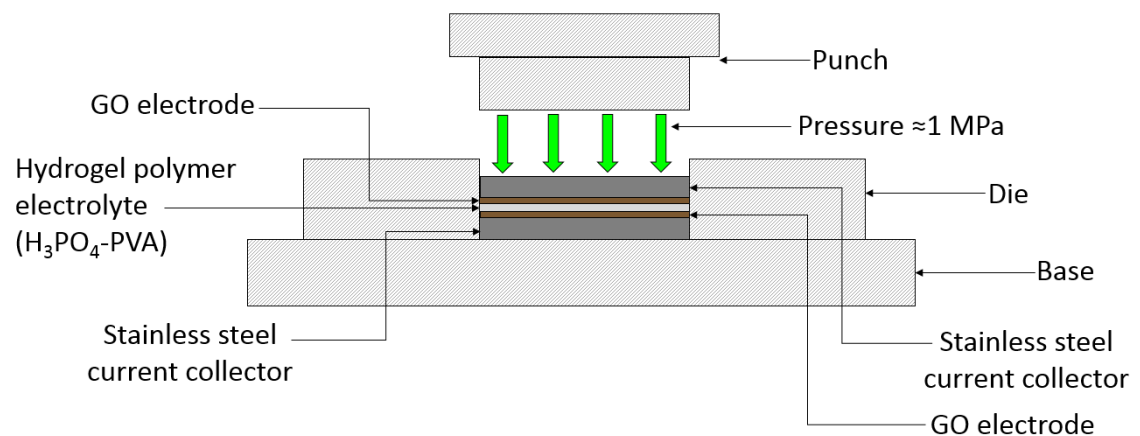


Figure 3.8 : Soft steel die sandwiching electrodes

3.4.6 GO characterisation

The morphology of the GO samples was characterised using High-Resolution Transmission Electron Microscopy (HRTEM). Elemental analysis was used to determine the carbon (C), hydrogen (H) sulphur (S), nitrogen (N) and oxygen (O) content in each GO sample. The chemical bonds in the graphite precursors and GO samples were determined by Fourier Transform Infrared (FTIR) spectroscopy.

The structure of the graphite precursors and GO samples were characterised by Raman spectroscopy at laser line wavelength of 514 nm. The intensities, full width at half maximum (FWHM), positions and integrated areas of the D band (I_D), G band (I_G), and 2D band (I_{2D}) were measured on the Raman spectrum for each sample. The ratio of I_D and I_G (I_D/I_G) gives the degree of disorder or amount of defects in the graphite and GO structure. The estimated crystallite size is determined from the Raman spectrum using (3.1) [37].

$$L_a = (2.4 \times 10^{-10}) \lambda_l^4 \left(\frac{A_D}{A_G} \right)^{-1} \quad (3.1)$$

where,

- L_a = Estimated Crystallite size (nm)
- λ_l = Laser line wavelength (nm)
- A_D = Integrated intensity (area) of D band
- A_G = Integrated intensity (area) of G band

The Raman spectra were baseline corrected by subtracting the baseline with baseline mode asymmetric least squares smoothing. Fitting of the Raman spectra was attained using the multi-peak Gaussian method by (3.2) for two peaks. Scaling was done by Levenberg-Marquardt algorithm with a tolerance of 0.0001.

$$y = y_0 + \left(\sqrt{\frac{2}{\pi}} \times \frac{A_1}{w_1} \times e^{-2 \times \frac{(x-x_{c1})^2}{w_1^2}} \right) + \left(\sqrt{\frac{2}{\pi}} \times \frac{A_2}{w_2} \times e^{-2 \times \frac{(x-x_{c2})^2}{w_2^2}} \right) \quad (3.2)$$

where,

- A_1 = Area of First Peak
- w_1 = Width of First Peak
- x_{c1} = Centre of First of Peak
- A_2 = Area of Second Peak
- w_2 = Width of Second Peak

- x_{c2} = Centre of Second of Peak

3.4.7 GO supercapacitor electrochemical measurement

CV was performed on the GO samples using a three-electrode system at typical scan rates [38] [39] of 10 mV.s^{-1} , 20 mV.s^{-1} , and 100 mV.s^{-1} . Since the electrolyte is inorganic and comprises of water (H_2O) which splits into hydrogen (H_2) and oxygen (O_2) gases at a voltage of 1.23 V, the supercapacitor was operated between 0 V and 1 V to avoid decomposition of the electrolyte.

CV was performed on the GO samples using a three-electrode system at scan rates of 10 mV.s^{-1} , 20 mV.s^{-1} , and 100 mV.s^{-1} . The operating potential window is 1 V which was determined from the H_3PO_4 electrolyte being inorganic.

To evaluate the energy storage capabilities, gravimetric (per mass) capacitance can be calculated using (3.3).

$$C = \frac{\int_{E_1}^{E_2} i(E)dE}{2vm(E_2 - E_1)} \quad (3.3)$$

where,

- $\int_{E_1}^{E_2} i(E)dE$ = Total Voltammetric Charge
- E_1 = Low Potential Limit (V)
- E_2 = High Potentials Limit (V)
- v = Scan Rate (V.s^{-1})
- m = Active Mass of the Sample GO (g).

Energy density was calculated using (3.4).

$$E = \frac{1}{2} CV^2 \quad (3.4)$$

where,

- E = Energy density (J.g^{-1})
- C = Specific Gravimetric Capacitance (F.g^{-1})
- V = Potential Difference (V)

3.5 Results and Discussion

The circular holes in Figure 3.9 are the holes in the carbon grid. In all samples, a sheet-like structure is seen, which is typical of GO. Another critical characteristic of GO is its minimal thickness regarded as 2D. All samples are highly transparent in the HRTEM images showing that the GO is exceptionally thin.

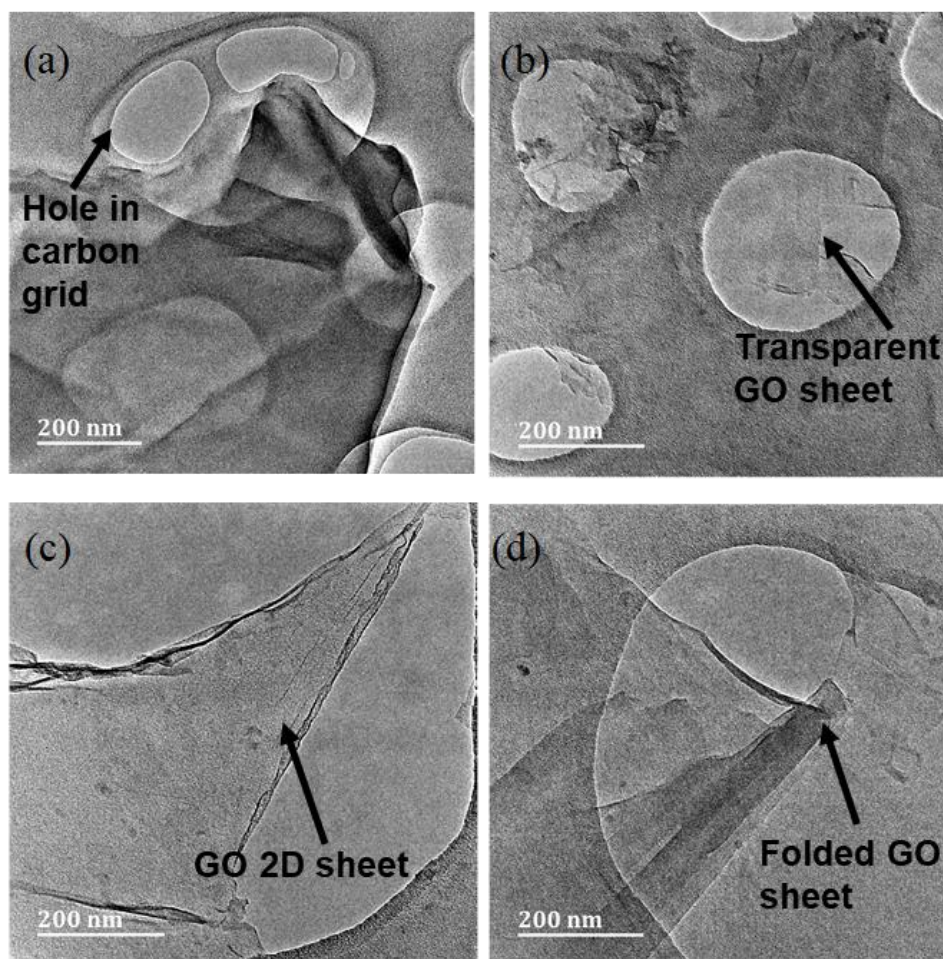


Figure 3.9 : HRTEM of (a) AN1-GO, (b) AN2-GO, (c) AN3-GO, (d) AN4-GO

The graphite precursors had some impurities of oxygen, sulphur and nitrogen as seen in the elemental results shown in Table 3.1. There is a trend with the GO samples where the increase in flake size of their graphite precursor increases sulphur content. Sulphur has been shown to increase capacitance in supercapacitors by enhancing conductivity, wettability and overall performance .

Table 3.1. These impurities are inherent in natural occurring graphite. AN1-GO sample has the highest oxygen content as compared to the other GO samples as seen in Table 3.1. There is a trend with the GO samples where the increase in flake size of their graphite precursor increases sulphur content. Sulphur has been shown to increase capacitance in supercapacitors by enhancing conductivity, wettability and overall performance .

Table 3.1. This means that AN1-GO had achieved the highest oxidation and therefore had a more significant number of oxygen functional groups than the other GO samples. This result was expected since AN1-GO was produced using natural graphite precursor with the smallest flake size (0.045 mm).

There is a trend with the GO samples where the increase in flake size of their graphite precursor increases sulphur content. Sulphur has been shown to increase capacitance in supercapacitors by enhancing conductivity, wettability and overall performance [40] [41] [42].

Table 3.1 : Elemental Analysis Results

Sample	C (%)	O (%)	S (%)	N (%)	H (%)
AN1-Graphite	97.180	1.139	1.268	0.413	0.000
AN2-Graphite	93.815	1.182	1.127	3.876	0.000
AN3-Graphite	94.297	1.112	0.994	3.597	0.000
AN4-Graphite	95.342	0.925	0.145	3.588	0.000
AN1-GO	41.80	53.095	1.881	0.05	3.174
AN2-GO	57.91	35.733	3.314	0.01	3.033
AN3-GO	61.63	30.573	4.576	0.01	3.211
AN4-GO	58.98	32.699	5.213	0.00	3.108

In order to confirm oxidation was not affected by flake size, FTIR analysis was conducted on the smallest (AN1) and largest (AN4) flake sizes. In **Figure 3.10**, the FTIR spectra of AN1-Graphite and AN4-Graphite has a noticeable variation. The significant variation is that the O–H bond of AN4-Graphite sample is broader (3700 cm^{-1} to 2200 cm^{-1}) than AN1-Graphite (3700 cm^{-1} to 3000 cm^{-1}). This bond is attributed to the water that naturally occurs in graphite. Therefore, it can be deduced that the large flake sized (0.450 mm) graphite precursor has more water content than the small flaked sized (0.045 mm) graphite precursor. The vibration mode of C–H bonds at 2934 cm^{-1} and 2860 cm^{-1} are attributed by the aldehyde functional group are seen in AN1-Graphite sample but not in AN4-Graphite sample.

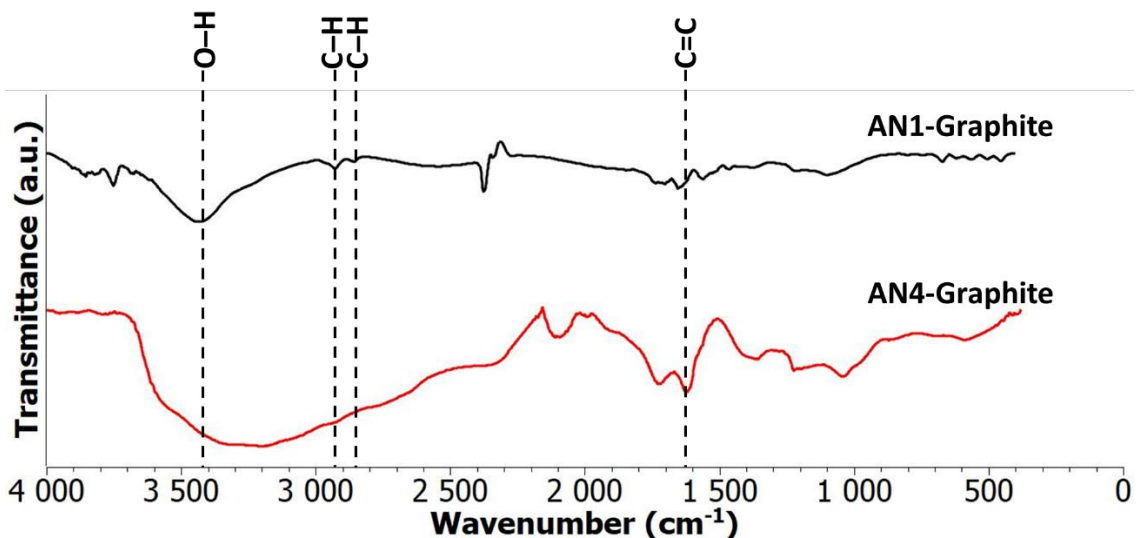


Figure 3.10 : FTIR spectra of AN1-Graphite and AN4-Graphite

In **Figure 3.11**, a broad O–H is seen for AN1-GO. This result means that after synthesis, AN1-GO was significantly oxidised. This observation agrees with the elemental analysis results of AN1-GO having a high oxygen content. AN1-GO and AN4-GO have similar FTIR spectra with AN1-GO with marginally broader peak for the O–H bond as seen in Fig. 11. The bonds C=O (1880 cm^{-1} to 1680 cm^{-1}), C=C (1680 cm^{-1} to 1500 cm^{-1}) and C–O (1150 cm^{-1} to 890 cm^{-1}) are attributed to the vibration modes of ketonic, sp²-hybridised aromatic and ether more specific epoxide species respectively.

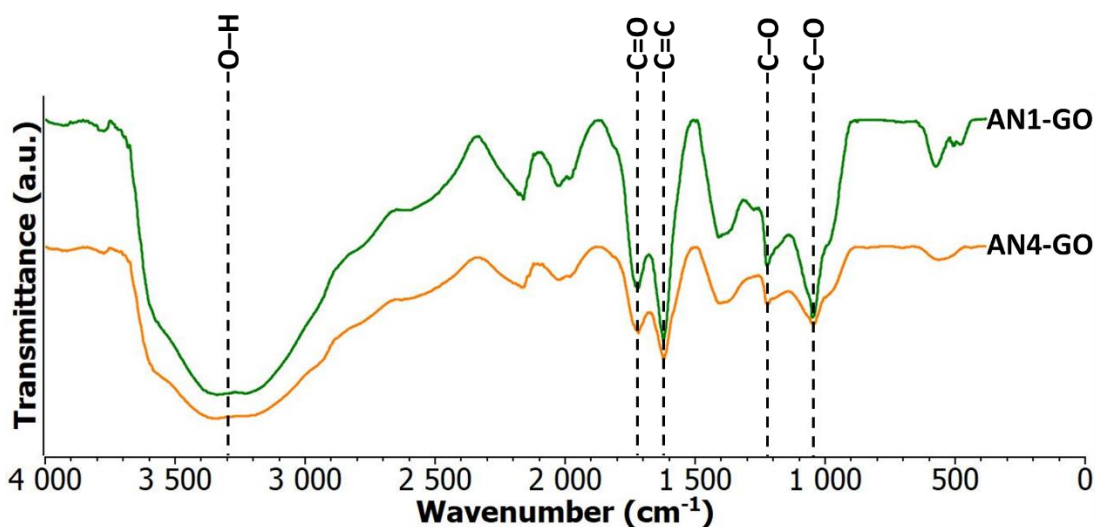


Figure 3.11 : FTIR spectra of AN1-GO and AN4-GO

The results obtained from the Raman spectra for graphite precursors are shown in **Figure 3.13**, the Raman spectra for GO samples showed only D band and G band with no 2D band being observed. GO samples show a high amount of defects, as seen in **Table 3.3** with the average ID/IG ratio of 0.87. The defects are due to sp³ hybridisation caused by oxygen functional groups. The crystallite sizes are relatively small, with an average of 11.11 nm. This result means that GO produced from natural graphite has low crystallinity.

Table 3.2. Raman spectra for natural graphite precursor samples shows two prominent bands G band 2D band, as seen in **Figure 3.12**. The G band is attributed to vibration of the sp² hybridisation in the graphitic structure.

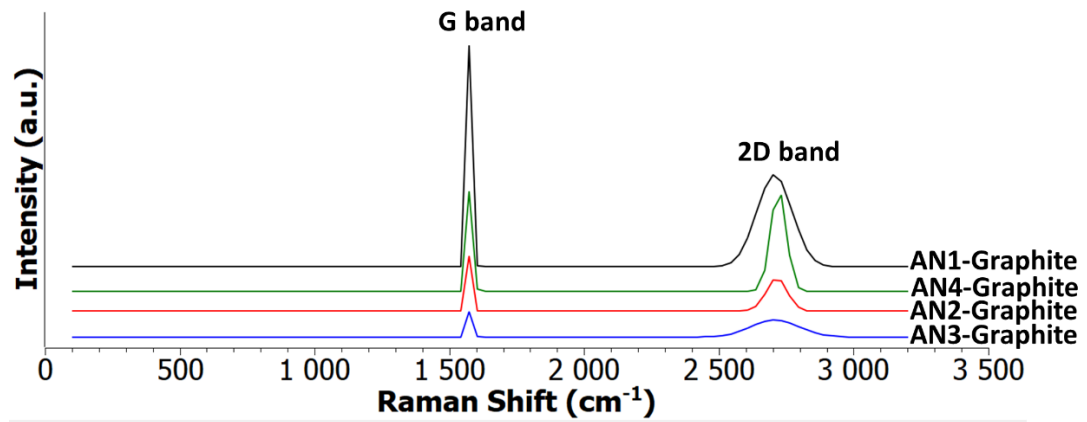


Figure 3.12 : Raman spectra of graphite precursors

The D band was not observed for graphite precursors, and therefore their crystallite sizes were not estimated, and disorder could not be determined. The D band is due out of plane vibration caused by defects in the graphitic structure. This factor does not mean that the natural graphite precursors' structure had no defects but minute defects that can be negligible. These minor defects could be from the little oxygen, sulphur and nitrogen content in the graphite precursors, as shown in **Table 3.1**.

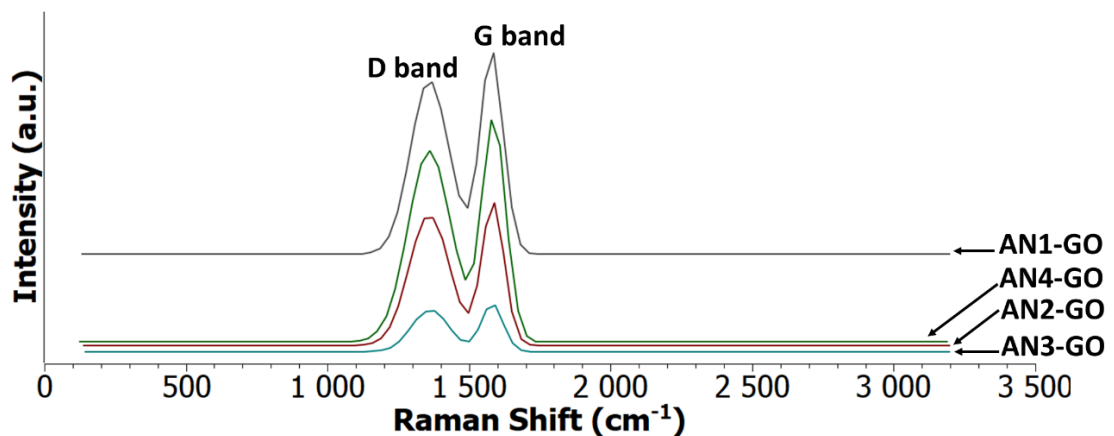


Figure 3.13 : Raman spectra of GO samples

In **Figure 3.13**, the Raman spectra for GO samples showed only D band and G band with no 2D band being observed. GO samples show a high amount of defects, as seen in **Table 3.3** with the average ID/IG ratio of 0.87. The defects are due to sp³ hybridisation caused by oxygen functional groups. The crystallite sizes are relatively small, with an average of 11.11 nm. This result means that GO produced from natural graphite has low crystallinity.

Table 3.2 : Raman Results for Graphite Precursors

Samples		AN1-Graphite	AN2-Graphite	AN3-Graphite	AN4-Graphite
G	Position	1575.17	1579.24	1581.74	1581.74

Band	FWHM	17.52	16.03	14.94	14.71
2D Band	Position	2705.84	2714.68	2707.58	2720.58
	FWHM	130.44	78.08	178.67	58.18

Table 3.3 : Raman Results for GO samples

Samples		AN1-GO	AN2-GO	AN3-GO	AN4-GO
D Band	Position	1361.13	1359.51	1362.82	1360.57
	FWHM	135.64	141.61	130.02	153.16
G Band	Position	1580.64	1585.00	1582.05	1588.14
	FWHM	20.68	24.47	17.38	21.37
I_D/I_G		0.85	0.91	0.87	0.86
L_a (nm)		11.63	10.33	11.63	10.84

The cyclic voltammograms of the GO samples are shown in Figure 3.14, Figure 3.15, and Figure 3.16.

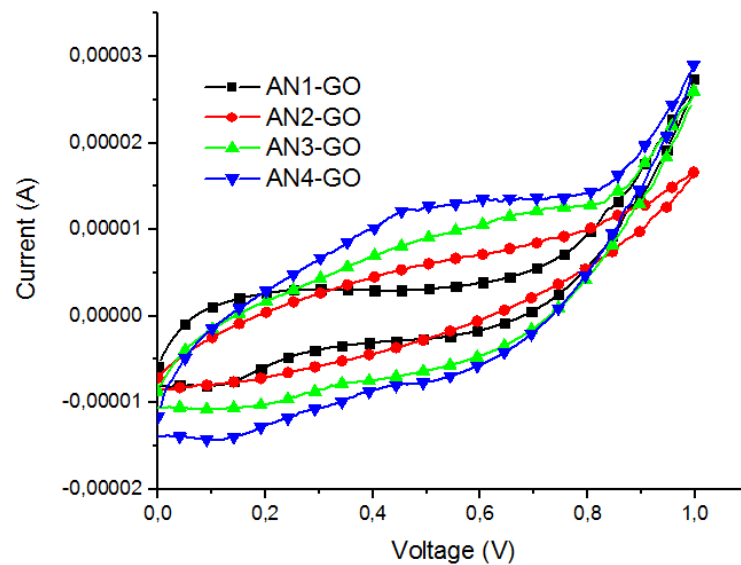


Figure 3.14 : CV curves for GO samples at 10 mV.s⁻¹ scan rate

Figure 3.14 shows a nearly symmetric curve for all samples showing a typical electrical double layer capacitive behaviour. Even at a high scan rate of 100 mV.s⁻¹ a similar shape is seen for the CV curves as seen in Figure 3.16.

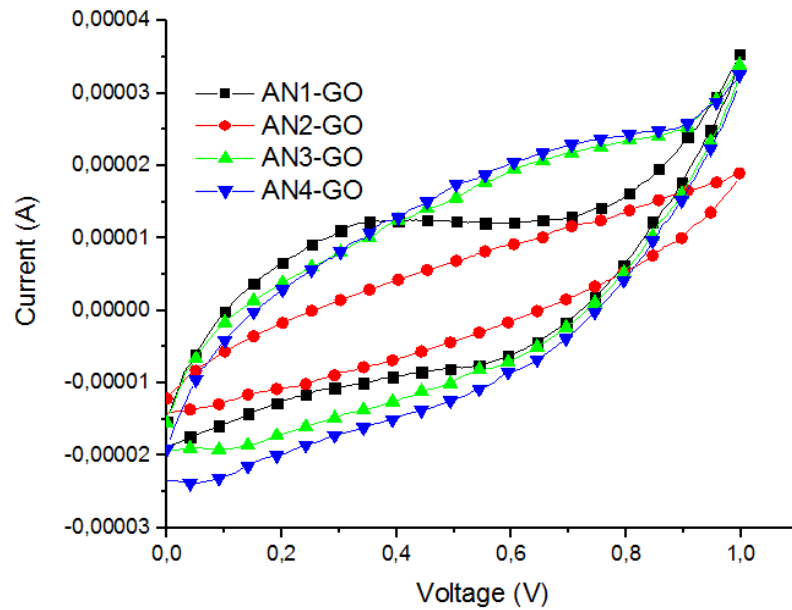


Figure 3.15 : CV curves for GO samples at $20 \text{ mV}\cdot\text{s}^{-1}$

The gravimetric capacitances for each sample were calculated from the CV curves. AN4-GO has the highest specific gravimetric capacitance of $204.22 \text{ F}\cdot\text{g}^{-1}$ at a scan rate of $10 \text{ mV}\cdot\text{s}^{-1}$ almost four times higher than AN1-GO as shown in Figure 3.17.

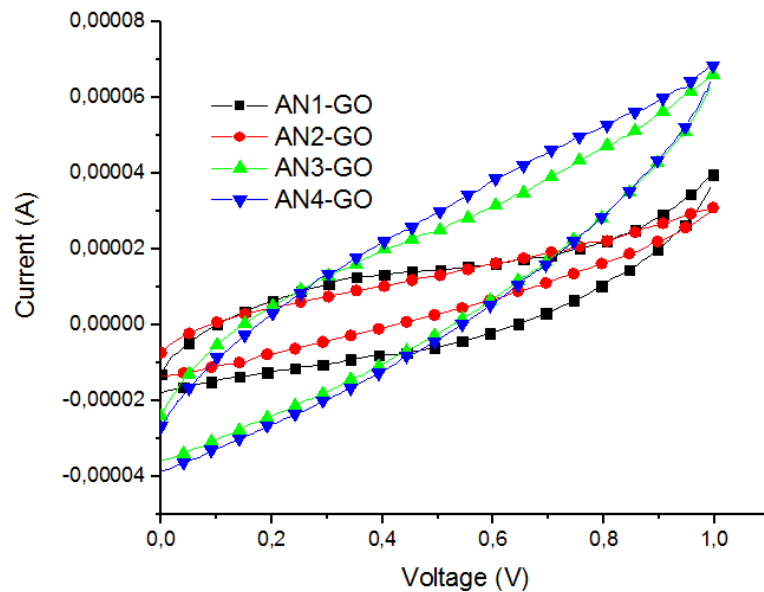


Figure 3.16 : CV curves for GO samples at $100 \text{ mV}\cdot\text{s}^{-1}$

AN4-GO specific gravimetric capacitance is of similar order of magnitude than ultrahigh-level functionalized graphene supercapacitor [43]. AN4-GO had a specific gravimetric capacitance almost double compared to nitrogen doped carbon aerogel supercapacitor's specific gravimetric capacitance of $115 \text{ F}\cdot\text{g}^{-1}$ [44].

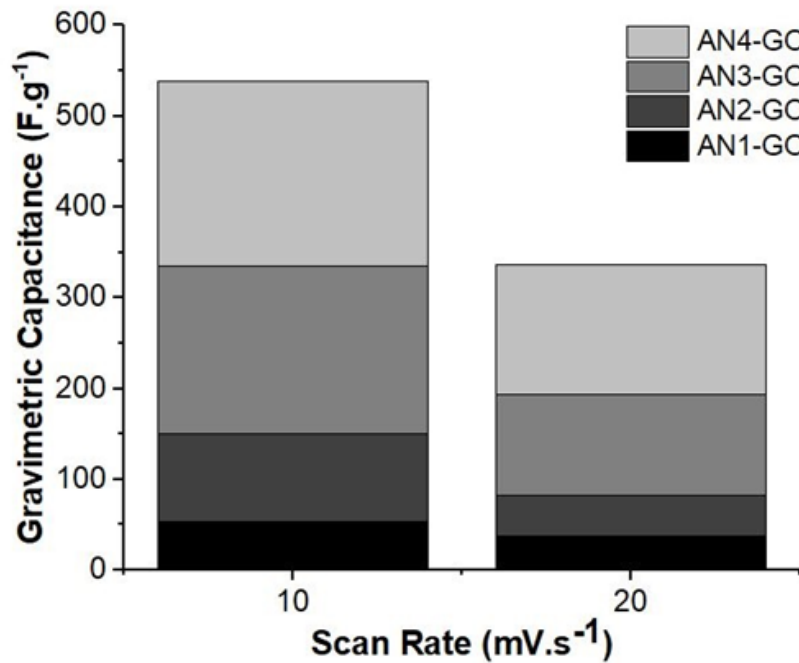


Figure 3.17: Gravimetric Capacitance vs. Scan Rate

AN1-GO having higher oxygen content does not have higher capacitance as expected due to more pseudocapacitance effect. It is the changing of particle size of the precursor graphite that influences the capacitance of the GO produced as seen in **Figure 3.19**.

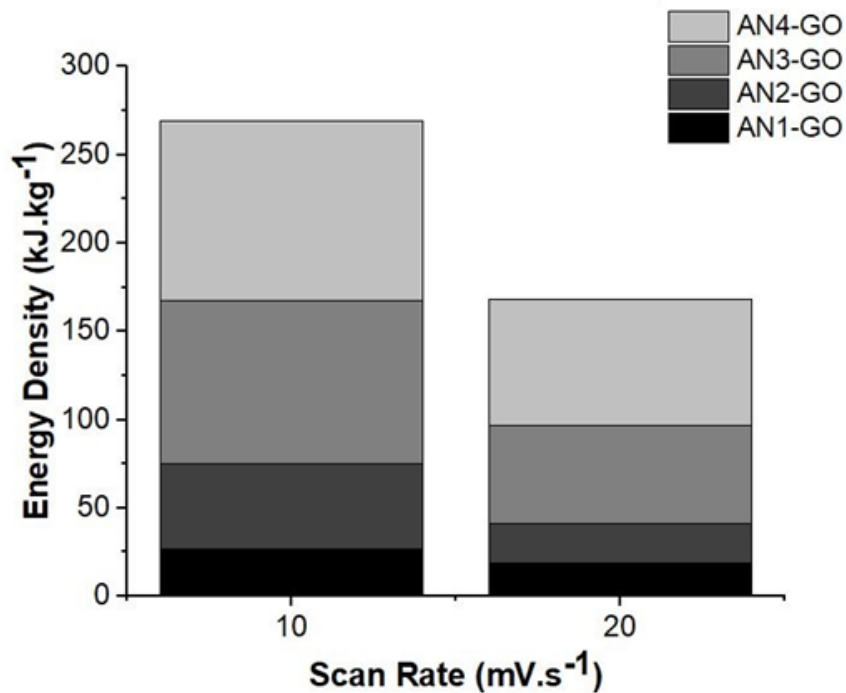


Figure 3.18: Energy Density vs. Scan Rate

The average particle size from 0.0405 mm to 0.1250 mm has a steep almost linear increase in the specific capacitance, but from 0.1250 mm to 0.4500 mm there is a gradual increase in specific capacitance suggesting there is a limiting point for the average particle size.

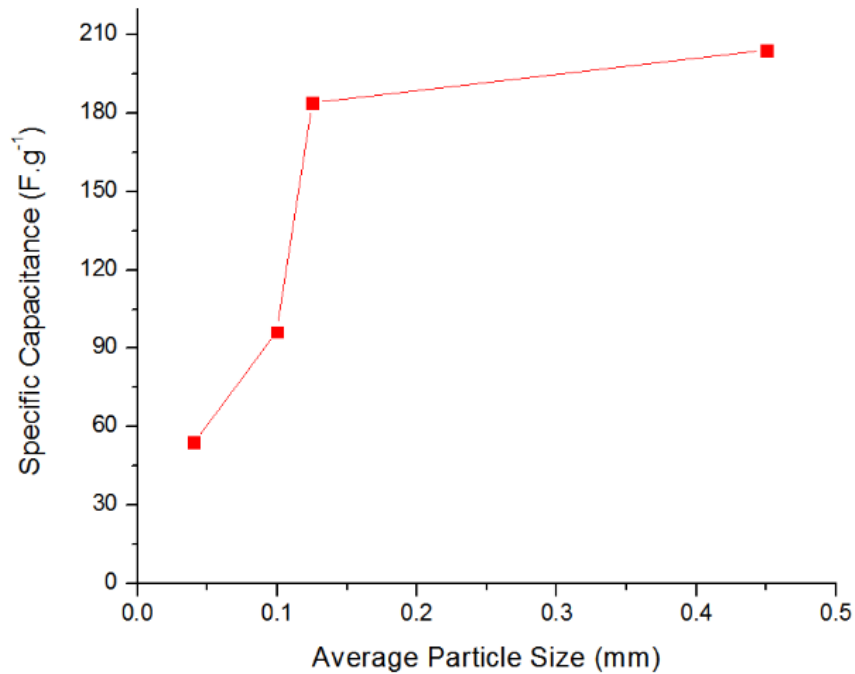


Figure 3.19 : Specific capacitance as a function of average particle size at scan rate 10 mV.s⁻¹

Figure 3.20 shows the specific capacitance as a function of the scan rate. It is clear that the specific capacitance values of AN4-GO are higher than those of all other samples at scan rates 10 mV.s⁻¹ and 20 mV.s⁻¹. AN4-GO produced from graphite precursor with the larger flake has the highest energy density of 102.11 kJ.kg⁻¹ as shown in **Figure 3.18** meaning it is more suitable for energy storage application. This energy density achieved is much higher than energy density of commercially available carbon-based supercapacitors of 18 kJ.kg⁻¹ [45]. The energy density of AN4-GO is almost five times greater than supercapacitors compared to other recent developments in supercapacitor research [43] [46] [47].

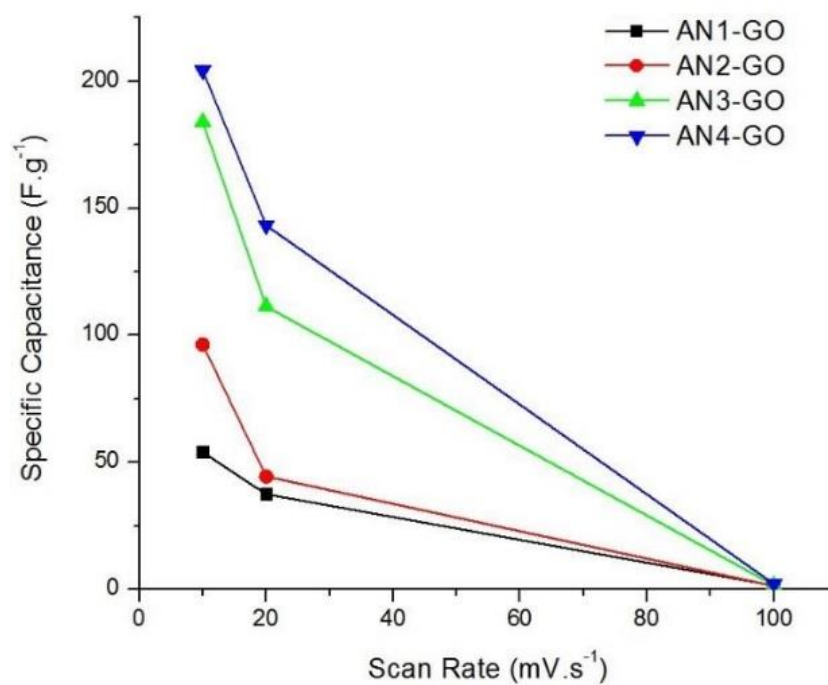


Figure 3.20 : Specific capacitance as a function of the scan rate

3.6 Conclusion

It was found, in the particle size range 0.0405 mm to 0.4500 mm, GO produced from smaller flake size (0.0405 mm) graphite precursor, has a more significant amount of oxygen functional groups, and lower capacitance than larger flaked (0.4500 mm) based GO. This observation implies that the pseudocapacitance effect does not have a significant impact on GO.

The energy density of GO samples synthesised from graphite precursor of a larger flake size is higher than GO synthesised from a smaller flake size graphite precursor, thus making it the preferred flake size when fabricating GO electrodes for supercapacitors for energy storage applications.

3.7 Acknowledgments

The graphite used in this research was kindly donated by Asbury Carbons. I would like to thank them for their generous contribution along with Eskom.

References

- [1] R. Inglesi, "Aggregate electricity demand in South Africa: Conditional forecasts 2030," *Applied Energy*, vol. 87, pp. 197-204, 2010.
- [1] R. Inglesi, "Aggregate electricity demand in South Africa: Conditional forecasts 2030," *Applied Energy*, vol. 87, pp. 197-204, 2010.
- [2] S.SA, "Energy and the poor: a municipal breakdown," 4 June 2018. [Online]. Available: <http://www.statssa.gov.za/p=11181>. [Accessed 24 July 2019].
- [3] H. Yang, "A Review of Supercapacitor-based Energy Storage Systems for Microgrid Applications," in *IEEE Power & Energy Society General Meeting (PESGM)*, Portland, 2018.
- [4] B. Xu, H. Wang, Q. Zhu, N. Sun, B. Anasori, L. Hu, F. Wang, Y. Guan and Y. Gogotsi, "Reduced graphene oxide as a multi-functional conductive binder for supercapacitor electrodes," *Energy Storage Materials*, vol. 12, pp. 128-136, 2018.
- [5] C. V. V. M. Gopi and H.-J. Kim, "Design of Supercapacitor for Electric and Hybrid Vehicles : Supercapacitor," in *International Conference on Information and Communication Technology Robotics (ICT-ROBOT)*, Busan, 2018.
- [6] W. Ma, S. Chen, S. Yang, W. Chen, W. Weng, Y. Cheng and M. Zhu, "Flexible all-solid-state asymmetric supercapacitor based on transition metal oxide nanorods/reduced graphene oxide hybrid fibers with high energy density," *Carbon*, vol. 113, pp. 151-158, 2017.
- [7] M. Ye, J. Gao, Y. Xiao, T. Xu, Y. Zhao and L. Qu, "Metal/graphene oxide batteries," *Carbon*, vol. 125, pp. 299-307, 2017.
- [8] J.-Q. Huang, T.-Z. Zhuang, Q. Zhang, H.-J. Peng, C.-M. Chen and F. Wei, "Permselective Graphene Oxide Membrane for Highly Stable and Anti-Self-Discharge Lithium–Sulfur Batteries," *ACS Nano*, vol. 9, no. 3, pp. 3002-3011, 2015.
- [9] K. Fu, Y. Wang, C. Yan, Y. Yao, Y. Chen, J. Dai, S. Lacey, Y. Wang, J. Wan, T. Li, Z. Wang, Y. Xu and L. Hu, "Graphene Oxide-Based Electrode Inks for 3D-Printed Lithium-Ion Batteries," *Advanced Materials*, vol. 28, p. 2587–2594, 2016.
- [10] C. Kim, J. W. Kim, H. Kim, D. H. Kim, C. Choi, Y. S. Jung and J. Park, "Graphene Oxide Assisted Synthesis of Self-assembled Zinc Oxide for Lithium-Ion Battery Anode," *Chemistry of Materials*, vol. 28, no. 23, p. 8498–8503, 2016.
- [11] Y. Jiang, F. Chen, Y. Gao, Y. Wang, S. Wang, Q. Gao, Z. Jiao, B. Zhao and Z. Chen, "Inhibiting the shuttle effect of Li–S battery with a graphene oxide coating separator: Performance improvement and mechanism study," *Journal of Power Sources*, vol. 342, pp. 929-938, 2017.
- [12] S. Yuan, Z. Guo, L. Wang, S. Hu, Y. Wang and Y. Xia, "Leaf-Like Graphene-Oxide-Wrapped Sulfur for High-Performance Lithium–Sulfur Battery," *Advanced Science*, vol. 2, pp. 1-10, 2015.
- [13] B. Xu, S. Yue, Z. Sui, X. Zhang, S. Hou, G. Cao and Y. Yang, "What is the choice for supercapacitors: graphene and graphene oxide?," *Energy & Environmental Science*, no. 4, pp. 2826-2830, 2011.
- [14] S. Korkmaz and A. Kariper, "Graphene and graphene oxide based aerogels: Synthesis, characteristics and supercapacitor applications," *Journal of Energy Storage*, vol. 27, pp. 1-12, 2020.
- [15] M. Down, S. J. Rowley-Neale, G. Smith and C. E. Banks, "Fabrication of Graphene Oxide Supercapacitor Devices," *ACS Applied Energy Materials*, vol. 1, no. 2, pp. 707-714, 2018.
- [16] H. Xian, T. Peng and H. Sun, "Effect of Particle Size of Natural Graphite on the Size and Structure of Graphene Oxide Prepared by the Modified Hummers Method," *Materials Science Forum*, vol. 814, pp. 185-190, 2015.
- [17] D. R. Chowdhury, C. Singh and A. Paul, "Role of graphite precursor and sodium nitrate in graphite oxide synthesis," *RSC Advances*, no. 29, pp. 15138-15145, 2014.
- [18] A. S. Aricò, P. Bruce, B. Scrosati, J.-M. Tarascon and W. V. Schalkwijk, "Nanostructured

- materials for advanced energy conversion and storage devices," *Nature Materials*, vol. 4, pp. 366-377, 2005.
- [19] R.Kötz and M.Carlen, "Principles and applications of electrochemical capacitors," *Electrochimica Acta*, vol. 45, no. 15-16, pp. 2483-2498, 2000.
- [20] B. E. Conway, *Electrochemical Supercapacitors, Scientific Fundamentals and Technological Applications*, New York: Kulwer Academic/Plenum Publishers, 1999.
- [21] Y. Li, M. V. Zijil, S. Chiang and N. Pan, "KOH modified graphene nanosheets for supercapacitor electrodes," *Journal of Power Sources*, vol. 196, no. 14, pp. 6003-6006, 2011.
- [22] W. K. Chee, H. N. Lim, Z. Zainal, N. M. Huang, I. Harrison and Y. Andou, "Flexible Graphene-Based Supercapacitors: A Review," *The Journal of Physical Chemistry C*, vol. 120, no. 8, pp. 4153-4172, 2016.
- [23] L. Gouy, "Constitution of the electric charge at the surface of an electrolyte," *Journal of Physical Theory and Applications*, vol. 9, pp. 457-468, 1910.
- [24] D. Chapman, "A contribution to the theory of electrocapillarity," *Philosophical Magazine Series 6*, vol. 25, pp. 475-481, 1913.
- [25] J. O. Bockris, M. Devanathan and K. Muller, "On the Structure of Charged Interfaces," in *Royal Society of London. Series A. Mathematical and Physical Sciences*, London, 1963.
- [26] W. Pell and B. Conway, "Voltammetry at a de Levie brush electrode as a model for electrochemical supercapacitor behaviour," *Journal of Electroanalytical Chemistry*, vol. 500, no. 1-2, pp. 121-133, 2001.
- [27] F. Beguin and E. Frackowiak, *Supercapacitors: Materials, Systems and Applications*, Germany: Wiley-VCH Verlag GmbH & Co. KGaA, 2013.
- [28] J. G. S. Moo, B. Khezri, R. D. Webster and M. Pumera, "Graphene Oxides Prepared by Hummers', Hofmann's, and Staudenmaier's Methods: Dramatic Influences on Heavy-Metal-Ion Adsorption," *ChemPhysChem*, vol. 15, no. 14, pp. 2922-2929, 2014.
- [29] D. A. Dikin, S. Stankovich, E. J. Zimney, R. D. Piner, G. H. B. Dommett, G. Evmenenko, S. T. Nguyen and R. S. Ruoff, "Preparation and characterization of graphene oxide paper," *Nature*, vol. 448, p. 457-460, 2007.
- [30] J. Tian, S. Wu, X. Yin and W. Wu, "Novel preparation of hydrophilic graphene/graphene oxide nanosheets for," *Applied Surface Science*, vol. 496, no. 143696, pp. 1-11, 2019.
- [31] C. Botas, P. Álvarez, C. Blanco, R. Santamaría, M. Granda, P. Ares, F. Rodríguez-Reinoso and R. Menéndez, "The effect of the parent graphite on the structure of graphene oxide," *Carbon*, vol. 50, no. 1, pp. 275-282, 2012.
- [32] D. C. Marcano, D. V. Kosynkin, J. M. Berlin, A. Sinitskii, Z. Sun, A. Slesarev, L. B. Alemany, W. Lu and J. M. Tour, "Improved Synthesis of Graphene Oxide," *ACS Nano*, vol. 4, no. 8, pp. 4806-4814, 2010.
- [33] I.-L. Tsai, J. Cao, L. L. Fevre, B. Wang, R. Todd, R. A. Dryfe and A. J.Forsyth, "Graphene-enhanced electrodes for scalable supercapacitors," *Electrochimica Acta*, vol. 257, pp. 372-379, 2017.
- [34] A. Y. S. Eng, C. Kiang and C. M. Pumera, "Intrinsic electrochemical performance and precise control of surface porosity of graphene-modified electrodes using the drop-casting technique," *Electrochemistry Communications*, vol. 59, pp. 86-90, 2015.
- [35] M. Kaempgen, C. K. Chan, J. Ma, Y. Cui and G. Gruner, "Printable Thin Film Supercapacitors Using Single-Walled Carbon Nanotubes," *Nano Letters*, vol. 9, no. 5, pp. 1872-1876, 2009.
- [36] Q. Chen, X. Li, X. Zang, Y. Cao, Y. He, P. Li, K. Wang, J. Wei, D. Wu and H. Zhu, "Effect of different gel electrolytes on graphene-based solid-state supercapacitors," *RSC Advances*, vol. 4, no. 68, pp. 36253-36256, 2014.
- [37] L. G. Caçadoa, K. Takai, T. Enoki, M. Endo, Y. A. Kim, H. Mizusaki, A. Jorio, L. N. Coelho, R. Magalhães-Paniago and M. A. Pimenta, "General equation for the determination of the crystallite size L_a of nanographite by Raman spectroscopy," *Applied Physics Letters*, vol. 88, no. 16, pp. 1-3,

2006.

- [38] Q. Li, X. Guo, Y. Zhang, W. Zhang, C. Ge, L. Zhao, X. Wang, H. Zhang, J. Chen, Z. Wang and L. Sun, "Porous graphene paper for supercapacitor applications," *Journal of Materials Science & Technology*, vol. 33, no. 8, pp. 793-799, 2017.
- [39] J. Yu, M. Wang, P. Xu, S.-H. Cho, J. Suhr, K. Gong, L. Meng, Y. Huang, J.-H. Byun, Y. Oh, Y. Yan and T.-W. Chou, "Ultrahigh-rate wire-shaped supercapacitor based on graphene fiber," *Carbon*, vol. 119, pp. 332-338, 2017.
- [40] Y. Zhou, S. L. Candelaria, Q. Liu, Y. Huang, E. Uchaker and G. Cao, "Sulfur-rich carbon cryogels for supercapacitors with improved conductivity and wettability," *Journal of Materials Chemistry A*, vol. 2, no. 22, pp. 8472-8482, 2014.
- [41] Y. Zhou, R. Ma, S. L. Candelaria, J. Wang, Q. Liu, E. Uchaker, P. Li, Y. Chen and G. Cao, "Phosphorus/sulfur Co-doped porous carbon with enhanced specific capacitance for supercapacitor and improved catalytic activity for oxygen reduction reaction," *Journal of Power Sources*, vol. 314, pp. 39-48, 2016.
- [42] X. Yu, Y. Kang and H. S. Park, "Sulfur and phosphorus co-doping of hierarchically porous graphene aerogels for enhancing supercapacitor performance," *Carbon*, vol. 101, pp. 49-56, 2016.
- [43] Z. Li, S. Gadipelli, Y. Yang, G. He, J. Guo, J. Li, Y. Lu, C. A. Howard, D. J. Brett, I. P. Parkin, F. Li and Z. Guo, "Exceptional supercapacitor performance from optimized oxidation of graphene-oxide," *Energy Storage Materials*, vol. 17, pp. 12-21, 2019.
- [44] F.-Y. Zeng, Z.-Y. Su, S. Liu, H.-P. Liang, H.-H. Zha and B.-H. Han, "Nitrogen-doped carbon aerogels with high surface area for supercapacitors and gas adsorption," *Materials Today Communications*, vol. 16, pp. 1-7, 2018.
- [45] J. Xu, Z. Tan, W. Zeng, G. Chen, S. Wu, Y. Zhao, K. Ni, Z. Tao, M. Ikram, H. Ji and Y. Zhu, "A Hierarchical Carbon Derived from Sponge-Templated Activation of Graphene Oxide for High-Performance Supercapacitor Electrodes," *Advanced Materials*, vol. 28, no. 26, pp. 5222-5228, 2016.
- [46] Z. Lei, J. Zhang, L. L. Zhang, N. A. Kumar and X. S. Zhao, "Functionalization of chemically derived graphene for improving its electrocapacitive energy storage properties," *Energy & Environmental Science*, vol. 9, no. 6, pp. 1891-1930, 2016.
- [47] R. Raccichini, A. Varzi, S. Passerini and B. Scrosati, "The role of graphene for electrochemical energy storage," *Nature Materials*, vol. 14, p. 271-279, 2015.

Chapter 4

Journal Article 2

Influence of Type of Graphite Precursor on Energy Storage Characteristics of Graphene Oxide Supercapacitor

Solan Perumal, Alan Leigh Lawrence Jarvis, and
Ajay Bissessur

In Manuscript Form: *To be submitted*

In this chapter, the research objective of investigating different type of graphite precursor and evaluating the electrochemical properties of graphene oxide synthesised from these graphite precursors as an electrode material for supercapacitors was achieved. In the previous chapter, for natural graphite precursor, the graphite precursor size of 0.450 mm gave the GO with highest energy density of 102 kJ.kg⁻¹ and low oxygen content of 32.699 %wt in comparison to natural graphite precursors with smaller flake sizes showing that the pseudocapacitance effect does not have a significant impact on the electrochemical properties of natural GO. In the present chapter, it was determined that for the synthetic graphite precursors, the flake size needed to be ten times smaller than that which gave the highest energy density for natural graphite precursors and in this case the resultant energy density was 521.49 kJ.kg⁻¹ which was about 500 % that of GO from natural graphite precursors.

4.1 Abstract

Graphene oxide (GO) as an electrode material for supercapacitors were investigated using graphite precursors with varying type and analogous flake sizes. GO was synthesised using the Hummers method with additional potassium permanganate and yield recorded for each sample. GO was characterised by elemental analysis, Fourier Transform Infrared (FTIR) spectroscopy and Raman spectroscopy. Electrochemical measurements were conducted using cyclic voltammetry to obtain the specific capacitance and energy density of the samples. GO produced from synthetic graphite precursor had the smallest flake size, higher oxygen content, higher crystallinity and a lower amount of defects in its structure compared to GO produced from natural graphite precursor; and yield the highest yield, specific gravimetric capacitance and energy density of 107.67 %, 1042.99 F.g⁻¹ and 521.49 kJ.kg⁻¹ respectively. This synthetic graphite precursor with small flake size 0.045 mm is the most suitable to use to fabricate GO electrode material with remarkable energy storage characteristics.

4.2 Introduction

Supercapacitors have caught the attention of many researchers in the field of energy storage applications due to their higher power density compared to lithium-ion batteries [1]. The disadvantage of supercapacitors is their lower energy density as compared to batteries [2]. Improvement in the electrode material of the supercapacitor has been flagged as a means to improve the low energy density problem. Graphene oxide (GO) has proven to be an excellent candidate as an electrode material compared to graphene (G) [3]. In the chemical route to synthesise G, GO is cheaper to manufacture since it is a precursor to graphene. Deionised water is used as a solvent for GO which is inexpensive compared to expensive organic solvents for G which include 1-methyl-2-pyrrolidinone (NMP), dimethyl sulfoxide (DMSO), sodium dodecylbenzene sulfonate (SDBS) and sodium dodecyl sulfate (SDS). GO can be used binder-free [4] as an electrode material in supercapacitors. GO does not tend to agglomerate and has a higher capacitance compared to G.

Graphite is the main precursor materials for the synthesis of GO. The variation in characteristics of this precursor material has been carried out by researchers to optimise the GO and G obtained after synthesis. Zhong-Shuai Wu *et al.* studied different graphite precursors, i.e. highly-oriented pyrolytic graphite, natural flake graphite, Kish graphite, flake graphite powder and synthetic graphite to determine if the number of layers of the resulting graphene can be controlled [5]. They found that synthetic graphite, flake graphite powder and Kish graphite with the smaller lateral size; and lower crystallinity gives G having few (1-3) layers.

In 2012, Cristina Botas *et al.* investigated the precursor synthetic graphite with the same average particle size and varying crystallinity on the GO structure. It was shown that synthetic graphite with higher crystallinity outputs GO with oxygen functional groups mainly epoxy groups at the basal plane while graphite with lower crystallinity outputs GO with oxygen functional groups predominantly hydroxyl and carboxyl groups located at the edges of the sheets [6]. In 2013, Cristina Botas *et al.* showed natural graphite with higher crystallinity (larger crystal size) outputs GO with higher yield percentage during sonication and larger lateral size sheets as compared to GO synthesised from synthetic graphite with lower crystallinity (smaller crystal size) independent of the carbon/ oxygen (C/O) ratio [7].

The role of the graphite precursor in GO synthesis was also investigated by Debarati Roy Chowdhury *et al.* in 2014. Debarati and her two co-authors studied synthetic graphite with varying particle size (between 20 and 150 μm) and found that there is a direct correlation with the crystallite sizes of the graphite precursor and GO [8]. Also, a crystallite size of graphite with 45 μm shows most oxidation on the basal plane of graphitic sheets in GO. In 2017, Seyyedeh Saadat Shojaeenezhad *et al.* determined the effect of the shape and size of the graphite precursor on the oxidation time for GO. Clod powder graphite precursor (6 μm and 18 μm) results in oxidation time of several days as compared to flake powder precursor

graphite (25 μm) with 2 hours oxidation time to yield GO [9]. The possible reasons are higher thickness and lower active surface area of clod powder graphite precursor which takes a longer time for the acid and existing agents to diffuse and therefore takes a long time to oxidise to obtain GO.

The above shows how characteristics of graphite precursors affect GO as a material and not for a specific application. Not much research has been directed toward finding the effect of the graphite precursor on GO used in energy storage application. This paper aims to determine the relationship between the type of precursor graphite used for GO synthesis and GO supercapacitor energy storage characteristics.

4.3 Background

Graphite is one of the four allotropic forms of carbon found in nature. The structure of graphite is shown in **Figure 4.1**. The bonding of the carbon atoms occurs hexagonally and comprises of sp² hybridisation, meaning that the s and 2p atomic orbitals form a trigonal structure [10]. In the basal plane, the bonding of carbon atoms is a strong metallic bonding. These carbon bonded atoms are in layers with each layer being held together by weak van der Waals forces. Each layer of graphite is known as graphene. The lateral size of the graphite is the particle size along the plane direction perpendicular to the c-axis.

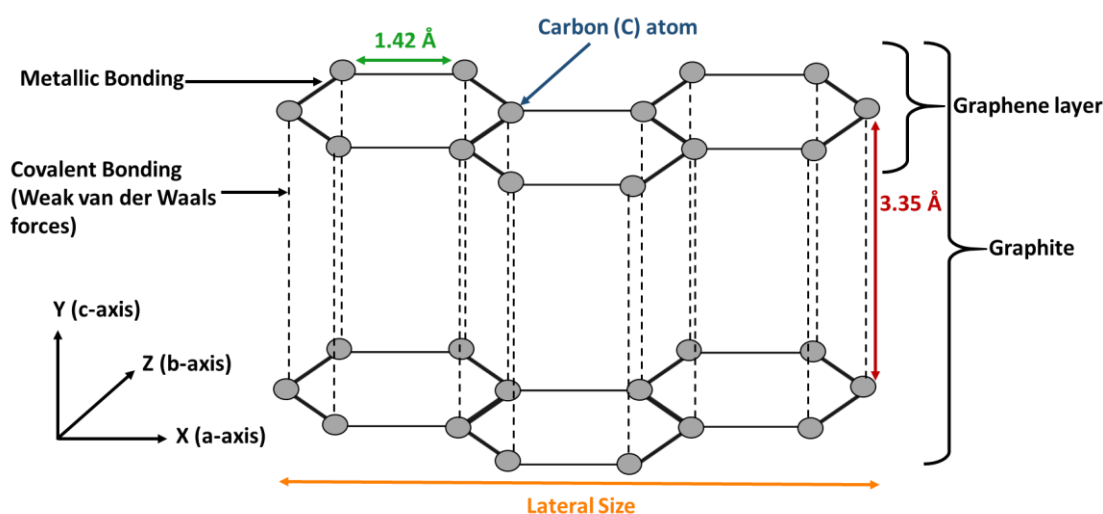


Figure 4.1 : Structure of graphite

Graphite is anisotropic, which gives it the ability to be intercalated between the graphite layers by acids, e.g. sulphuric acid (H₂SO₄) [11]. This intercalation is required to break up the graphite layers to oxygenate the graphite to produce GO. There are different types of graphite which are shown in **Figure 4.2**. The focus of this paper is natural flake graphite and primary synthetic graphite since they are the most common used for GO synthesis [12].

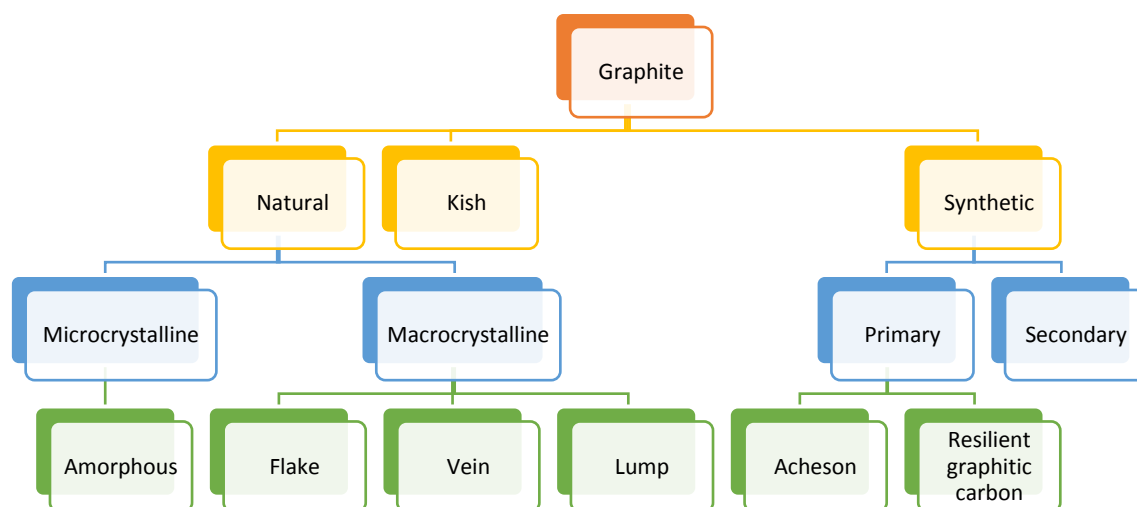


Figure 4.2 : Categorisation of graphite

Natural flake graphite is mined from geological environments that have been subjected to extremely high temperatures and pressures most commonly metamorphic rock [13]. From the processing of natural flake graphite, impurities become inherent. This type of graphite has a flaky and platy morphology [14]. The crystallinity of the natural flake graphite is high, which implies a large average crystal size and has a low production cost.

Primary synthetic graphite is made from two constituents, the main being calcined petroleum coke (unstructured carbon) and the other coal tar pitch as a binder [15]. These two constituents are graphitised by being subjected to temperatures around 2800 °C. This process, therefore, makes primary synthetic graphite costly to manufacture. However, synthetic graphite still forms the most substantial portion of the graphite market. Since primary synthetic graphite is human-made, there are almost no impurities in this graphite.

4.4 Experimental

4.4.1 Synthesis of GO

Eight graphite precursors were obtained from Asbury Carbons and were used as received. The eight graphite precursors were named the following for simple identification: AN1-GO, AN2-GO, AN3-GO, AN4-GO, AS1-GO, AS2-GO, AS3-GO and AS4-GO. The A stands for Asbury, N for natural graphite precursor, S for synthetic graphite precursor and the numbers 1, 2, 3, 4 indicate the flake sizes 0.045 mm, 0.105 mm, 0.125mm and 0.450 mm respectively. The flakes sizes for the natural and synthetic are analogous. GO was synthesised using the Hummers method with additional potassium permanganate [16] and some of as-prepared GO samples are shown in **Figure 4.3**. The variation of colour in the GO powders can be used as an indicator for degree of oxidation. For example, AN4-GO has a greenish-grey colour compared to AS2-GO, which is a yellowish-brown colour. GO that is a yellowish-brown colour is said to be well-oxidised compared to GO that is greenish-grey. Observing colour variation alone cannot be used to determine degree of oxidation; hence, elemental analysis was used to verify degree of oxidation.

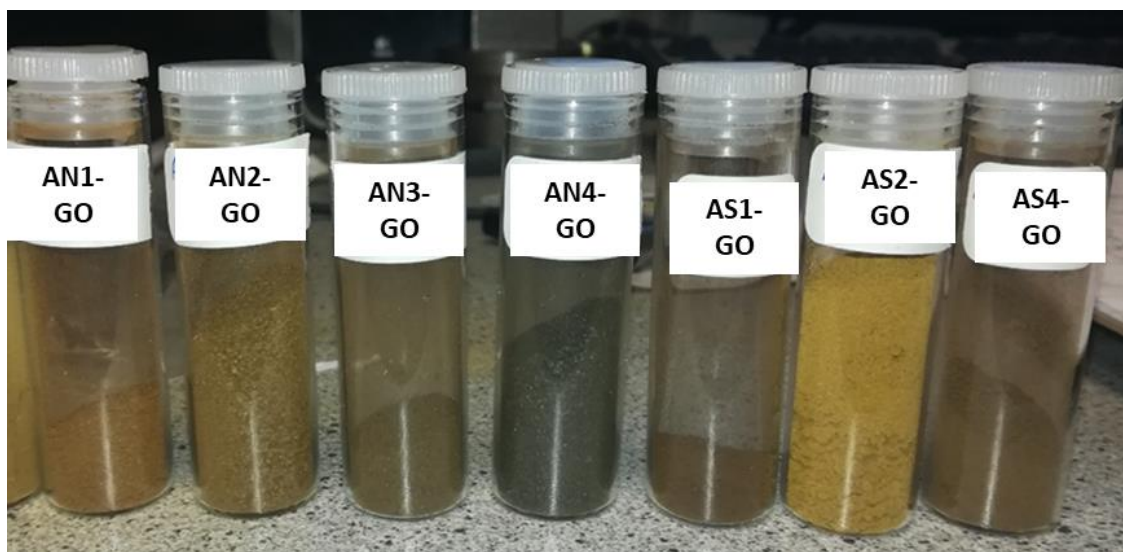


Figure 4.3 : GO as-prepared powder samples

4.4.2 Elemental Analysis

The elemental composition of the graphite and GO samples were determined using elemental analysis. The elements analysed were carbon (C), oxygen (O), hydrogen (H), sulphur (S) and nitrogen (N).

4.4.3 Fourier Transform Infrared (FTIR) Spectroscopy

The chemical bonds in the graphite precursors and GO samples are determined by FTIR. The graphite and GO samples were tested as received and as prepared respectively.

4.4.4 Raman Spectroscopy

Graphite precursors' and GO samples' structures are characterised by Raman spectroscopy at laser line wavelength of 514 nm. The intensities, full width at half maximum (FWHM), positions and integrated areas of the D band (I_D), G band (I_G), and 2D band (I_{2D}) were measured on the Raman spectrum for each sample. The ratio of I_D and I_G (I_D/I_G) gives the degree of disorder or amount of defects in the graphite and GO structure. The estimated crystallite size is determined from the Raman spectrum using (4.1) [17]:

$$L_a = (2.4 \times 10^{-10}) \lambda_l^4 \left(\frac{A_D}{A_G} \right)^{-1} \quad (4.1)$$

where,

L_a = Estimated Crystallite size (nm)

λ_l = laser line wavelength (nm)

A_D = Integrated intensity (area) of D band

A_G = Integrated intensity (area) of G band

4.4.5 Cyclic Voltammetry

CV was performed on the GO samples using a three-electrode system at scan rates of 10 mV.s⁻¹ and 20 mV.s⁻¹. Samples were immersed in phosphoric acid (H₃PO₄) electrolyte and sonicated for an hour. An operating potential window between 0 V and 1 V was used to ensure no decomposition of electrolyte occurs.

The energy storage characteristics of the GO samples were determined using (4.2), (4.3), (4.4), and (4.5):

$$C = \frac{\int_{E_1}^{E_2} i(E) dE}{2\nu(E_2 - E_1)} \quad (4.2)$$

where,

integral term = total voltammetric charge (area under the curve as shown in **Figure 4.4**),

E_2 = High potential limit (V)

E_1 = Low potential limit (V)

ν = scan rate (V.s⁻¹).

$$C_{SG} = \frac{C}{m} \quad (3.3)$$

where C_{SG} is the specific gravimetric capacitance; m is the mass of the active material GO.

$$C_{SA} = \frac{C}{A} \quad (4.4)$$

where C_{SA} is the specific areal capacitance; A is the area of the electrode, which is 5.76 cm^2 .

$$E = \frac{1}{2} C_{SG} V^2 \quad (4.5)$$

where E is the energy density (kJ.kg^{-1}); V is the operating voltage which is set to 1 V.

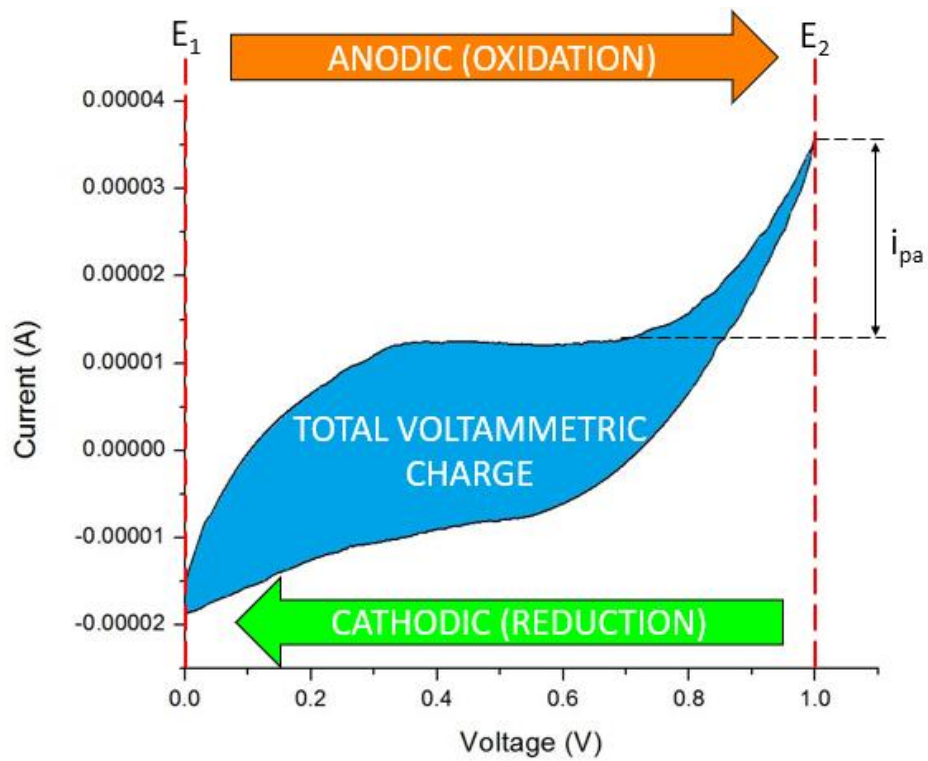


Figure 4.4 : Typical CV curve showing critical values

4.5 Results and Discussion

The yield of GO samples was recorded by measuring the quantities of graphite precursor and GO as the input and output, respectively of the GO synthesis process, as shown in **Table 4.1**. The average yield for synthetic GO samples of 87 % was higher than natural GO samples of 70.25 %. This evaluation alludes two points. One, lesser unoxidised graphite is washed away and discarded when using synthetic graphite precursor during the GO synthesis process compared to using natural graphite precursor. Two, a higher quantity of synthetic graphite oxidises compared to natural graphite precursor during the GO synthesis process. From a manufacturing point of view, with using synthetic graphite precursor, there will be lesser losses and higher profitability than using natural graphite precursor. The low yields for AN1-GO, AN3-GO and AS3-GO were due to oxidised GO being discarded with supernatant into waste containers during washing process. AS1-GO had the highest yield of 107.67 %.

Table 4.1 : Yield results of GO samples from GO synthesis process

Sample	Input Graphite (g)	Output GO (g)	Yield (%)
AN1-GO	3.00	1.42	47.33
AN2-GO	3.00	3.03	101.00
AN3-GO	3.00	1.17	39.00
AN4-GO	3.00	2.81	93.67
AS1-GO	3.00	3.23	107.67
AS2-GO	3.00	2.80	93.33
AS3-GO	3.00	1.54	51.33
AS4-GO	3.00	2.87	95.67

From **Table 4.2**, it can be deduced that all graphite precursor samples were effectively oxidised. This deduction is made from observing the average C/O ratio of all graphite precursor samples being 1:0.012 and their respective GO samples increasing to an average C/O ratio of 1:1.253. Synthetic GO samples showed a higher average C/O ratio of 1:1.320 than natural GO samples with average C/O ratio of 1:1.187. AS4-GO had the highest oxidation from all samples with a C/O ratio of 1:1.505. This result is contrary to a previous report [8] which have shown smaller flake size (0.045 mm) synthetic graphite precursor yield GO with higher oxidation using UV-Vis, the colour of samples and not elemental analysis.

A correlation can be seen with the increase of sulphur content of the natural GO samples and the increase in flake size. This outcome means that GO synthesised from a larger flake size (0.450 mm) natural graphite precursor has higher impurities remaining after synthesis. This trend is not seen in the synthetic GO samples.

Table 4.2 : Elemental analysis results of graphite precursors and GO samples

Sample	C (%)	O (%)	H (%)	S (%)	N (%)
AN1-Graphite	97.180	1.139	1.268	0.413	0.000
AN2-Graphite	93.815	1.182	1.127	3.876	0.000
AN3-Graphite	94.297	1.112	0.994	3.597	0.000
AN4-Graphite	95.342	0.925	0.145	3.588	0.000
AS1-Graphite	95.728	1.246	0.862	2.164	0.000
AS2-Graphite	92.618	1.138	1.362	4.882	0.000
AS3-Graphite	93.550	1.228	2.011	3.211	0.000
AS4-Graphite	93.997	1.157	0.903	3.943	0.000
AN1-GO	43.053	51.842	3.174	1.881	0.050
AN2-GO	44.791	48.852	3.033	3.314	0.010
AN3-GO	40.568	51.635	3.211	4.576	0.010
AN4-GO	42.077	49.602	3.108	5.213	0.000
AS1-GO	40.042	53.587	3.163	3.198	0.010
AS2-GO	41.693	51.974	3.148	3.176	0.010
AS3-GO	43.189	51.457	3.115	2.149	0.090
AS4-GO	37.357	56.227	3.192	3.214	0.010

In **Figure 4.5** (left), the FTIR spectra of AN1-Graphite and AS1-Graphite are almost undistinguishable. This observation shows that graphite precursors with a small flake size (0.045 mm) of different type have similar chemical bonding. The large flake sized (0.450 mm) natural and synthetic graphite precursors FTIR spectra have distinct variations, as shown in **Figure 4.5** (right). The significant distinction is that the O–H bond of AN4-Graphite sample is broader than AS4-Graphite. This bond is attributed to the water that naturally occurs in graphite. Therefore, it can be deduced that the natural graphite precursor sample (AN4-Graphite) has more water content than the synthetic graphite precursor sample (AS4-Graphite) for a large flake size (0.450 mm). The vibration mode of C–H bonds are seen in AS4-Graphite sample but not in AN4-Graphite sample are attributed by the aldehyde functional group.

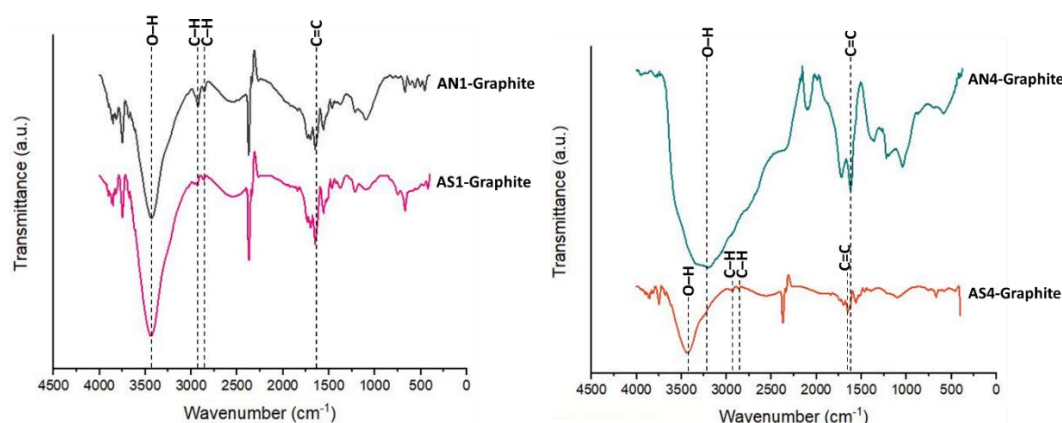


Figure 4.5 : FTIR spectra of: AN1-Graphite and AS1-Graphite (left); and AN4-Graphite and AS4-Graphite (right)

In **Figure 4.6** (left), a broader O–H is seen for AN1-GO compared to AS1-GO. This result could suggest that after synthesis, GO synthesised from natural graphite holds more water content than GO synthesised from synthetic graphite for a small flake size (0.045 mm). AN4-GO and AS4-GO have similar FTIR spectra with AN4-GO having a slightly broader peak for the O–H bond, as seen in **Figure 4.6** (right). The bonds C=O, C=C and C–O are attributed to the vibration modes of ketonic, sp²-hybridised aromatic and ether more specific epoxide species respectively.

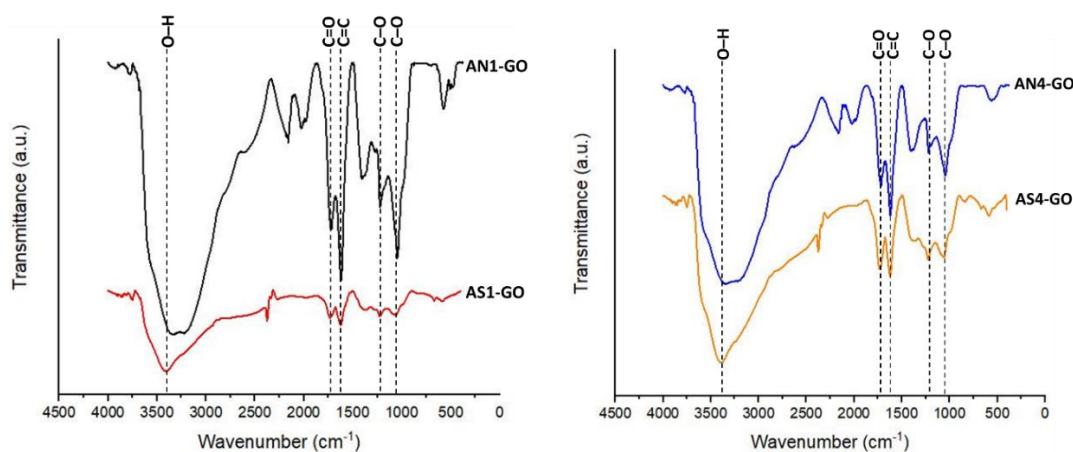


Figure 4.6 : FTIR spectra of: AN1-GO and AS1-GO (left); and AN4-GO and AS4-GO (right)

The results obtained from the Raman spectra for all samples are shown in **Table 4.3**. Raman spectra for natural graphite precursor samples shows two prominent bands G band 2D band, as seen in **Figure 4.7**. D band was not observed for these samples, and therefore their crystallite sizes were not estimated. The G band is attributed to vibration of the sp² hybridisation in the graphitic structure. For the synthetic graphite samples, all three bands, i.e. D band, G band, and 2D band, were observed as shown in **Figure 4.8**. The D band is due out of plane vibration caused by defects in the graphitic structure. The disorder in the graphitic structure for these samples is low, with an average I_D/I_G ratio of 0.17.

Table 4.3 : Results obtained from Raman spectra for all samples

Samples	D Band		G Band		2D band		I_D/I_G	L_a (nm)
	Position	FWHM	Position	FWHM	Position	FWHM		
AN1-Graphite	N/A	N/A	1575.17	17.52	2705.84	130.44	N/A	N/A
AN2-Graphite	N/A	N/A	1579.24	16.03	2714.68	78.08	N/A	N/A
AN3-Graphite	N/A	N/A	1581.74	14.94	2707.58	178.67	N/A	N/A
AN4-Graphite	N/A	N/A	1581.74	14.71	2720.58	58.18	N/A	N/A
AS1-Graphite	1351.38	28.53	1575.12	20.68	2702.62	73.45	0.17	69.44
AS2-Graphite	1355.53	55.36	1573.79	24.47	2697.17	83.40	0.18	41.02

AS3-Graphite	1351.38	25.86	1579.81	17.38	2711.22	65.32	0.09	131.06
AS4-Graphite	1354.00	33.61	1581.28	21.37	2711.31	66.22	0.24	44.63
AN1-GO	1361.13	135.64	1580.64	80.49	N/A	N/A	0.85	11.63
AN2-GO	1359.51	141.61	1585.00	79.49	N/A	N/A	0.91	10.33
AN3-GO	1362.82	130.02	1582.05	78.13	N/A	N/A	0.87	11.63
AN4-GO	1360.57	153.16	1588.14	84.76	N/A	N/A	0.86	10.84
AS1-GO	1355.29	53.68	1602.64	48.38	N/A	N/A	0.49	30.95
AS2-GO	1355.57	46.92	1594.19	47.63	N/A	N/A	0.21	79.67
AS3-GO	1358.46	156.45	1578.47	79.64	N/A	N/A	0.94	9.09
AS4-GO	1348.31	61.86	1593.63	51.26	N/A	N/A	0.52	26.89

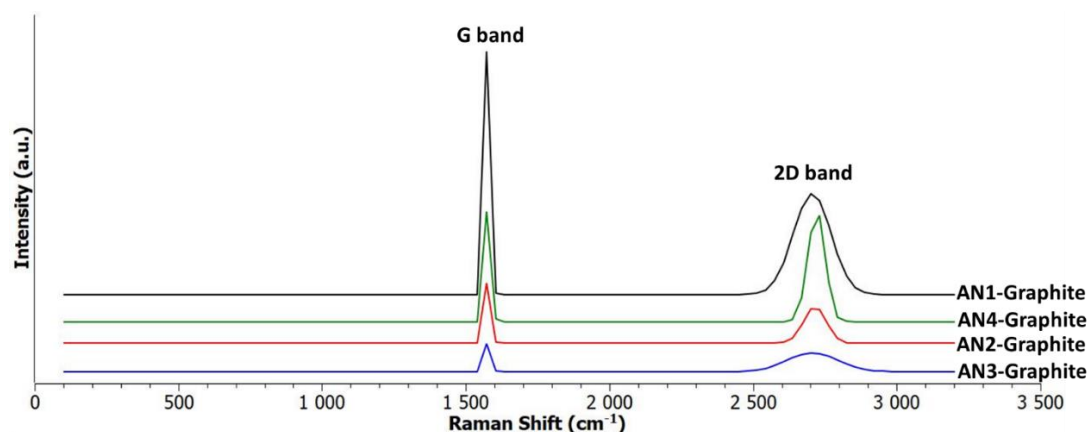


Figure 4.7 : Raman spectra of natural graphite precursor samples

The Raman spectra of the synthetic graphite precursors show a D band and 2D band which means the hexagonal crystal structure is highly ordered. The estimated crystallite sizes of the synthetic graphite precursor samples varied considerably with a standard deviation of 36.06. This result may be due to the artificial manufacturing processes rather than natural forming graphite. Synthetic graphite precursor samples have an average estimated crystallite size of 71.54 nm. This result cannot be referred to as high or low crystallinity compared to natural graphite precursors since the average estimated crystallite size of natural graphite precursors could not be calculated due to no D band observed. The FWHM of G band for all graphite samples were low with an average of 18.39 cm showing the graphite layers' mutual orientation has high reproducibility.

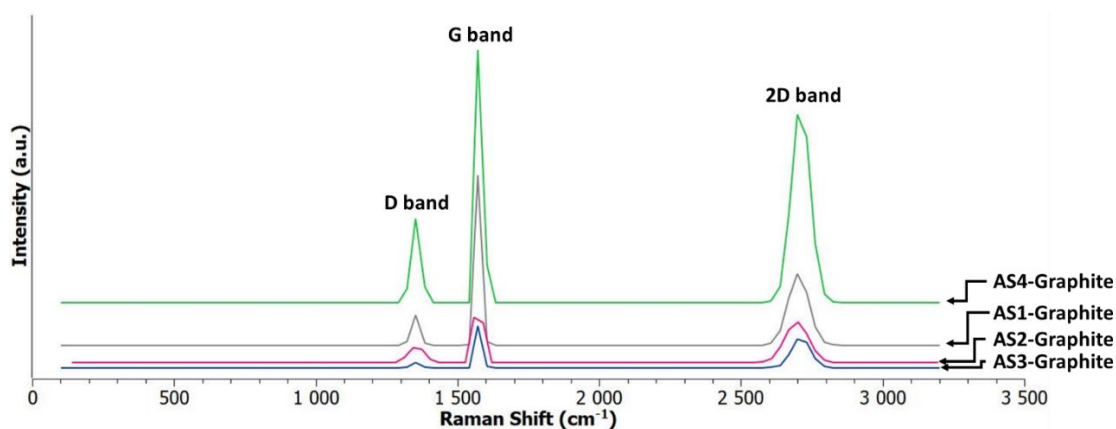


Figure 4.8 : Raman spectra of synthetic graphite precursor samples

In all GO samples, only D band and G band were observed with no 2D band, as seen in **Figure 4.9** and **Figure 4.10**. Natural graphite derived GO samples show a higher amount of defects than synthetic GO samples with average I_D/I_G ratios of 0.87 and 0.54, respectively. However, the oxidation of natural GO samples was lower than synthetic GO samples, as shown in Elemental analysis results (Refer to **Table 4.2**). Therefore, the defects are not due to sp³ hybridisation caused by oxygen functional groups but may be due to some other structural defects such as vacancy-like defects, charged impurities or hopping defects which is defects which distort the bonds between atoms.

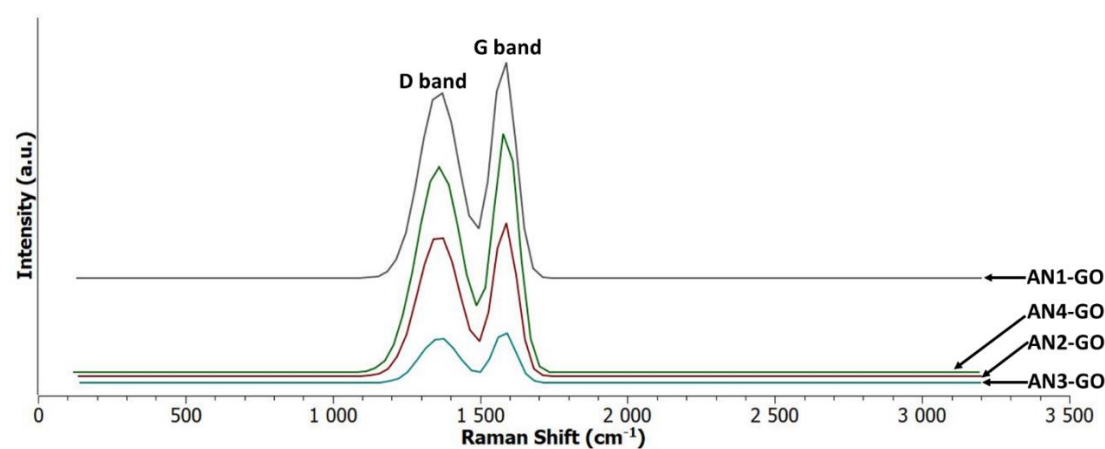


Figure 4.9 : Raman spectra of natural GO samples

The average crystallite sizes estimated by use of Raman spectroscopy for natural GO samples of 11.12 nm is lower than synthetic GO samples of 36.65 nm. This evaluation shows that synthetic GO samples have a higher crystallinity than natural GO samples. This observation is unexpected since their precursors according to previous research [7] has an opposite relationship. It is interesting to note that the estimated crystallite sizes for natural GO samples vary slightly with a standard deviation of 0.55 compared to synthetic GO samples that vary significantly with a standard deviation of 26.16. The natural GO samples vary marginally in crystallite sizes; it can be assumed that their natural graphite precursors have the same trend since synthetic GO samples follow the same trend to their synthetic graphite precursors in terms of crystallinity with significant variation.

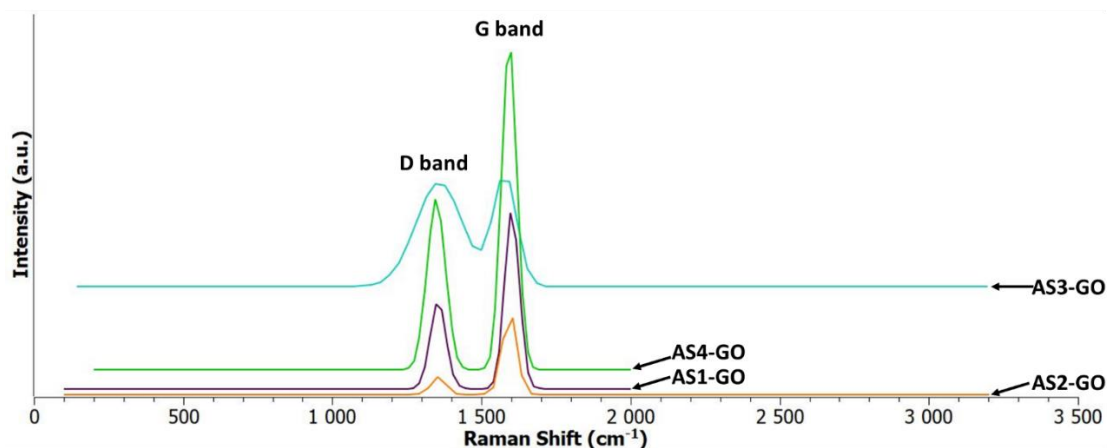


Figure 4.10 : Raman spectra of synthetic GO samples

For the natural GO samples, their CV curves have higher symmetry than synthetic GO samples, as seen in **Figure 4.11**. This observation means that natural GO samples electrochemical behaviour is electrical double layer capacitive. The peaks in the CV curves of the synthetic GO samples seen in **Figure 4.12** means their electrochemical behaviour is pseudocapacitive. AS1-GO has the highest specific gravimetric of 1042.99 F.g^{-1} at scan rate 10 mV.s^{-1} as shown in **Table 4.4** almost twice that of AS3-GO which has a larger flake size (0.1250 mm) graphite precursor and ten times that of AN1-GO which has an analogous flake size (0.045 mm) graphite precursor to AS1-GO but varies in type. The higher specific capacitance of AS1-GO could be due to the pseudocapacitance effect since AS1-GO has a higher oxygen content than AS3-GO. However, AS4-GO has the highest oxygen content (O% wt = 56.227 %); therefore, it should have a greater pseudocapacitance effect hence have the highest specific capacitance amongst all samples.

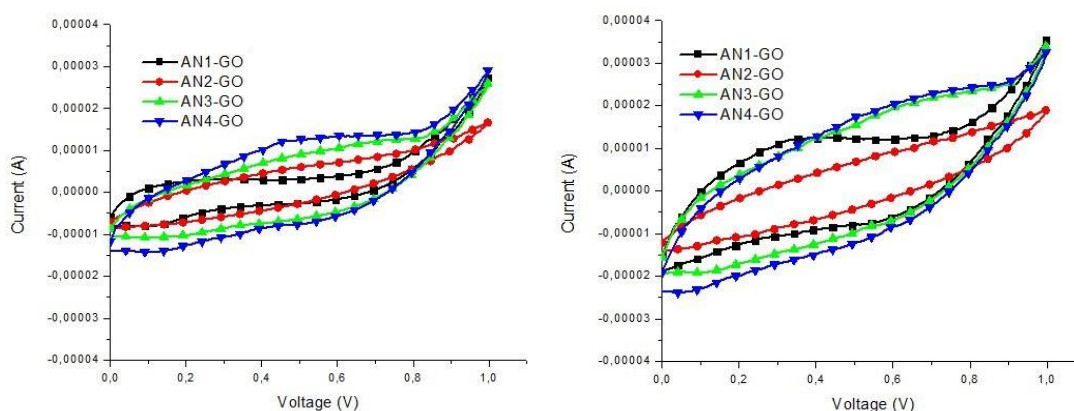


Figure 4.11 : CV curves for natural GO samples at: 10 mV.s^{-1} (left); and 20 mV.s^{-1} (right)

AN4-GO has the highest specific capacitance of 204.22 F.g^{-1} and 143.27 F.g^{-1} at 10 mV.s^{-1} and 20 mV.s^{-1} respectively amongst all natural GO samples, and therefore it was thought that a larger flake size (0.450 mm) graphite precursor would contribute to a higher capacitance. This result does not seem to be the case in the synthetic GO samples with the smallest flake size (0.045 mm) graphite precursor giving AS1-GO the highest specific capacitance amongst the synthetic GO samples.

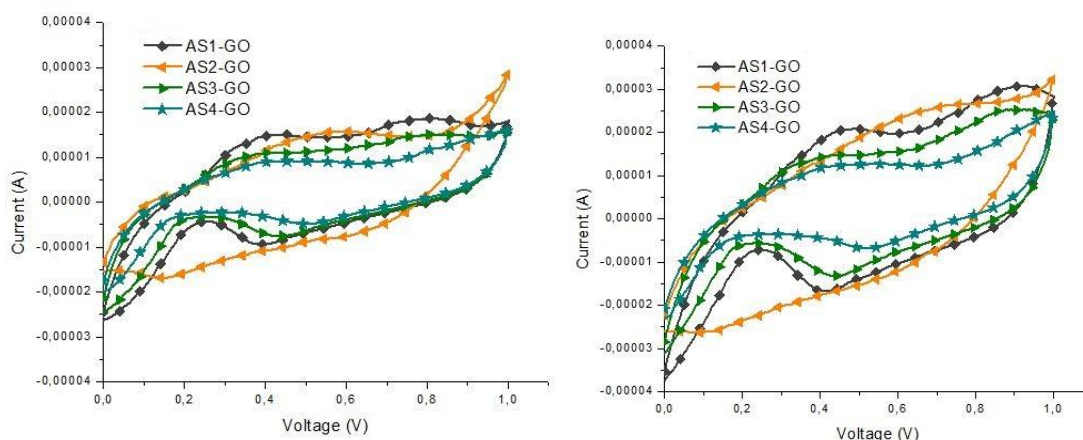


Figure 4.12 : CV curves for synthetic GO samples at: 10 $\text{mV}\cdot\text{s}^{-1}$ (left); and 20 $\text{mV}\cdot\text{s}^{-1}$ (right)

At all average particle sizes of the graphite precursors, synthetic GO samples had a higher specific capacitance than natural GO samples at scan rate 10 $\text{mV}\cdot\text{s}^{-1}$ as shown in **Figure 4.13**. With the increase in average particle size of the graphite precursor, synthetic GO samples showed a decrease in gravimetric specific capacitance while the opposite trend was seen in natural GO samples. Three factors possibly influence the higher specific capacitances of synthetic GO samples compared to natural GO samples, i.e. oxygen content, crystallinity and amount of defects.

Table 4.4 : Results obtained from CV curves for natural and synthetic GO samples

Sample	Scan Rate ($\text{mV}\cdot\text{s}^{-1}$)	Gravimetric Capacitance ($\text{F}\cdot\text{g}^{-1}$)	Areal Capacitance ($\mu\text{F}\cdot\text{cm}^{-2}$)	Energy Density ($\text{kJ}\cdot\text{kg}^{-1}$)
AN1-GO	10	54,00	48.49	27
AN2-GO	10	96,33	53.07	48.16
AN3-GO	10	183,97	92.62	91.98
AN4-GO	10	204,22	117.36	102.11
AN1-GO	20	37,38	64.54	18.69
AN2-GO	20	44,42	36.76	22.21
AN3-GO	20	111,29	83.23	55.64
AN4-GO	20	143,27	92.69	71.63
AS1-GO	10	1042,99	140.575	521.49
AS2-GO	10	274,91	142.143	137.45
AS3-GO	10	539,93	113.479	269.97
AS4-GO	10	279,20	83.072	139.60
AS1-GO	20	129,19	105.152	64.60
AS2-GO	20	240,23	110.804	120.12
AS3-GO	20	106,42	83.684	53.26
AS4-GO	20	59,93	55.724	29.97

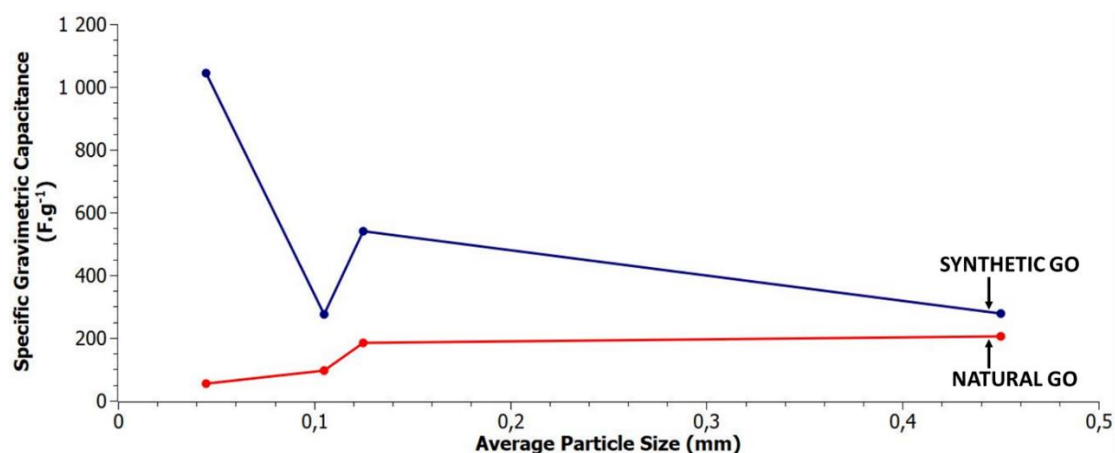


Figure 4.13 : Specific gravimetric capacitance of GO samples vs average particle size of graphite precursors

The highest specific capacitance of AS1-GO can be explained not by one single factor of the precursor graphite but by a combination of factors such as smaller flake size graphite precursor (0.045 mm) and synthetic type resulting in higher oxygen content (O % wt = 51.587 %) giving additional pseudocapacitance effect, and a lower amount of defects in the graphitic structure of GO promoting efficient ion transport. AS1-GO had the highest energy density of 521.49 kJ.kg⁻¹ and with a yield of 107.67 % makes it the most suitable electrode material to use for GO supercapacitors. This energy density obtained is higher than recent development in supercapacitor technology by Sandesh Y.Sawant et. al using a more complex method of fabricating supercapacitor electrodes, nitrogen doped metal-free and non-precious multifunctional 3D carbon foam, obtaining an energy density of 399.6 kJ.kg⁻¹ at potential scan rates of 1 to 40 mV.s⁻¹ within a potential range of 0 to 1 V.

4.6 Conclusion

During this investigation, it was observed that GO produced from synthetic graphite precursor have a higher specific capacitance than GO produced from natural graphite precursor with analogous average particle size (flake size) between the range 0.045 mm and 0.450 mm. GO produced from small flake size (0.045 mm) synthetic graphite precursor has the highest specific capacitance due to the pseudocapacitance effect of the oxygen functional groups as well as a lower amount of defects in the GO structure.

It was found that the desired characteristics of a graphite precursor are a small flake size producing highly oxidised GO with high yield, and a synthetic type with highly ordered graphitic structure fabricating GO with a low amount of defects. AS1-Graphite had these desired characteristics making it the preferred graphite precursor which produced AS1-GO with exceptional energy storage characteristics resulting in the optimal electrode material to use to fabricate GO supercapacitors.

4.7 Acknowledgments

I would like to thank Asbury Carbons for kindly donating the graphite used in this research.

References

- [1] J. R. Miller and P. Simon, "Electrochemical Capacitors for Energy Management," *Science*, vol. 321, no. 5889, pp. 651-652, 2008.
- [2] J. Biener, M. Stadermann, M. Suss, M. A. Worsley, M. M. Biener, K. A. Rosea and T. F. Baumann, "Advanced carbon aerogels for energy applications," *Energy & Environmental Science*, vol. 4, no. 3, pp. 656-667, 2011.
- [3] B. Xu, S. Yue, Z. Sui, X. Zhang, S. Hou, G. Cao and Y. Yang, "What is the choice for supercapacitors: graphene or graphene oxide?," *Energy & Environmental Science*, vol. 4, no. 8, pp. 2826-2830, 2011.
- [4] S. Wang and R. A. W. Dryfe, "Graphene oxide-assisted deposition of carbon nanotubes on carbon cloth as advanced binder-free electrodes for flexible supercapacitors," *Journal of Materials Chemistry A*, vol. 1, no. 17, pp. 5279-5283, 2013.
- [5] Z.-S. Wu, W. Ren, L. Gao, B. Liu, C. Jiang and H.-M. Cheng, "Synthesis of high-quality graphene with a pre-determined number of layers," *Carbon*, vol. 47, no. 2, pp. 493-499, 2009.
- [6] C. Botas, P. Álvarez, C. Blanco, R. Santamaría, M. Grandaa, P. Ares, F. Rodríguez-Reinoso and R. Menéndez, "The effect of the parent graphite on the structure of graphene oxide," *Carbon*, vol. 50, no. 1, pp. 275-282, 2012.
- [7] C. Botas, A. M. Pérez-Mas, P. Álvarez, R. Santamaría, M. Granda, C. Blanco and R. Menéndez, "Optimization of the size and yield of graphene oxide sheets in the exfoliation step," *Carbon*, vol. 63, pp. 576-578, 2013.
- [8] D. R. Chowdhury, C. Singh and A. Paul, "Role of graphite precursor and sodium nitrate in graphite oxide synthesis," *RSC Advances*, vol. 4, no. 29, pp. 15138-15145, 2014.
- [9] S. S. Shojaenezhad, M. Farbod and I. Kazeminezhad, "Effects of initial graphite particle size and shape on oxidation time in graphene oxide prepared by Hummers' method," *Journal of Science: Advanced Materials and Devices*, vol. 2, no. 4, pp. 470-475, 2017.
- [10] D. D. L. Chung, "Review Graphite," *Journal of Materials Science*, vol. 37, p. 1475-1489, 2002.
- [11] M. Inagaki, "Graphite intercalation compounds. Synthesis, structure and application," *Journal of the Japan Institute of Energy*, vol. 77, no. 9, pp. 849-857, 1998.
- [12] M.-H. Tran and H. K. Jeong, "Influence of the Grain Size of Precursor Graphite on the Synthesis of Graphite Oxide," *New Physics: Sae Mulli*, vol. 63, no. 2, p. 206-209, 2013.
- [13] P. L. Weis, I. Friedman and J. P. Gleason, "The origin of epigenetic graphite: evidence from isotopes," *Geochimica et Cosmochimica Acta*, vol. 45, no. 12, pp. 2325-2332, 1981.
- [14] A. Kavanagh and R. Schlögl, "The morphology of some natural and synthetic graphites," *Carbon*, vol. 26, no. 1, pp. 23-32, 1988.
- [15] M. Wissler, "Graphite and carbon powders for electrochemical applications," *Journal of Power Sources*, vol. 156, no. 2, pp. 142-150, 2006.
- [16] D. C. Marcano, D. V. Kosynkin, J. M. Berlin, A. Sinitskii, Z. Sun, A. Slesarev, L. B. Alemany, W. Lu and J. M. Tour, "Improved Synthesis of Graphene Oxide," *ACS Nano*, vol. 4, no. 8, pp. 4806-4814, 2010.
- [17] L. G. Cançadoa, K. Takai, T. Enoki, M. Endo, Y. A. Kim, H. Mizusaki, A. Jorio, L. N. Coelho, R. Magalhães-Paniago and M. A. Pimenta, "General equation for the determination of the crystallite size L_a of nanographite by Raman spectroscopy," *Applied Physics Letters*, vol. 88, no. 16, pp. 1-3, 2006.

Chapter 5

Conclusions and Recommendations

5.1 Conclusion

In this investigation and research, natural and synthetic graphite precursors were effectively oxidised to GO using the Hummers method with additional potassium permanganate. First, GO obtained from natural graphite precursor with varying flake size between the range 0.045 mm and 0.450 mm was analysed to determine its effect on GO supercapacitor energy storage capabilities.

It was observed that an increase in flake size of natural graphite precursor showed an increase in specific capacitance of GO electrode materials obtained from natural graphite precursors. These results showed how specific capacitance could be improved for GO electrode materials. The actual results obtained was contrary to the expected result of GO produced from smallest flake size (0.045 mm) natural graphite precursor with highest oxygen content from all GO produced from natural graphite precursors to have the highest specific capacitance. The reason for this expected result was from previous research which indicated that GO has a higher capacitance than graphene due to the pseudocapacitance effect from oxygen functional groups.

In the initial experiment, the amount of oxygen functional groups natural GO samples was determined by elemental analysis. The specific capacitance of natural GO samples was obtained from CV and showed peaks at the voltage limits and not between them. These results showed pseudocapacitance effect has a minor effect on the overall specific capacitance of GO electrode produced from natural graphite precursors material and that some other factor had to be playing a role in the increase of specific capacitance.

Varying type of graphite precursors showed that synthetic graphite precursor with the smallest flake size (0.045 mm) displayed high specific capacitance obtained from the CV curve. It was observed that this GO had an effective combination of high oxygen content, high crystallinity and low amount of defects in its structure. The high oxygen content obtained from elemental analysis contributes to the pseudocapacitance effect in this sample. The pseudocapacitance effect is significant because the CV curves showed a few peaks between the voltage limits. The high crystallinity and low amount of defects determined from Raman may assist in allowing the ions from the electrolyte to move efficiently throughout the GO electrode material and into the pores.

5.2 Recommendation for Further Studies

Future work includes investigating the mechanisms of pseudocapacitance effect in GO and ion transportation in defective GO structure. More experiments and some modelling to be carried out of the hypothesised physical phenomena responsible for the established relations in this research.

Appendix A

First attempts at electrolyte preparation with incorrect heating process caused discolouration to polymer gel electrolyte as shown in Figure A.1. After many attempts, the correct heating process was realised, resulting in a transparent gel electrolyte, as shown in Figure A.2.

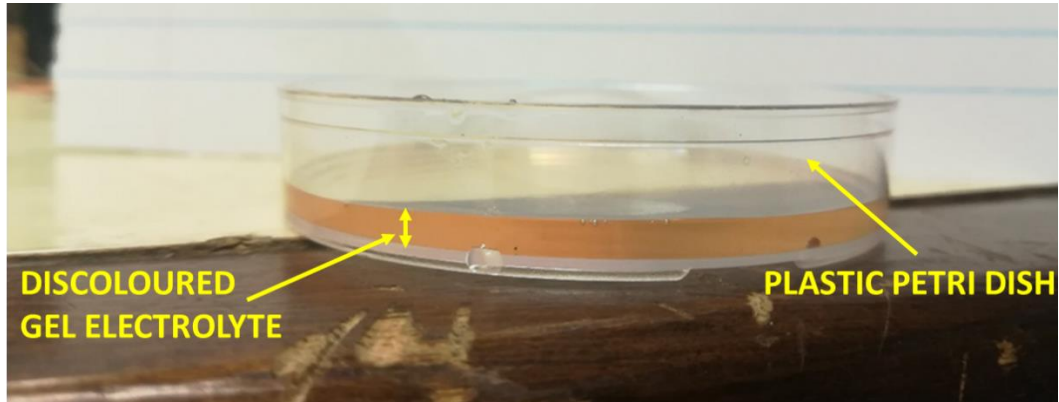


Figure A.1 : Discoloured gel electrolyte



Figure A.2 : Clear gel electrolyte: top view (left); and side view (right)

The hydraulic press was used to achieve this 1 MPa pressure to sandwich the electrodes together and is shown in Figure A.3. The die with sample (supercapacitor) in it is sitting raised from the bolster with the piston rod coming down onto the sample. The two control switches must be pressed together to bring down the slide/ram with piston rod if only one switch is pressed the slide/ram with piston rod will not move. This mechanism is a safety feature of the hydraulic press.

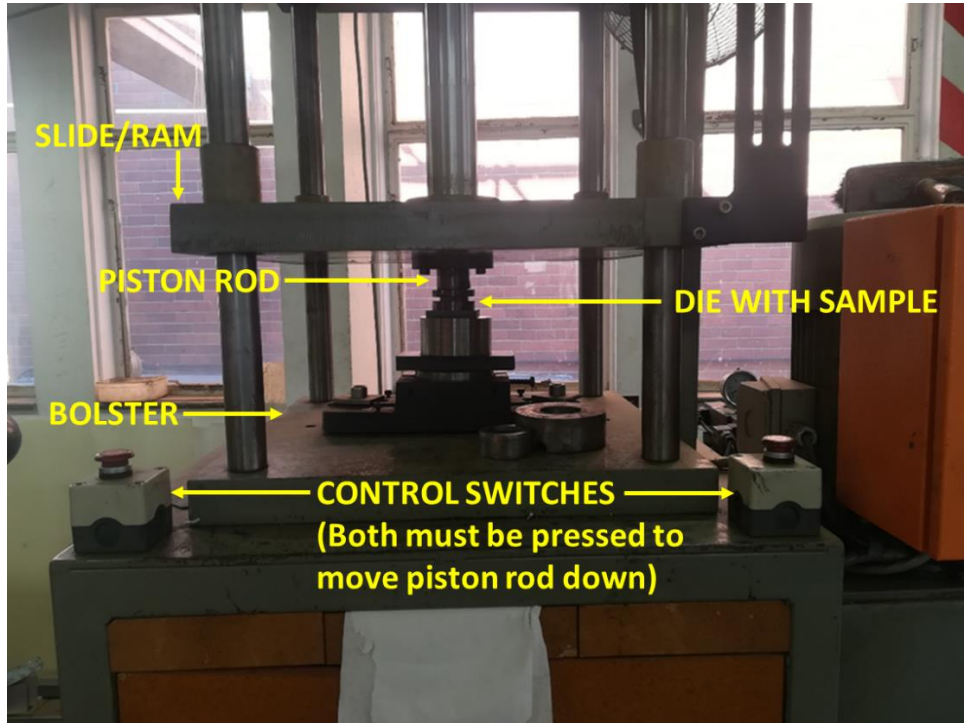


Figure A.3 : Hydraulic press sandwiching supercapacitor electrodes together

A complete assembled GO supercapacitor is shown in Figure A.4. Perspex was the material used for the encapsulation since it is an insulator. Bolts and nuts were fitted for a hermetic seal also to maintain consistent, even pressure on the supercapacitor.

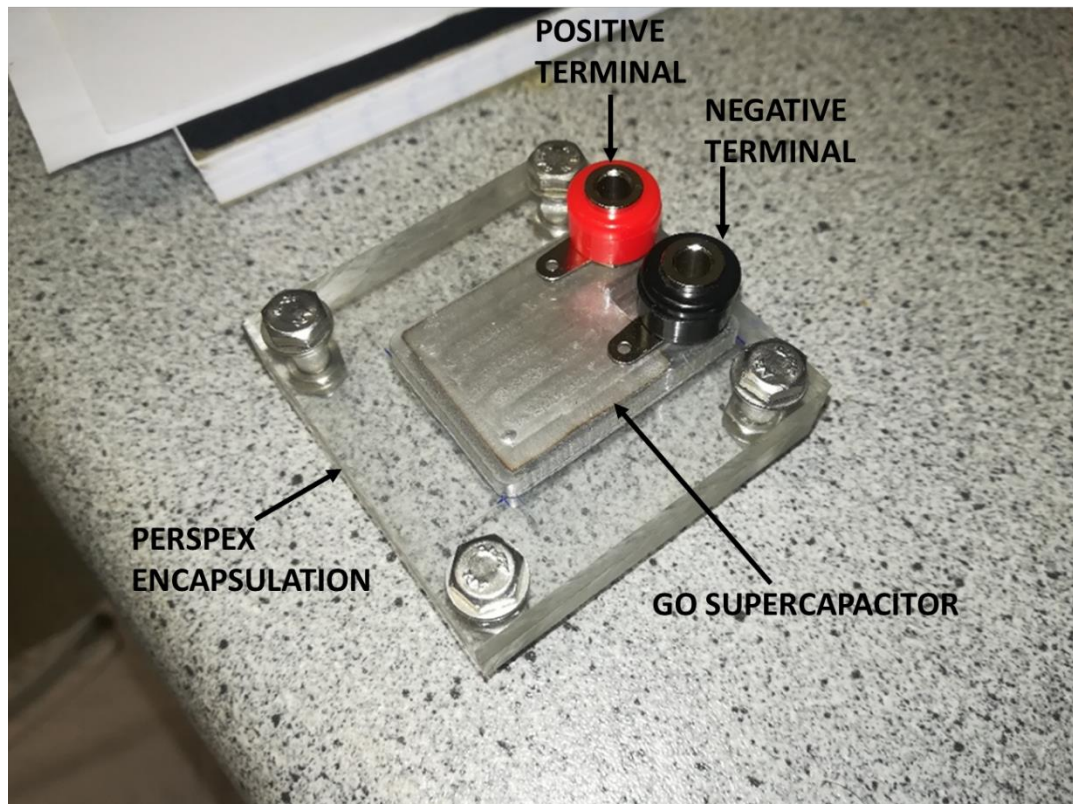


Figure A.4 : Fully assembled GO supercapacitor

Appendix B

Peer-Reviewed Conference Article

Effect of flake size of graphite precursor on graphene oxide supercapacitors for energy storage

Solan Perumal, Alan Leigh Lawrence Jarvis and
Mohammed Zaahid Gaffoor

Published: *Proceedings of International Southern African
Universities Power Engineering Conference 2020*

B.1 Abstract

In this research, supercapacitors were fabricated using graphene oxide (GO) as the electrode material. GO was synthesised using natural graphite precursor with varying flake sizes. GO was characterised by High-Resolution Transmission Electron Microscopy (HRTEM) and Elemental Analysis. Cyclic voltammetry was carried out at different scan rates to determine the specific capacitance and energy density of the electrode material. An increase in specific capacitance was seen with an increase in graphite precursor flake size. A specific capacitance and energy density of 204.22 F.g⁻¹ and 102.11 kJ.kg⁻¹ respectively at scan rate 10 mV.s⁻¹ was obtained for the GO sample synthesised from graphite precursor with an average particle size of 0.45 mm. This sample also had the highest specific capacitance for all scan rates.

B.2 Introduction

Eskom, South Africa's major electricity provider lacks the capacity to meet energy demand with their current non-renewable energy-based power plants [1]. In 2018, the Department of Energy pledged to get more renewable energy across the country and especially to rural areas [2]. The intermittent nature of renewable energy sources however creates many challenges in energy storage. Therefore, there's been great interest in finding efficient energy storage devices for renewable energy [3]. A promising candidate is the supercapacitor due to its high power density and good rate capability which is desirable in energy storage devices.

This has resulted in the supercapacitor technology having undergone considerable research and development in the recent years. Supercapacitors have a high power density and a low energy density as compared to lithium batteries [4]. For supercapacitors to realise their potential, it is important that their energy density is improved. An important way to address this is to develop advanced electrode materials. One of the interesting materials to use as the electrodes of the supercapacitor is graphene oxide (GO).

GO is a two-dimensional (2-D) material made from oxidising graphite. GO is hydrophilic meaning it is easily dispersible in water. Therefore, it is easy to work with, no expensive solvent or binders are required. GO was first reported as an electrode material for supercapacitors in 2011 by Bin Xu. *et al.* [5]. GO had a specific capacitance of 189 F.g⁻¹, higher than that of graphene. This was attributed by an additional pseudocapacitance effect of attached oxygen-functional groups on the basal plane [5]. In 2018, GO proved to be an excellent electrode material when combined with conductive electrode bulk ink with a specific capacitance of 423 F.g⁻¹ [6]. The properties of GO can be tailored by varying the graphite precursor used for synthesis. The size and structure of GO is affected by using graphite precursors with different flake sizes [7]. Oxidation of GO is greater when graphite precursor with shorter crystallite sizes were used [8]. So, if GO was synthesised with a graphite precursor of smaller flake size, it would be better oxidised and therefore have more oxygen functional groups. This greater amount of oxygen functional groups would give more pseudocapacitance effect and therefore have a higher capacitance than GO synthesised from graphite precursor with larger flake size. When purchasing commercially available natural graphite, the only difference in choice of natural graphite is varying flake sizes.

In this paper, an investigation into the link between the flake size of the graphite precursor used to synthesise GO and the energy storage characteristics of the GO supercapacitor is presented.

B.3 Background

A supercapacitor is an energy storage device with high surface area porous electrodes and a thin dielectric (electrolyte) [9]. The interface between the electrolyte and the electrode is the electric double layer. The capacitances gained from this type of architecture is orders of magnitude higher than conventional capacitors. Supercapacitors are categorised as per Figure B.1.

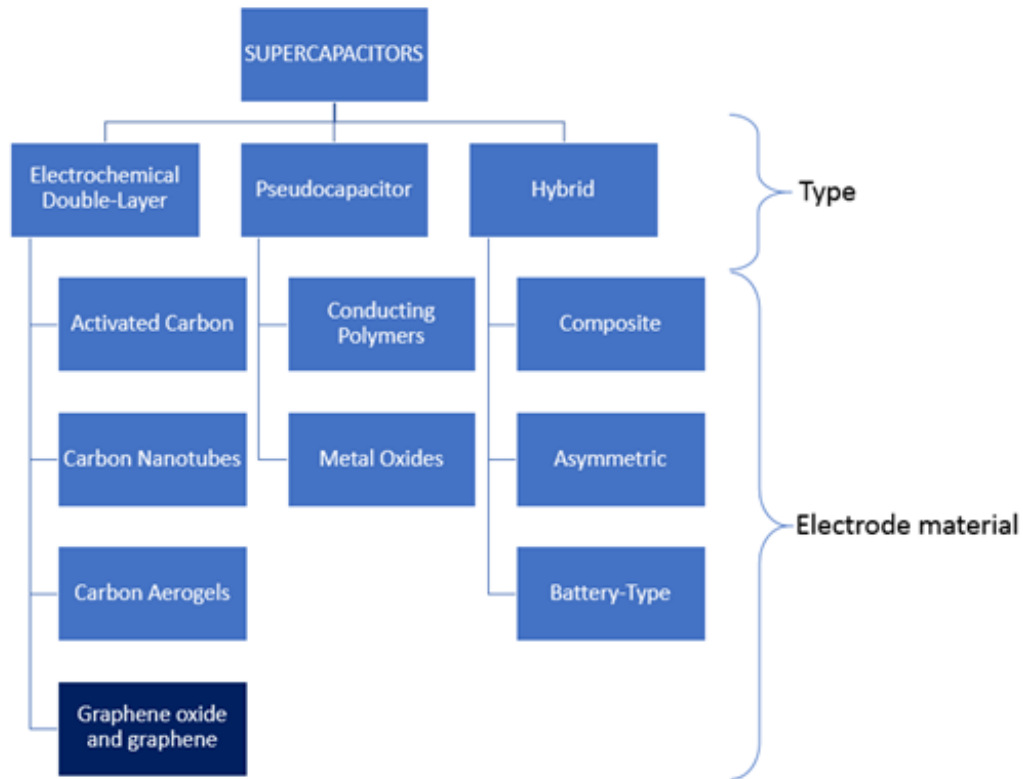


Figure B.1 : Categorisation of supercapacitors

The type of supercapacitor and electrode material of concern in this paper is Electrochemical Double Layer Capacitor (EDLC) and GO respectively. EDLC's mechanism for storing charge is non-Faradaic which means charges are distributed on surfaces by physical processes that do not involve the making or breaking of chemical bonds [10]. The double layer in name 'electrochemical double-layer capacitor' refers to the double layer of charge. One layer of charge accumulates on the electrode surface due to the voltage applied. The other layer of charge is the ions from the electrolyte that diffuse across the separator into the pores of the electrode of opposite charge as seen in Figure B.2. The capacitance gained from this mechanism is known as double-layer capacitance.

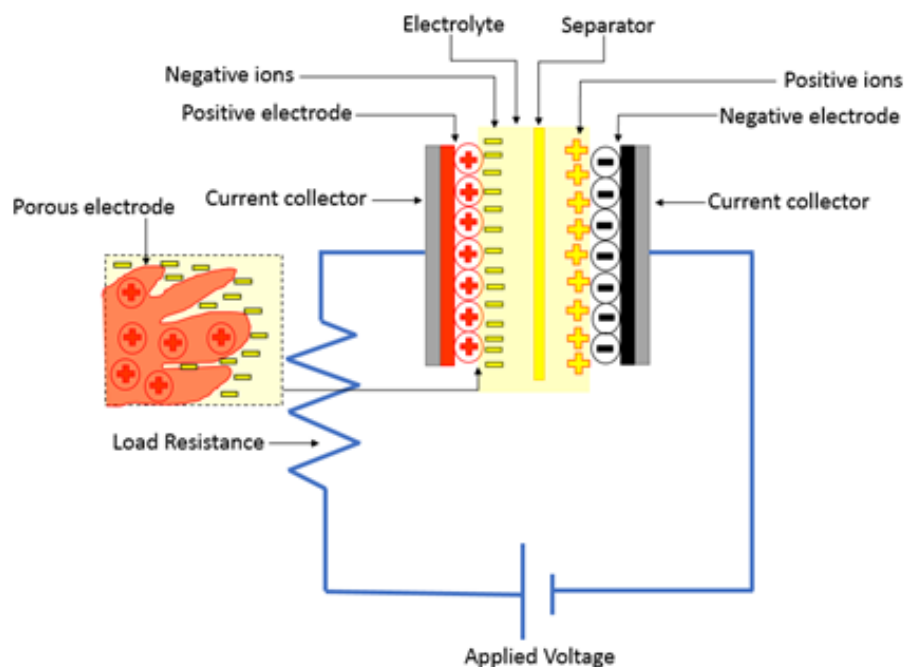


Figure B.2 : Schematic of supercapacitor

The capacitance of porous carbon materials like GO is mainly contributed by double-layer capacitance from electrostatic charge accumulation and about 1-5 % is contributed by pseudocapacitance [11]. This pseudocapacitance comes from the high content of oxygen functional groups [12] which is inherent in GO. Pseudocapacitance charge storing mechanism is Faradaic unlike double-layer capacitance and occurs as quick surface reduction and oxidation (redox) reactions.

The key parameters for supercapacitors are specific capacitance, equivalent series resistance (*ESR*), energy density and power density. Specific capacitance is the capacitance normalised by electrode mass (in grams), volume (in cm^3), or area (in cm^2). *ESR* is the internal resistance of the supercapacitor. Energy density is the amount of energy the supercapacitor can store and is presented as a specific energy density measured in J.kg^{-1} [13]. Obtaining these supercapacitor characteristics are most commonly done by cyclic voltammetry (CV).

CV can be performed to evaluate capacitance of the as prepared active electrode material GO and the operating voltage window of the electrolyte. CV is an analytical technique in which current produced via a redox reaction is monitored as a function of scanned potential applied to an electrode [14]. The instrumentation used in CV analysis consists of a signal generator, potentiostat, working electrode (WE), reference electrode (RE) and counter electrode (CE). CV can either be done using a two-electrode system or three-electrode system [15]. Three-electrode system is accurate in controlling the voltage at the WE while measuring the current flowing from the WE to CE since it uses a RE that is ideally non-polarisable proving to be consistent and reliable [11]. It is found that the three electrode system is also advantageous due to the quick electrode preparation.

B.4 Experimental

The GO supercapacitor comprised of four parts viz. electrode material, current collectors, electrolyte and encapsulation. The current collector, electrolyte and encapsulation were kept constant for all samples and the electrode material was varied.

B.4.1 Synthesis of GO

Four different graphite precursors from Asbury Carbons were used viz. Grade 230U, 3243, 3160 and 3061 and were called AN1-GO, AN2-GO, AN3-GO and AN4-GO respectively for easy identification. The average particle sizes for AN1-GO, AN2-GO, AN3-GO and AN4-GO are 0.045 mm, 0.105 mm, 0.1250 mm and 0.4500 mm respectively. Graphite precursors were used as received. GO was synthesised by oxidising the graphite precursor using Hummers method with additional potassium permanganate. The GO powders obtained at the end of synthesis process is shown in Figure B.3.



Figure B.3 : GO samples

B.4.2 Fabrication of current collectors

The design of the current collector was drawn using SolidWorks software as shown in Figure B.4. The current collectors were fabricated using stainless steel with 0.5 mm thickness. Symmetric current collectors were made by laser cutting. Stainless steel was chosen due to its low corrosion rate. This is a requirement due to the use of an acidic electrolyte. Stainless steel has been used as a current collector in many commercially available supercapacitors.

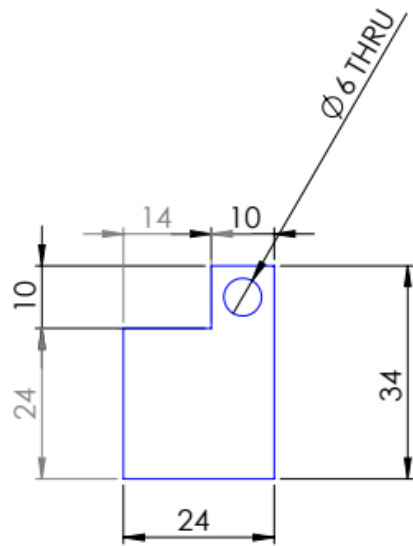


Figure B.4 : Stainless current collector with dimensions

B.4.3 Preparation of GO electrode

GO solution with 0.1 % wt concentration was made by adding 0.03 g of GO powder to 30 ml of deionised water. GO solution was then sonicated for 1 hour. Thereafter, GO solution was drop-casted onto stainless steel plates (Refer to Figure B.5) and left to dry in air overnight at room temperature. Five coats of GO solution were deposited onto the stainless steel. Before each drop-casting, the GO solution was sonicated for 10 minutes. Multiple coats of low concentration solution are preferred to single coat of high concentration solution. At high concentrations, aggregation of GO occurs.

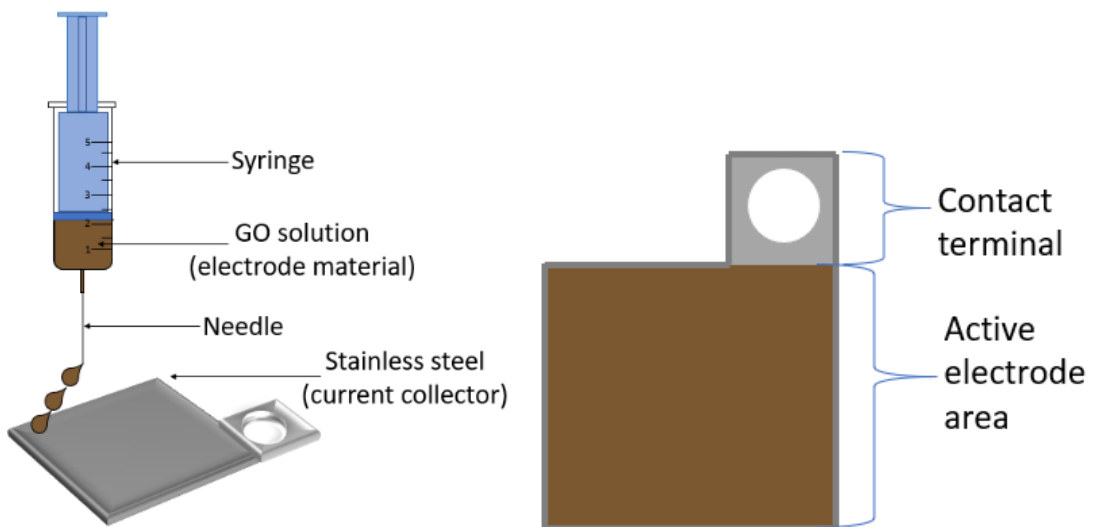


Figure B.5 : Drop-casting of GO on stainless steel current collectors

B.4.4 Synthesis of electrolyte

The hydrogel polymer electrolyte was made using poly(vinyl alcohol) (PVA) as a host matrix, water as a plasticizer and phosphoric acid (H_3PO_4) as the electrolyte solution. The preparation of the hydrogel polymer electrolyte began with mixing with a magnetic stirrer 1 g of PVA powder and 10 ml of deionised water into a 50 ml beaker. The mixture was then heated up to $\sim 80^\circ\text{C}$ until it turned from white to clear. This solution was cooled down to 50°C and then 0.03 mol (2.94 g) of H_3PO_4 was added to the solution. The viscous solution was mixed thoroughly for 1 hour. Thereafter, the clear, viscous solution was drop-cast into a glass Petri dish left overnight in air to allow the excess water to evaporate.

B.4.5 Assembly of GO supercapacitor

PVA gel electrolyte is applied to the GO coated electrodes. The electrodes are then sandwiched together using a die that was manufactured from soft steel as seen in Figure B.6. A pressure of ~ 1 MPa was applied to the electrodes. A load of 90 kg was used to achieve this pressure.

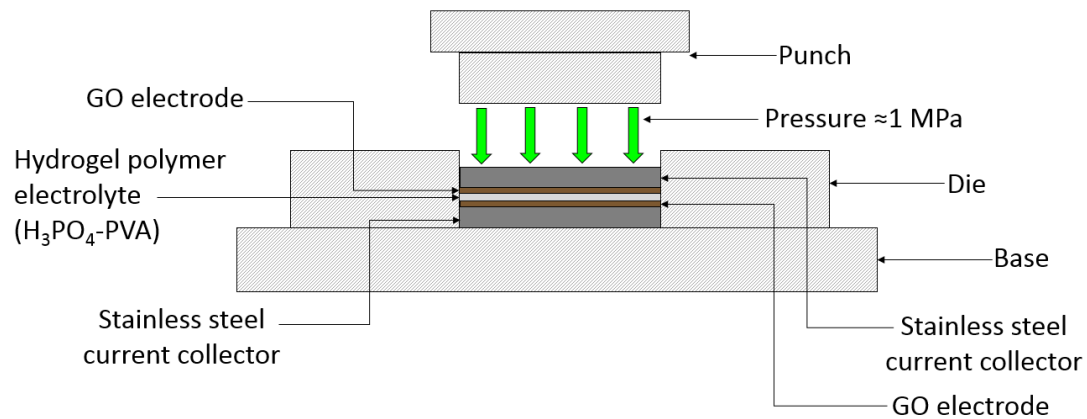


Figure B.6 : Soft steel die sandwiching electrodes

B.4.6 GO characterisation

The morphology of the GO samples was characterised using High-Resolution Transmission Electron Microscopy (HRTEM). Elemental analysis was used to determine the carbon (C), hydrogen (H) sulphur (S), nitrogen (N) and oxygen (O) content in each GO sample.

B.4.7 GO supercapacitor electrochemical measurement

CV was performed on the GO samples using a three-electrode system at scan rates of 10 mV.s⁻¹, 20 mV.s⁻¹ and 100 mV.s⁻¹. The operating potential window is 1 V which was determined from the H₃PO₄ electrolyte being inorganic.

To evaluate the energy storage capabilities, gravimetric (per mass), and surface/areal (per surface area) capacitance can be calculated using (B.1).

$$C = \frac{\int_{E_1}^{E_2} i(E)dE}{2(E_2 - E_1)\nu m} \quad (\text{B.1})$$

where the integral part which is the area under the curve as shown in Figure B.7 represents the total voltammetric charge, E_2 and E_1 and the high and low potentials limits (V) respectively, ν is the scan rate (V.s⁻¹) and m is the active mass of the sample GO.

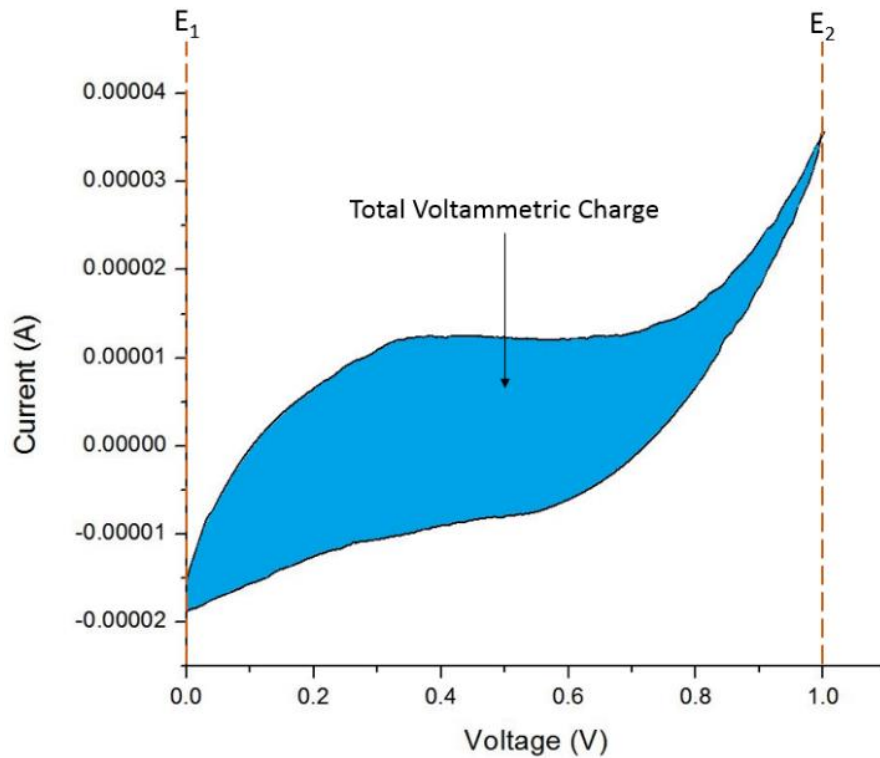


Figure B.7 : Typical CV curve

Energy density can be calculated using (B.2).

$$E = \frac{1}{2} CV^2 \quad (\text{B.2})$$

B.5 Results and Discussion

The circular holes in Figure B.8 are the holes in the carbon grid. In all samples, a sheet-like structure is seen which is typical of GO. Another key characteristic of GO is its very small thickness regarded as 2D. All samples are highly transparent in the HRTEM images showing that the GO is exceptionally thin.

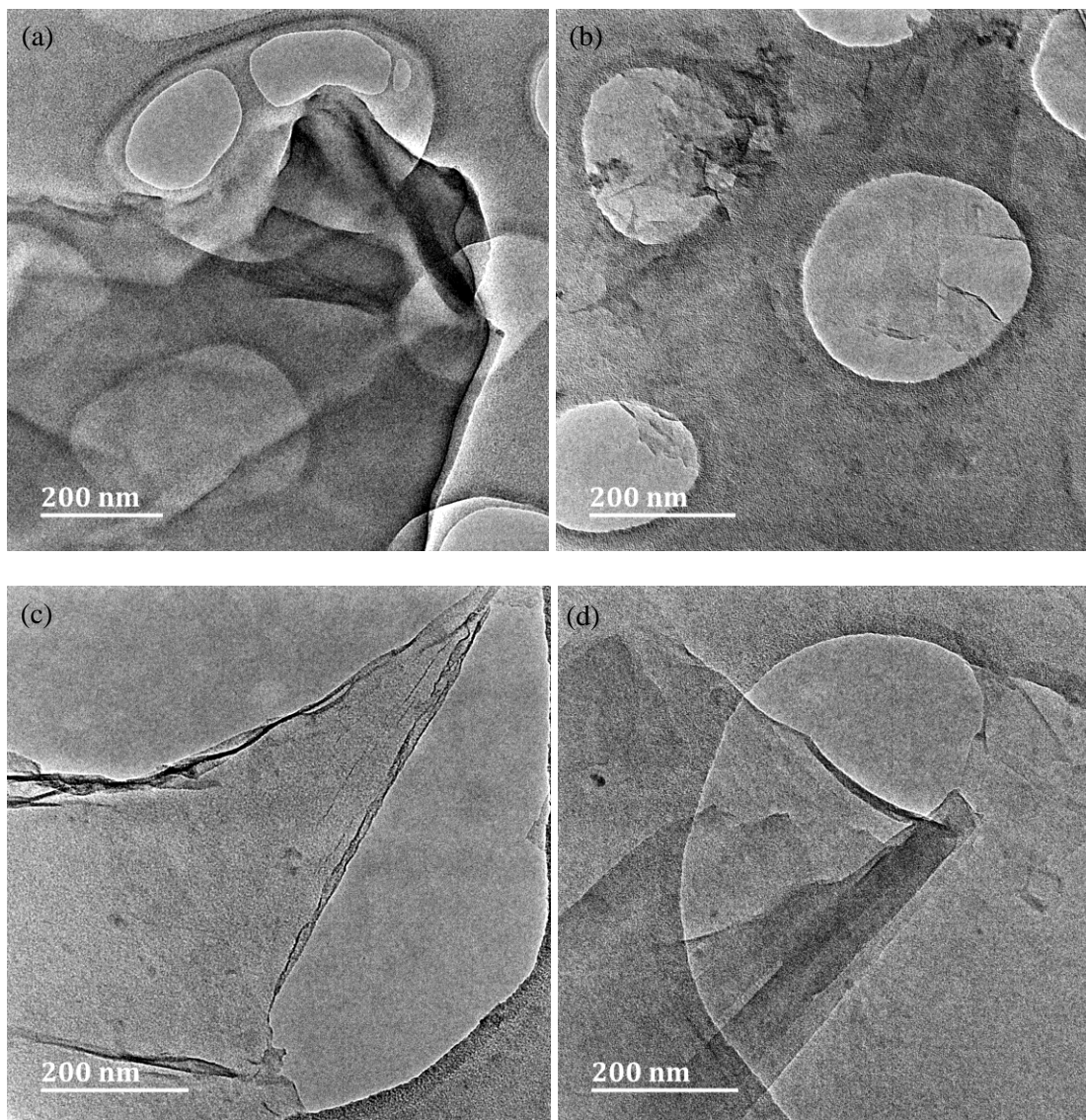


Figure B.8 : HRTEM of (a) AN1-GO, (b) AN2-GO, (c) AN3-GO, (d) AN4-GO

AN1-GO sample has the highest oxygen content as compared to the other GO samples as seen in Table B.1. This means that AN1-GO had achieved the highest oxidation and therefore had a greater number of functional groups than the other GO samples. This was expected since AN1-GO was produced using natural graphite with the smallest flake size.

Table B.1 : Elemental Analysis Results

Sample	C (%)	O (%)	S (%)	N (%)	H (%)
AN1-GO	41.80	53.095	1.881	0.05	3.174
AN2-GO	57.91	35.733	3.314	0.01	3.033
AN3-GO	61.63	30.573	4.576	0.01	3.211
AN4-GO	58.98	32.699	5.213	0.00	3.108

The cyclic voltammograms of the GO samples are shown in Figure B.9, Figure B.10 and Figure B.11.

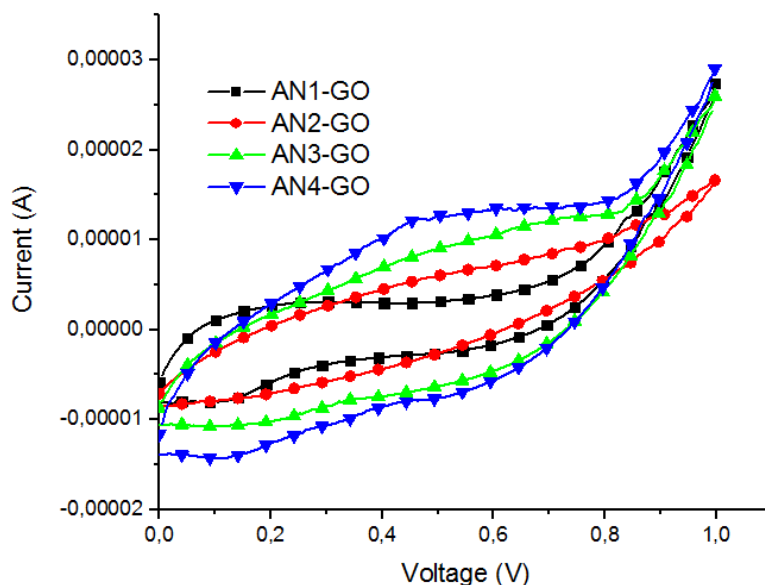


Figure B.9 : CV curves for GO samples at 10 mV.s^{-1}

Figure B.9 shows a nearly symmetric curve for all samples showing a typical electrical double layer capacitive behaviour. Even at a high scan rate of 100 mV.s^{-1} a similar shape is seen for the CV curves as seen in Figure B.10.

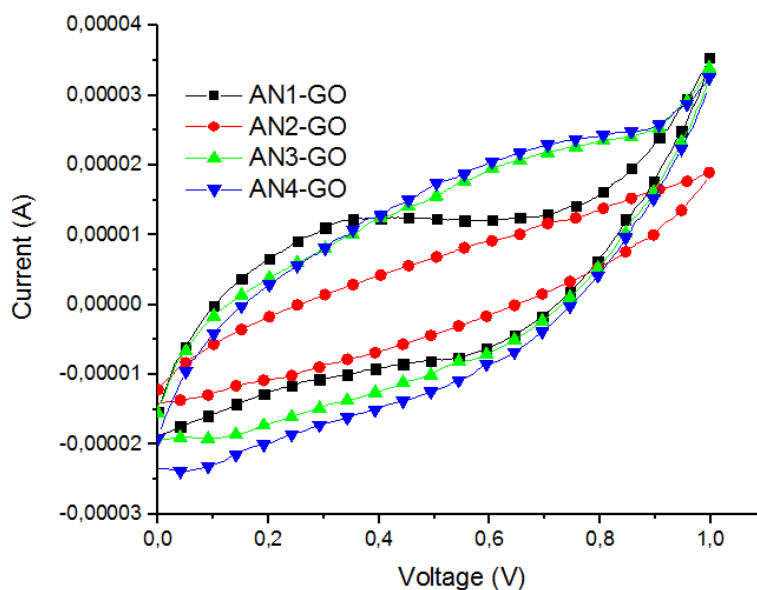


Figure B.10 : CV curves for GO samples at 20 mV.s^{-1}

The gravimetric capacitances for each sample was calculated from the CV curves as is shown in Table B.2. The areal capacitances were calculated for the fabricated supercapacitors having an electrode area of 5.76 cm² using the CV curves.

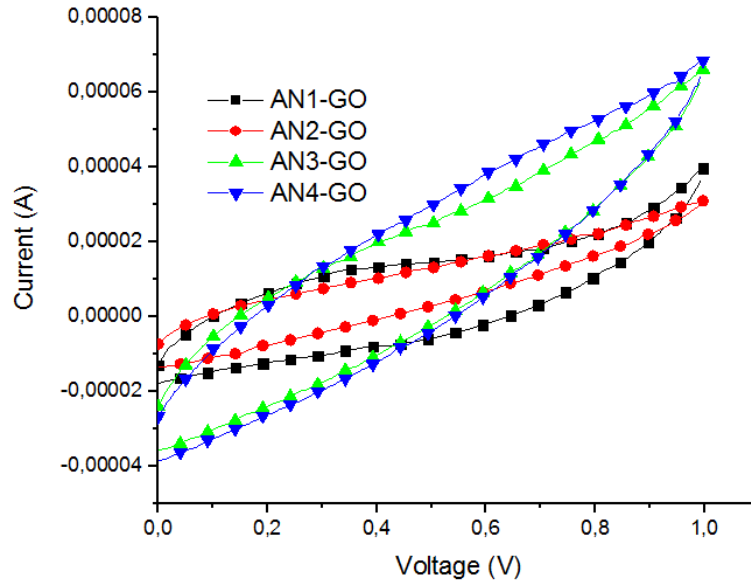


Figure B.11 : CV curves for GO samples at 100 mV.s⁻¹

AN4-GO has the highest capacitance of 204.22 F.g⁻¹ at a scan rate of 10 mV.s⁻¹ almost 4 times higher than AN1-GO.

Table B.2 : Results calculated from CV curves

Sample	Scan Rate (mV.s ⁻¹)	Gravimetric Capacitance (F.g ⁻¹)	Areal Capacitance (μF.cm ⁻²)	Energy Density (kJ.kg ⁻¹)
AN1-GO	10	54.00	48.49	27
AN2-GO	10	96.33	53.07	48.16
AN3-GO	10	183.97	92.62	91.98
AN4-GO	10	204.22	117.36	102.11
AN1-GO	20	37.38	64.54	18.69
AN2-GO	20	44.42	36.76	22.21
AN3-GO	20	111.29	83.23	55.64
AN4-GO	20	143.27	92.69	71.63
AN1-GO	100	1.47	13.34	0.73
AN2-GO	100	1.24	7.74	0.619
AN3-GO	100	1.59	19.76	0.79
AN4-GO	100	2.07	22.89	1.04

AN1-GO having higher oxygen content does not have higher capacitance as expected due to more pseudocapacitance effect. It is the changing of particle size of the precursor graphite that influences the capacitance of the GO produced as seen in Figure B.12. The average particle size from 0.0405 mm to 0.1250 mm has a steep almost linear increase in the specific capacitance but from 0.1250 to 0.4500 mm there is a gradual increase in specific capacitance suggesting there is a limiting point for the average particle size.

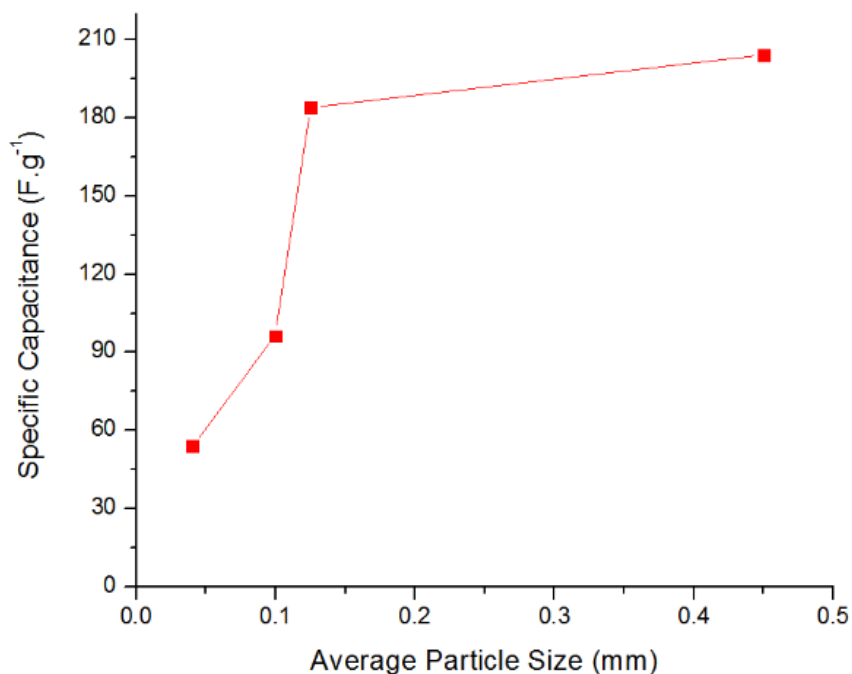


Figure B.12 : Specific Capacitance as a function of average particle size at scan rate 10 mV.s⁻¹

Figure B.13 shows the specific capacitance as a function of the scan rate. It is clear that the specific capacitance values of AN4-GO are higher than that of all other samples at scan rates 10 mV.s⁻¹ and 20 mV.s⁻¹. AN4-GO produced from graphite precursor with the larger flake has the highest energy density of 102.11 kJ.kg⁻¹ meaning it is more suitable for energy storage application.

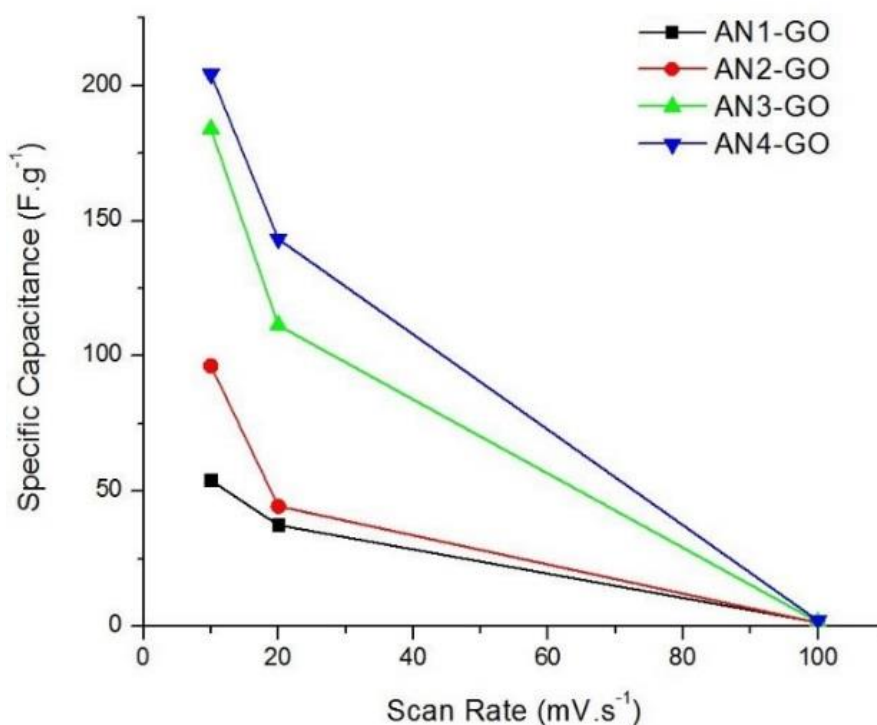


Figure B.13 : Specific capacitance as a function of scan rate

B.6 Conclusion

It was found, in the particle size range 0.0405 mm to 0.4500 mm, GO produced from smaller flake size (0.0405 mm) graphite precursor, has a greater amount of oxygen functional groups and lower capacitance than larger flaked (0.4500 mm) based GO. This implies that the pseudocapacitance effect does not have a significant impact on GO.

The energy density of GO samples synthesised from graphite precursor of a larger flake size is greater than GO synthesised from a smaller flake size graphite precursor, thus making it the preferred flake size when fabricating GO electrodes for supercapacitors for energy storage applications.

B.7 Acknowledgments

I would like to thank my colleagues in the Material Science Lab for their support during this research. Further thanks to Asbury Carbons for kindly donating the graphite used in this research.

References

- [1] R. Inglesi, "Aggregate electricity demand in South Africa: Conditional forecasts 2030," *Applied Energy*, vol. 87, pp. 197-204, 2010.
- [2] S.SA, "Energy and the poor: a municipal breakdown," 4 June 2018. [Online]. Available: <http://www.statssa.gov.za/p=11181>. [Accessed 24 2019 July].
- [3] H. Yang, "A Review of Supercapacitor-based Energy Storage Systems for Microgrid Applications," in *IEEE Power & Energy Society General Meeting (PESGM)*, Portland, 2018.
- [4] C. V. V. M. Gopi and H.-J. Kim, "Design of Supercapacitor for Electric and Hybrid Vehicles : Supercapacitor," in *International Conference on Information and Communication Technology Robotics (ICT-ROBOT)*, Busan, 2018.
- [5] B. Xu, S. Yue, Z. Sui, X. Zhang, S. Hou, G. Cao and Y. Yang, "What is the choice for supercapacitors: graphene and graphene oxide?," *Energy & Environmental Science*, no. 4, pp. 2826-2830, 2011.
- [6] M. Down, S. J. Rowley-Neale, G. Smith and C. E. Banks, "Fabrication of Graphene Oxide Supercapacitor Devices," *ACS Applied Energy Materials*, vol. 1, no. 2, pp. 707-714, 2018.
- [7] H. Xian, T. Peng and H. Sun, "Effect of Particle Size of Natural Graphite on the Size and Structure of Graphene Oxide Prepared by the Modified Hummers Method," *Materials Science Forum*, vol. 814, pp. 185-190, 2015.
- [8] D. R. Chowdhury, C. Singh and A. Paul, "Role of graphite precursor and sodium nitrate in graphite oxide synthesis," *RSC Advances*, no. 29, pp. 15138-15145, 2014.
- [9] A. S. Aricò, P. Bruce, B. Scrosati, J. M. Tarascon and W. V. Schalkwijk, "Nanostructured materials for advanced energy conversion and storage devices," *Nature Materials*, vol. 4, pp. 366-377, 2005.
- [10] R. Kötz and M. Carlen, "Principles and applications of electrochemical capacitors," *Electrochimica Acta*, vol. 45, no. 15-16, pp. 2483-2498, 2000.
- [11] B. E. Conway, *Electrochemical Supercapacitors, Scientific Fundamentals and Technological Applications*, New York: Kluwer Academic/Plenum Publishers, 1999.
- [12] Y. Li, M. V. Zijll, S. Chiang and N. Pan, "KOH modified graphene nanosheets for supercapacitor electrodes," *Journal of Power Sources*, vol. 196, no. 14, pp. 6003-6006, 2011.
- [13] W. K. Chee, H. N. Lim, Z. Zainal, N. M. Huang, I. Harrison and Y. Andou, "Flexible Graphene-Based Supercapacitors: A Review," *Journal of Physical Chemistry C*, vol. 120, no. 8, pp. 4153-4690, 2016.
- [14] W. Pell and B. Conway, "Voltammetry at a de Levie brush electrode as a model for electrochemical supercapacitor behaviour," *Journal of Electroanalytical Chemistry*, vol. 500, p. 121-133, 2005.
- [15] F. Beguin and E. Frackowiak, *Supercapacitors: Materials, Systems and Applications*, Germany: Wiley-VCH Verlag GmbH & Co. KGaA, 2013.